NASA/TM–2011-217163(Corrected Copy)

Evaluation of Aluminum Alloy 2050-T84 Microstructure and Mechanical Properties at Ambient and Cryogenic Temperatures

Robert A. Hafley, Marcia S. Domack, and Stephen J. Hales
Langley Research Center, Hampton, Virginia

Ravi N. Shenoy
Lockheed Martin Corporation, Hampton, Virginia

July 2011

NASA STI Program . . . in Profile

Since its founding, NASA has been dedicated to the advancement of aeronautics and space science. The NASA scientific and technical information (STI) program plays a key part in helping NASA maintain this important role.

The NASA STI program operates under the auspices of the Agency Chief Information Officer. It collects, organizes, provides for archiving, and disseminates NASA's STI. The NASA STI program provides access to the NASA Aeronautics and Space Database and its public interface, the NASA Technical Report Server, thus providing one of the largest collections of aeronautical and space science STI in the world. Results are published in both non-NASA channels and by NASA in the NASA STI Report Series, which includes the following report types:

- TECHNICAL PUBLICATION. Reports of completed research or a major significant phase of research that present the results of NASA programs and include extensive data or theoretical analysis. Includes compilations of significant scientific and technical data and information deemed to be of continuing reference value. NASA counterpart of peer-reviewed formal professional papers, but having less stringent limitations on manuscript length and extent of graphic presentations.

- TECHNICAL MEMORANDUM. Scientific and technical findings that are preliminary or of specialized interest, e.g., quick release reports, working papers, and bibliographies that contain minimal annotation. Does not contain extensive analysis.

- CONTRACTOR REPORT. Scientific and technical findings by NASA-sponsored contractors and grantees.

- CONFERENCE PUBLICATION. Collected papers from scientific and technical conferences, symposia, seminars, or other meetings sponsored or co-sponsored by NASA.

- SPECIAL PUBLICATION. Scientific, technical, or historical information from NASA programs, projects, and missions, often concerned with subjects having substantial public interest.

- TECHNICAL TRANSLATION. English-language translations of foreign scientific and technical material pertinent to NASA's mission.

Specialized services also include creating custom thesauri, building customized databases, and organizing and publishing research results.

For more information about the NASA STI program, see the following:

- Access the NASA STI program home page at *http://www.sti.nasa.gov*

- E-mail your question via the Internet to help@sti.nasa.gov

- Fax your question to the NASA STI Help Desk at 443-757-5803

- Phone the NASA STI Help Desk at 443-757-5802

- Write to:
  NASA STI Help Desk
  NASA Center for AeroSpace Information
  7115 Standard Drive
  Hanover, MD 21076-1320

NASA/TM–2011-217163(Corrected Copy)

Evaluation of Aluminum Alloy 2050-T84 Microstructure and Mechanical Properties at Ambient and Cryogenic Temperatures

Robert A. Hafley, Marcia S. Domack, and Stephen J. Hales
Langley Research Center, Hampton, Virginia

Ravi N. Shenoy
Lockheed Martin Corporation, Hampton, Virginia

National Aeronautics and
Space Administration

Langley Research Center
Hampton, Virginia 23681-2199

July 2011

Available from:

NASA Center for AeroSpace Information
7115 Standard Drive
Hanover, MD 21076-1320
443-757-5802

Errata

Issued May 2016 for

NASA-TM-2011-217163

Evaluation of Aluminum Alloy 2050-T84 Microstructure Mechanical Properties at Ambient and Cryogenic Temperatures

Hafley, Robert A.; Domack, Marcia S.; Hales, Stephen J.; Shenoy, Ravi N.

Summary of Changes:

Added statement "Fracture toughness data, J-curves, and images showing fracture path for individual tests are included in Appendix E." in the second paragraph of the fracture toughness section.

In Table 14, corrected K_{QJIC} for L-S orientation at RT to 37.7 ksi√in.

In Table B5 corrected K_{QJIC} for specimen L-S-3 to 38.0 ksi√in.

In Table B5 corrected average K_{QJIC} for L-S orientation specimens to 37.7 ksi√in.

Added Appendix E, showing individual fracture toughness data, J-curves, and images showing fracture path.

Contents

List of Tables

List of Figures

Symbols and Abbreviations

Al	aluminum
Al-Li	aluminum-lithium
AMS	Aerospace Material Specification
ASTM	American Society for Testing and Materials
°C	temperature, degrees Celsius
C(T)	compact tension specimen
C_p	temperature-dependent specific heat
DSC	differential scanning calorimetry
e_T	total elongation, measured in %
E	Young's modulus in tension, measured in Msi
E_c	Young's modulus in compression, measured in Msi
°F	temperature, degrees Fahrenheit
F_{cy}	0.2% offset compression yield strength, measured in ksi
F_{tu}	ultimate tensile strength, measured in ksi
F_{ty}	0.2% offset tension yield strength, measured in ksi
Hz	Hertz, cycles per second
ipm	inches per minute
ksi	1,000 pounds/in^2
K_{QJIC}	conditional fracture toughness, measured in ksi$\sqrt{\text{in}}$
L	direction parallel to plate rolling direction
LN_2	liquid nitrogen
LOX	liquid oxygen
L-S	denotes fracture plane normal to L with crack propagation in ST
L-T	denotes fracture plane normal to L with crack propagation in LT
LT	direction perpendicular to plate rolling direction
L45ST	direction 45° from the L direction in the ST plane
micron	10^{-6} meters
mli	mean lineal intercept, method of measuring approximate grain dimensions
Msi	1,000,000 pounds/in^2
μm	micrometers
ODF	orientation distribution function
psia	absolute pressure, pounds per square inch
RD	plate rolling direction
RT	room temperature, approximated as 75°F
SD	standard deviation
ST	direction perpendicular to L and LT
t	thickness, measured in inches
t_0	thickness position near plate surface
t/6, 5t/6	plane 1/6 from either surface of plate
t/2	through thickness midplane of plate
TEM	transmission electron microscopy
T-L	denotes fracture plane normal to LT with crack propagation in L
VHN	Vickers hardness number

Abstract

Aluminum alloy 2050 is being considered for the fabrication of cryogenic propellant tanks to reduce the mass of future heavy-lift launch vehicles. The alloy is available in section thicknesses greater than that of the incumbent aluminum alloy, 2195, which will enable designs with greater structural efficiency. While ambient temperature design allowable properties are available for alloy 2050, cryogenic properties are not available. To determine its suitability for use in cryogenic propellant tanks, tensile, compression and fracture tests were conducted on 4 inch thick 2050–T84 plate at ambient temperature and at -320°F. Various metallurgical analyses were also performed in order to provide an understanding of the compositional homogeneity and microstructure of 2050.

1. Introduction

Aluminum alloy 2050 is an aluminum-copper-lithium alloy produced by Alcan Global Aerospace. The alloy was designed to provide improvements in strength, toughness, elastic modulus and fatigue crack growth resistance, together with a reduction in density, as compared to conventional non-lithium bearing 2XXX and 7XXX series alloys (refs. 1, 2, 3, 4). The alloy also exhibits excellent stress corrosion cracking resistance and is weldable. It is available in plate thicknesses from 0.5 to 5.0 inches.

Launch vehicle cryogenic propellant tanks typically employ integrally stiffened skins, a structural design that requires extensive machining of thick plate for fabrication. Recent design studies (ref. 5) have indicated significant mass reduction for future heavy lift launch vehicle cryogenic propellant tanks through the use of taller, more widely spaced stiffening elements to optimize structural design. However, the maximum available plate thickness of the current cryogenic tank alloy, 2195, is 1.95 inches, thus limiting the tank stiffener height to less than 2 inches. This thickness limitation is due to the quench rate senstivity of the alloy (ref. 6) which gives rise to inhomogeneity and a drop in properties. In contrast, 2050 is reported to be significantly less quench sensitive, retaining uniform strength and toughness properties in thicknesses up to 5 inches. Room temperature mechanical properties and density (0.098 lbs/in^3) of 2050 are similar to those of 2195 (ref. 2, 4); however, no cryogenic temperature mechanical properties are presently available for 2050. Thus, a study was undertaken to measure mechanical properties of 2050 including tensile strength, compression strength and fracture toughness at ambient and cryogenic temperatures; characterize its microstructure via optical microscopy, orientation distribution function (ODF) x-ray texture analysis and differential scanning calorimetry (DSC); and determine the liquid oxygen compatibility of the alloy.

2. Material

Two plates of 2050 from two different lots of material were procured to AMS 4413 specifications (ref. 3). One 2 inch thick plate in the –T84 temper (44 inches by 30 inches by 2 inches, lot number 805751) was used for liquid oxygen compatibility testing. One 4 inch thick plate in the –T84 temper (120 inches by 64 inches by 4 inches, lot number 278111) was used for all mechanical property testing and metallography. The chemical compositions of the two plates, as provided on the mill certifications, are presented in Table 1, along with the AMS specification range for this alloy (ref. 3). The mill certifications for the plates are included in Appendix A. The compositions of both plates were within the AMS specification. Through-thickness chemical analysis was performed using direct current plasma spectroscopy at two lengthwise locations in the 4 inch thick plate. Results shown in Table 2 for positions near the plate surface (t_o), t/4, and t/2 indicated uniform composition throughout the plate.

Table 1. Composition of 2050 Plates Used in this Study Compared to AMS 4413 (ref. 3) Specification Range (weight percent)

Plate Thickness	Lot	Al	Cu	Li	Mg	Mn	Ag	Zr	Si	Fe	Zn
2 in.	805751	Bal.	3.56	0.88	--	0.38	0.35	0.10	0.03	0.05	--
4 in.	278111	Bal.	3.48	0.90	0.34	0.36	0.36	0.09	0.03	0.05	0.01
AMS 4413	Min.		3.20	0.70	0.20	0.20	0.20	0.06	--	--	--
AMS 4413	Max.		3.90	1.30	0.60	0.50	0.70	0.14	0.08	0.10	0.25

Table 2. Through-Thickness Variation in Composition of 4 inch 2050 Plate (weight percent)

		Cu	Li	Mg	Mn	Ag	Zr
Location #1	t_o	3.35	0.80	0.31	0.33	0.33	0.09
	t/4	3.41	0.83	0.32	0.33	0.32	0.11
	t/2	3.32	0.85	0.31	0.33	0.33	0.08
Location #2	t_o	3.41	0.82	0.31	0.34	0.33	0.12
	t/4	3.30	0.83	0.31	0.32	0.33	0.09
	t/2	3.38	0.81	0.31	0.33	0.34	0.09

2.1. Microstructure

Microstructure of the 2 inch and 4 inch 2050-T84 plates was evaluated in the three principal planes, i.e., normal to L, LT, and ST. In addition, these microstructures were examined at three through thickness locations, t/6, t/2 and 5t/6 to evaluate through-thickness variability. Specimens extracted from these locations were mounted, polished, and then anodized using Barker's reagent and examined under cross-polarized illumination. Micrographs for the 2 inch thick plate are presented in Figure **1**; those for the 4 inch thick plate are presented in Figure 2.

The grain morphology observed in both the 2 inch and 4 inch plates was elongated and lamellar, typical of rolled Al-Li plate. As expected, the grain aspect ratio was larger in the 2 inch plate than in the 4 inch plate at all through-thickness positions due to the greater reduction in thickness experienced by the 2 inch plate during rolling.

During cross-polarized imaging, the anodized specimens were rotated 45° in order to maximize contrast in the microstructures being observed. The resulting micrographs for the 4 inch plate in the L-S and T-S planes are presented in Figure 3. These images revealed a largely unrecrystallized microstructure with high aspect ratio grain morphology (approximately L:T=2.5:1 and L:S=10:1), with evidence of some sub-structure present. The microstructure was uniform both parallel (L-S) and perpendicular (T-S) to the rolling direction (L). Approximate grain dimensions, based on the mean lineal intercept (mli) method, were 500 µm in the L direction, 200 µm in the T direction, and 50 µm in the S direction.

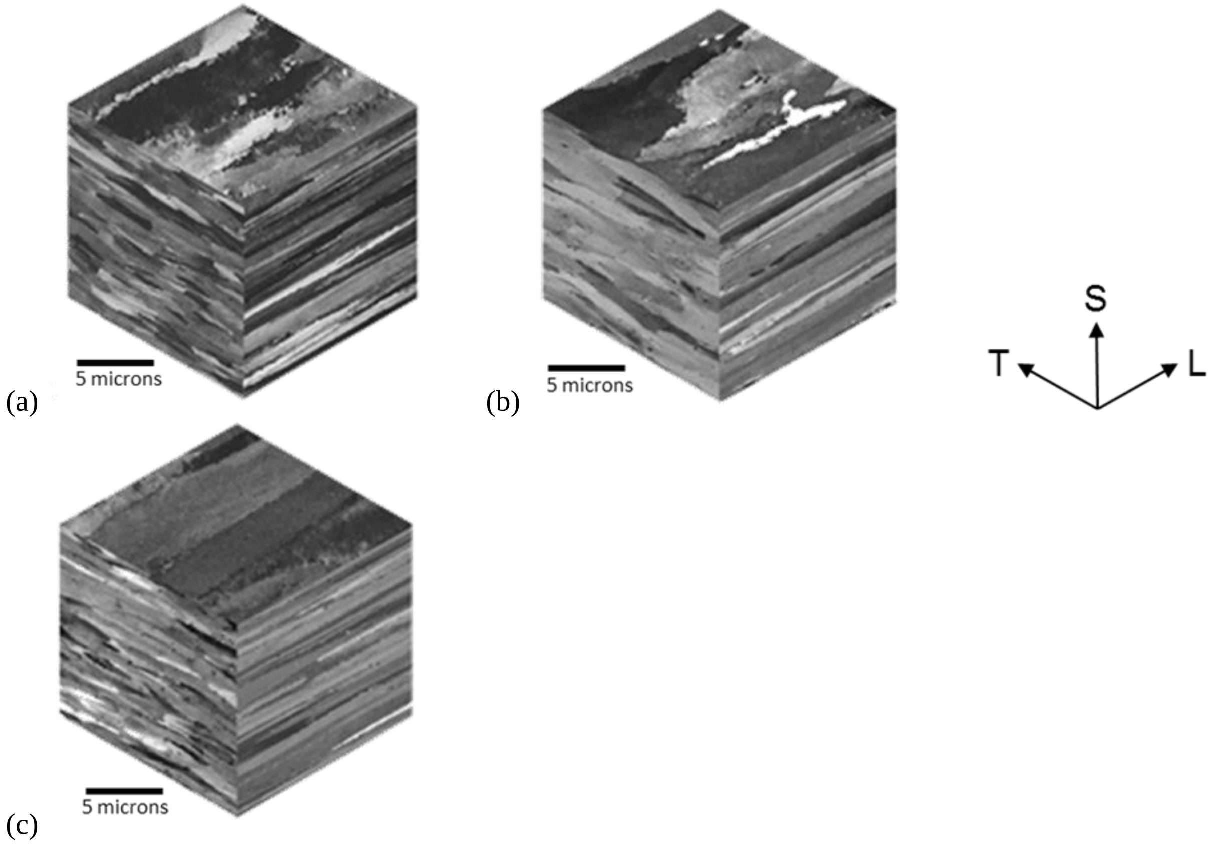

Figure 1. Microstructure of 2 inch thick 2050-T84 plate at three through thickness locations: (a) t/6, (b) t/2, (c) 5t/6.

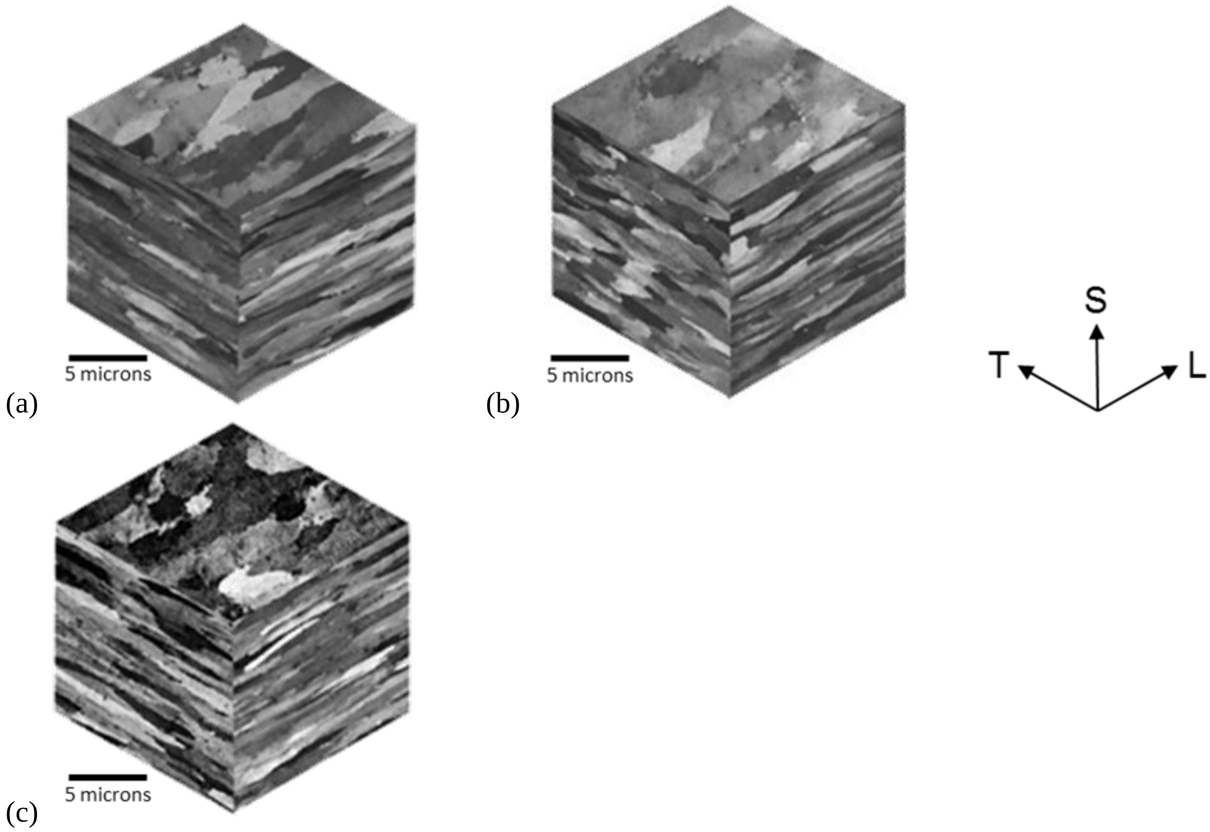

Figure 2. Microstructure of 4 inch thick 2050-T84 plate at three through thickness locations: (a) t/6, (b) t/2, (c) 5t/6.

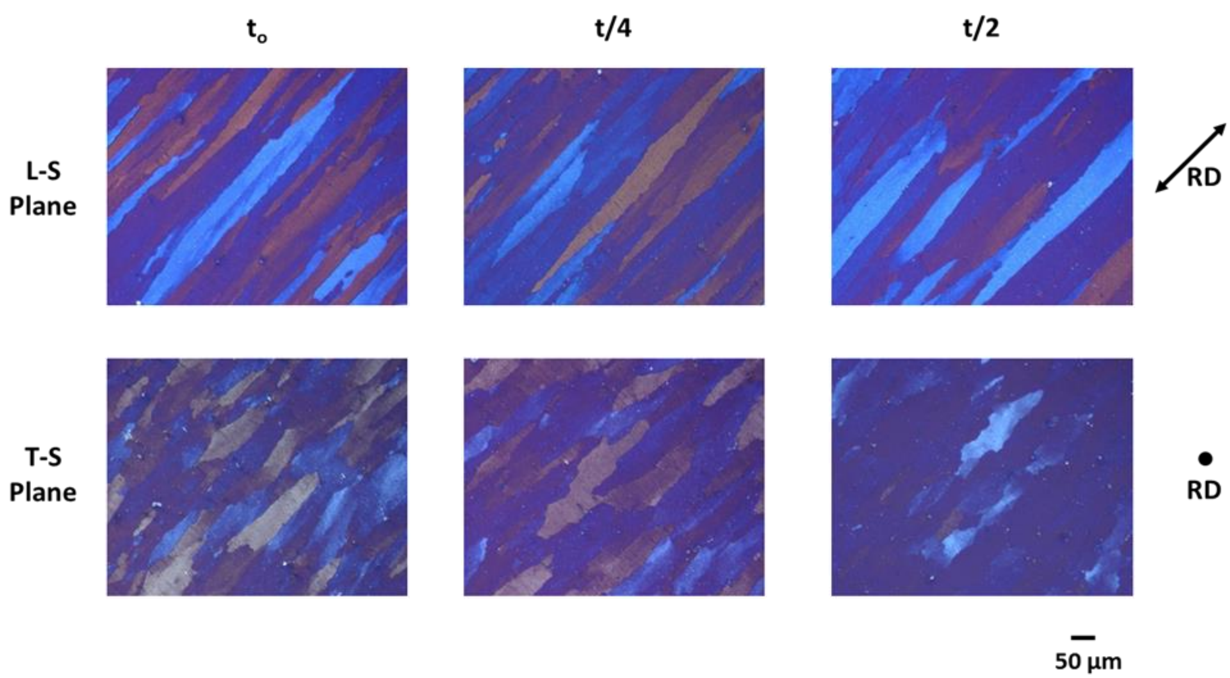

Figure 3. Microstructure of 4 inch thick 2050-T84 plate at three through thickness locations, near surface (t_o), t/4, and t/2, rotated 45 degrees using cross-polarized illumination.

2.2. Texture Analysis

X-ray texture analysis using Orientation Distribution Functions (ODF) of the 4 inch thick plate was performed to correlate crystallographic texture characteristics and the observed grain morphologies with the measured mechanical properties. ODF plots were derived from the texture components obtained from more basic x-ray pole figures corresponding to the [111], [200], and [311] x-ray reflections of the aluminum matrix (ref. 7). Samples for this analysis were measured at various locations through the thickness of the 4 inch plate. The results presented in Figure 4 show variations in the intensities of texture components through the plate thickness direction. The types of texture components and their spatial distribution are typical of those documented for aluminum alloys in plate forms subjected to cold deformation and/or recrystallization anneals (ref. 8, 9).

In Figure 4a, many of the deformation components were particularly strong through the midplane region, reflecting the overlapping strain fields during rolling deformation. Intensities of all deformation components were weak between t/4 and t/8. Intensities of some of the recrystallization components, shown in Figure 4b, were strongest at t/2, though of lower intensity than those of the deformation components. Other recrystallization texture components exhibited moderate intensity peaks between t/4 and t/8, that were weaker at t/2.

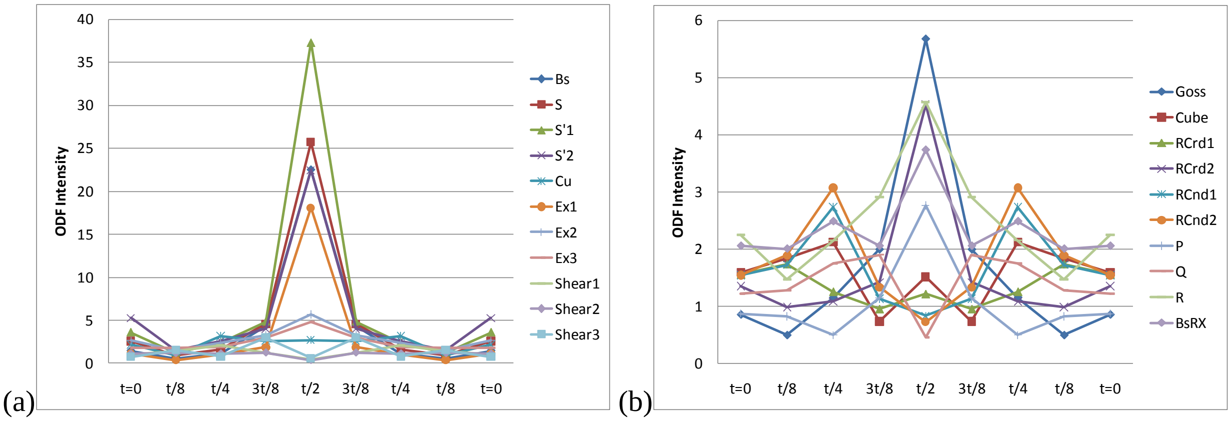

Figure 4. Through-thickness variation in the intensity of selected texture components in 4 inch thick 2050-T84 plate: (a) deformation and (b) recrystallization.

2.3. Hardness

Hardness may be used as an indication of strength in ductile metals, and determination of its distribution in a product form may be used to assess compositional or microstructural homogeneity of the alloy. Through-thickness hardness measurements were performed on cross-sections of both the 2 inch and 4 inch plates, employing a Vickers indenter with a 2000 gram load. Full surface-to-surface hardness scans were performed on the 2 inch plate, while only surface-to-mid-plane scans were performed on the 4 inch plate. Duplicate hardness profiles (scan #1 and scan #2) for each plate, shown in Figure 5, revealed uniform through-thickness hardness throughout both plates. The mean hardness values were essentially identical for both plates, as summarized in Table 3. The uniformity in the hardness data and similarity in values for both plates indicates a high degree of microstructural homogeneity throughout each of the 2 inch and 4 inch plates examined.

Table 3. Measured Mean and Standard Deviation VHN Hardness Values Across Duplicate Scans on 2050-T84 Plate

Plate Thickness	VHN, Scan #1	VHN, Scan #2
2 in.	140.9±3.5	140.5±4.1
4 in.	140.6±3.5	140.7±3.5

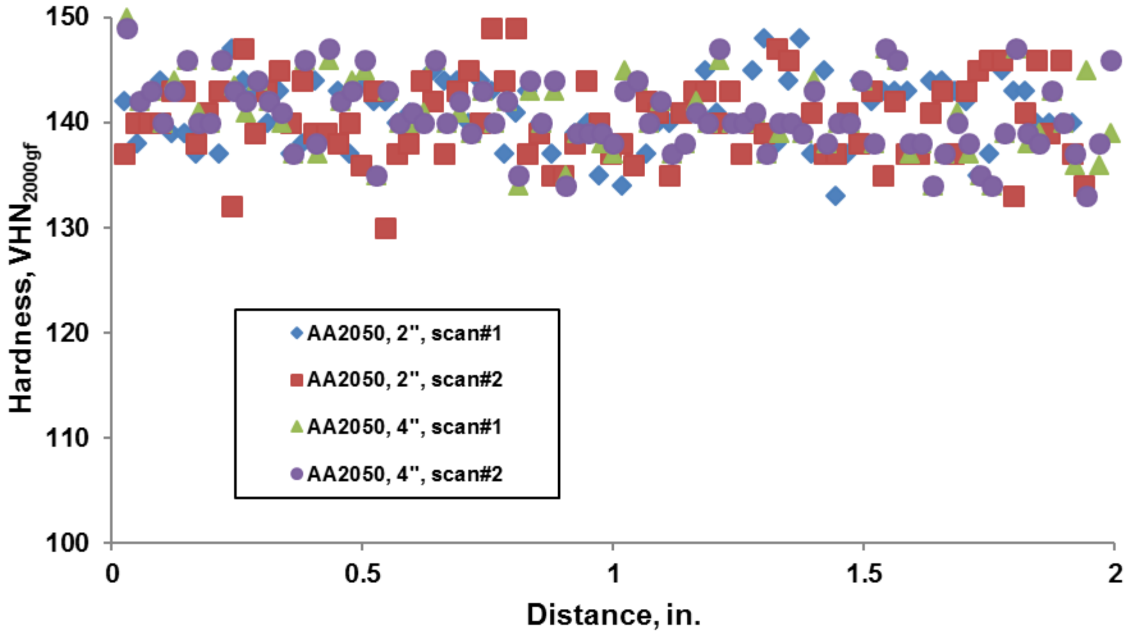

Figure 5. Through-thickness variation in hardness of the 2 inch and 4 inch thick 2050-T84 plates.

2.4. Thermal Analysis

Temperature-dependent specific heat (C_p) of an alloy is a function of composition, homogeneity, and precipitate microstructure. Differential scanning calorimetry (DSC) is a sensitive technique for C_p measurements in aerospace aluminum alloys. Together with transmission electron microscopy (TEM), DSC enables identification of alloy tempers, relative volume fractions of various stable and metastable phases in the microstructure, and evaluation of compositional or microstructural inhomogeneities. Employing a heating rate of 18°F/min (10°C/min) in flowing nitrogen gas, samples were scanned from room temperature (RT) to 1022°F (550°C). C_p measurements were made using the 3-Curve Ratio method described in ASTM E1269 (ref. 10), using a sapphire standard. Duplicate samples were tested for both the 2 inch and the 4 inch plates from selected through-thickness locations.

At least seven thermal events are noted in the C_p versus temperature curve; these are identified in Figure 6 based on compositional and temper similarity of 2050 to 2195. The C_p curves for the 2 inch plate at t/8 and t/2 and for the 4 inch plate at t/8, t/4, and t/2 are shown in Figure 7. The temperature peaks from duplicate DSC runs are presented in Table 4, where the thermal events are referenced to Figure 6. These C_p curves are similar within $\pm$5% (the instrument's limit of repeatability), including the occurrence of peaks and their associated temperatures as shown in Table 4. These results imply that alloy chemistries and precipitate microstructures are uniform throughout the thickness of each plate and that the 2 inch plate and 4 inch plates are chemically and microstructurally similar.

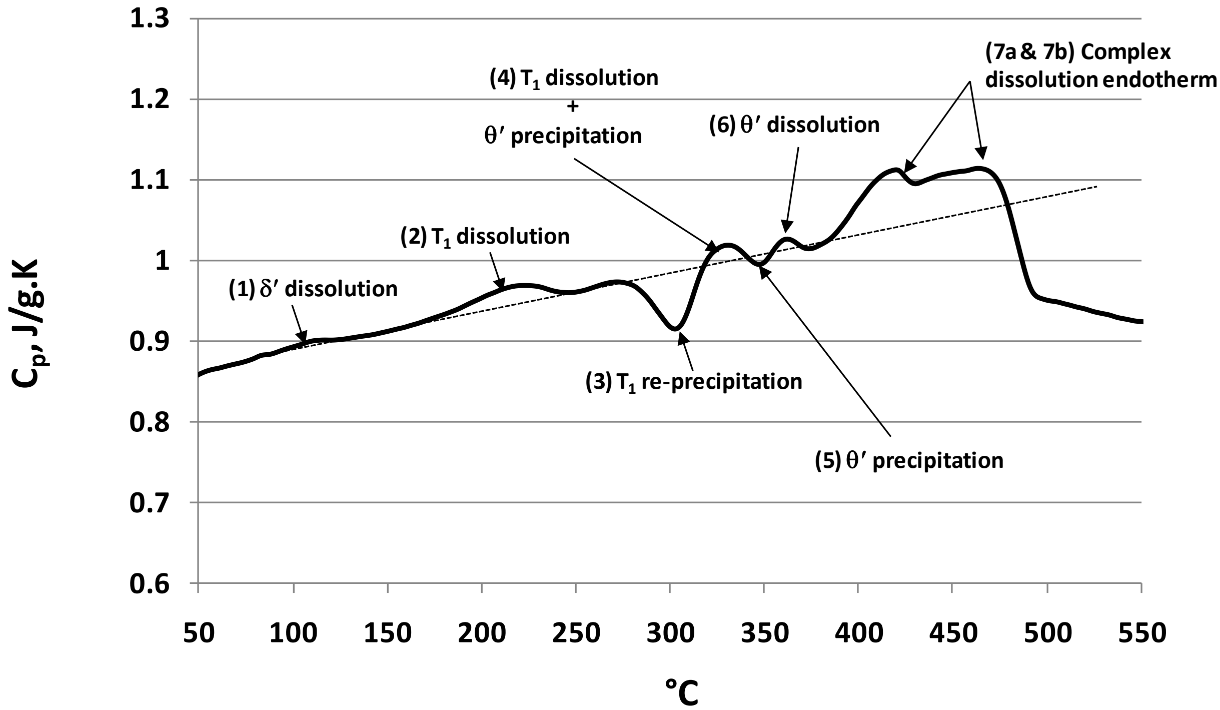

Figure 6. Tentative phase identification of thermal events in the C_p curve for 2050-T84 plate.

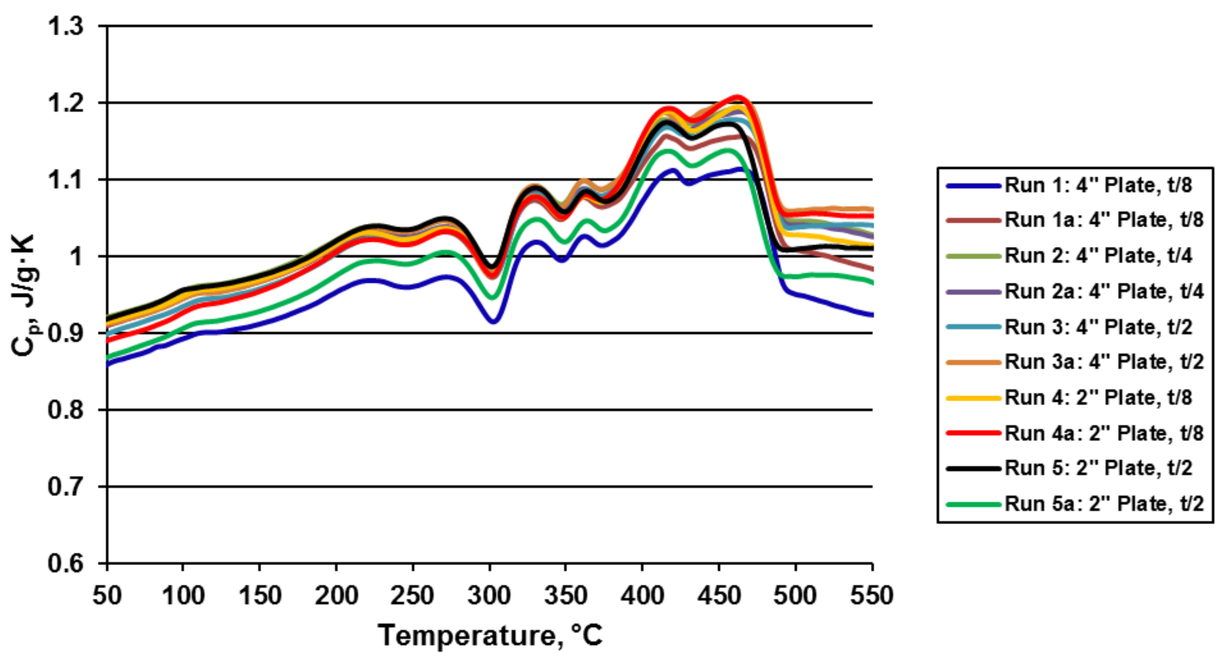

Figure 7. Specific heat curves for the 2 inch and 4 inch thick 2050-T84 plates.

Table 4. Peak Temperatures in the C_p Curves at Various Locations in the 2 inch and 4 inch thick Plates of 2050-T84

Thermal Event	2 in., t/8	2 in., t/2	4 in., t/8	4 in., t/4	4 in., t/2	2 in. Avg. ± SD	4 in. Avg. ± SD
1	103.4 102.5	96.4 102.8	105.8 103.5	100.7 100.2	104.8 102.3	103.1±0.4	104.1±2.5
2	212.4 213.5	219.4 213.8	213.8 213.5	215.7 214.2	220.8 219.3	213.1±1.0	216.5±3.9
3	295.4 297.5	298.4 297.8	297.8 297.5	296.7 295.2	297.8 295.3	296.6±1.7	296.6±1.7
4	323.4 323.5	325.4 325.8	324.8 324.5	323.7 323.2	324.8 323.3	324.6±1.7	324.8±1.1
5	341.4 342.5	345.4 344.8	341.8 341.5	340.7 340.2	342.8 341.3	343.1±2.4	341.6±0.4
6	357.4 358.5	359.4 359.8	357.8 357.5	356.7 356.2	358.8 356.3	358.6±1.7	357.6±1.1
7a	410.4 411.5	411.4 410.8	414.8 412.5	407.7 410.2	410.8 408.3	410.6±0.3	411.6±4.6
7b	456.4 456.5	452.4 451.8	458.8 460.5	459.7 459.2	455.8 457.3	454.1±3.3	458.1±1.1

3. Liquid Oxygen Compatibility Testing

In order to use a material in the presence of high concentrations of oxygen, it must be evaluated per NASA-STD-(I)-6001B - Flammability, Offgassing, And Compatibility Requirements And Test Procedures (ref. 11) and NASA-STD-6016 - Standard Materials And Processes Requirements For Spacecraft (ref. 12). Oxygen compatibility testing was conducted by the Materials Test Branch (EM10) at NASA's George C. Marshall Space Flight Center. The tests conducted per NASA-STD-6001 included Test 17 (Promoted Ignition-Combustion (Upward Flammability of Metals)) and Tests 13A and 13B (Ambient Pressure and High Pressure Liquid Oxygen Mechanical Impact).

Specimens were extracted from the 2 inch 2050-T84 plate. Specimens for Test 17 consisted of rectangular bars 0.126 inch by 0.126 inch by 4 inches. This alternate specimen geometry was used due to difficulty in machining the primary 0.126 inch diameter specimen with a length of 6-12 inches. Specimens were cleaned per ASTM G86 (ref. 13) to remove any contaminants that could affect the test results. A 0.38 gram titanium promoter was attached to the end of the specimen which was then installed in the test chamber. The test chamber was sealed, purged several times with pure oxygen, then pressurized to the desired test conditions. An aluminum-palladium igniter wire was used to ignite the promoter. After the test, the unburned length of specimen was recorded.

Specimens for Tests 13A and 13B were discs 0.69 inch diameter by 0.127 inch thick. Prior to testing, the specimens were cleaned per ASTM G86 (ref. 13) to remove any contaminants that could affect the test results. The specimen was inserted into the test cup, installed in the test apparatus and immersed in liquid oxygen at the desired pressure. The specimens were then impacted with an energy of 72 ft·lbf and observed for signs of ignition such as flash, char marks, etc.

All specimens burned during Test 17; however, at most pressures tested, the specimens self-extinguished before they were completely consumed. Average burn lengths for each tested pressure are presented in Table 5. For the mechanical impact Tests 13A and 13B, no reactions were observed at the three conditions tested; results are summarized in Table 6. These initial results indicate that 2050 compares favorably with current cryogenic tank alloys 2195 and 2219 (ref. 14).

Table 5. 2050 Promoted Combustion Test Results (Test 17)

Pressure (psia)	Burn Length (in.)
50	0.84
60	0.86
75	0.75
100	1.33
125	0.81
150	1.90
160	2.39
170	3.38
180	4.12 (total burn)
190	1.81
200	1.75
210	1.79
226	4.12 (total burn)
250	4.12 (total burn)
300	4.12 (total burn)

Table 6. 2050 Mechanical Impact Test Results (Tests 13A and 13B)

LOX Pressure (psia)	Reactions/Tests
14.7	0/20
300	0/20
400	0/20

4. Tensile Testing

Tensile tests were conducted per ASTM E8-09 (ref. 15), using sub-size round specimens with a test section diameter of 0.250 inches as illustrated in Figure 8. Specimens were extracted from t/6 and t/2 locations from the 4 inch 2050 plate in the following orientations: L, LT, 45, ST (t/2 only) and L45ST (t/2 only), as shown in Figure 9. Testing was conducted using a servohydraulic test stand at a constant crosshead speed of 0.010 ipm. Strain was measured using two back-to-back extensometers with a 1.000 inch gage length. Tests were conducted at ambient temperature (approx. 75°F) in laboratory air and at cryogenic temperature (approx. -320°F) immersed in liquid nitrogen. Test data were recorded at 10 Hz.

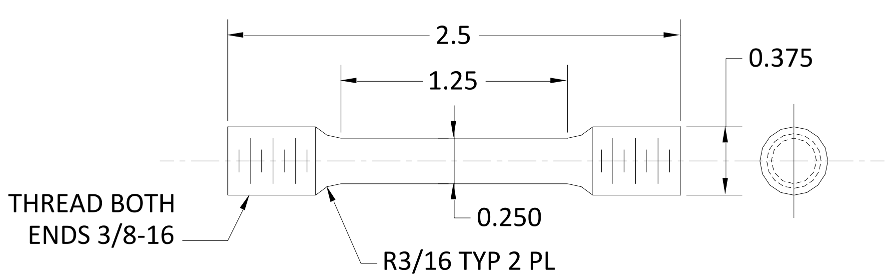

Figure 8. Tensile specimen (all dimensions in inches). (ref. 15)

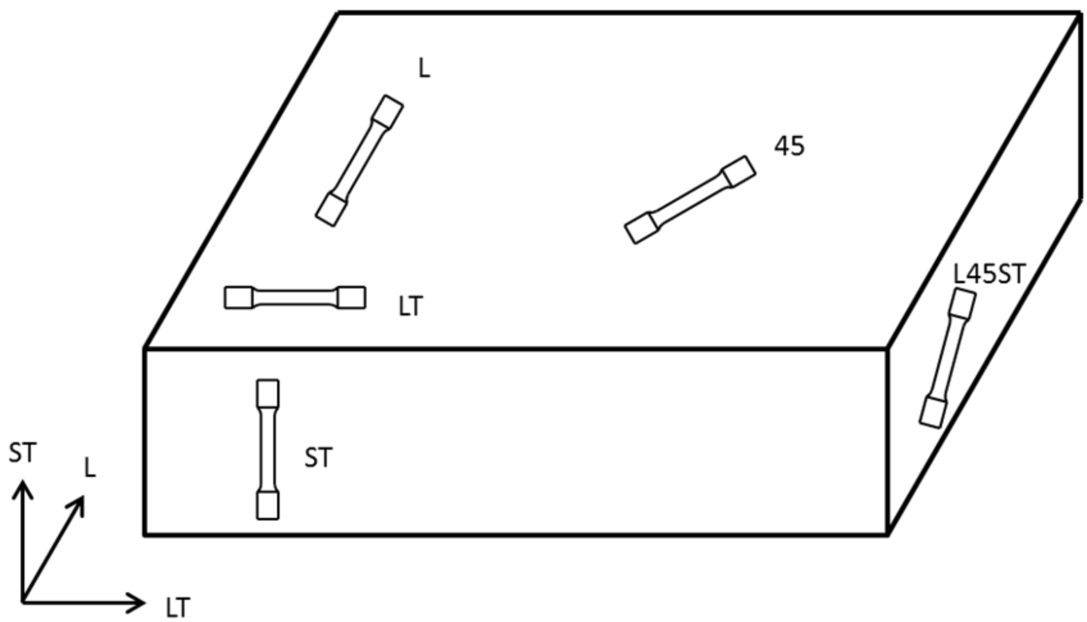

Figure 9. Diagram of tensile and compression specimen orientations extracted from 4 inch thick 2050-T84 plate.

The published A-Basis tensile properties (ref. 2), which are also the material specification (ref. 3) minimum, are presented in Table 7. The average of the three replicate tests is presented in Table 8 for ambient temperature tests and in Table 9 for cryogenic temperature tests. The individual test results are tabulated in Appendix B and the stress-strain curves are included in Appendix C.

The ambient temperature tensile properties of the four principal orientations (L, LT, ST and 45°) exceeded the published A-Basis mechanical properties for 2050 (ref. 2). Through-thickness location dependent variations were noted in the L and LT orientations. In the L orientation, parallel to the rolling direction, the specimens machined from the t/2 location had 6-7% higher strengths and 35% lower elongation values as compared to the t/6 location. For the LT orientation, tensile strength is 1-3% lower and elongation is 25% lower at t/2 than at t/6. However, the 45° orientation showed no variation in strength with through-thickness location, although elongation was higher at t/6 than at t/2. The L45ST strength and elongation values are the lowest of the orientations tested.

Examining individual data shown in Appendix B reveals that the standard deviations on these data are less than 1%. This anisotropy in the tensile properties is expected, based upon the elongated microstructure in the L orientation and the higher intensity deformation texture components in the near-midplane region of the 4 inch 2050 plate. The anisotropy is attributed to the strain gradients introduced into the plate during rolling, resulting in increased strain that occurs nearer to the t/2 location. The lower but more isotropic yield strengths at the t/6 location is consistent with the weaker deformation texture components calculated in the ODF analysis.

As 2050 was originally intended for use at ambient temperatures, no cryogenic mechanical property data are available for comparison with those obtained in the present study. Specimens in all orientations exhibited an increase in strength and modulus as temperature was decreased from ambient temperature to -320°F. Over the same temperature range, elongation increased for all orientations except LT, for which it decreased slightly. Through-thickness variations in properties similar to those observed at ambient temperature were also observed at cryogenic temperature.

For comparison, Table 10 shows the typical tensile properties for 1.85 inch thick 2195-T8 plate (ref. 16), which is the thickest plate available for 2195 used in current cryotank applications. The strength and elongation values for the 4 inch 2050-T84 plate were less than 3% lower than that of 2195-T8, both at ambient (75°F) and at cryogenic (-320°F) temperatures. Elongation reductions observed for the LT orientation in 2050 at -320°F were similar to those for 2195.

Table 7. A-Basis Tensile Properties of 4 inch thick 2050-T84 Plate (ref. 2, 3)

Orient.	F_{ty} (ksi)	F_{tu} (ksi)	E (Msi)	e_T (%)
L	66	71	10.9	6
LT	64	71	10.9	3
ST	59	69	10.5	1.5
45	65	73	--	-

Table 8. Average Ambient Temperature Tensile Results for 4 inch thick 2050-T84 Plate

Orient.	Plate Location	F_{ty} (ksi)	F_{tu} (ksi)	E (Msi)	e_T (%)
L	t/2	74.6	79.2	11.0	8.8
	t/6	70.6	73.9	10.9	13.8
LT	t/2	67.9	74.8	11.0	8.5
	t/6	69.6	75.7	10.9	11.3
ST	t/2	64.2	73.3	10.7	4.8
45	t/2	65.6	72.4	10.8	9.9
	t/6	65.4	72.8	10.8	12.0
L45ST	t/2	63.1	68.1	10.9	2.5

Table 9. Average Cryogenic Temperature Tensile Results for 4 inch thick 2050-T84 Plate

Orient.	Plate Location	F_{ty} (ksi)	F_{tu} (ksi)	E (Msi)	e_T (%)
L	t/2	85.9	95.7	12.2	10.7
	t/6	81.5	88.8	11.9	16.9
LT	t/2	78.9	91.4	12.3	7.8
	t/6	79.9	91.6	12.1	12.3
ST	t/2	73.1	87.3	11.9	5.3
45	t/2	74.2	86.4	11.8	11.2
	t/6	74.5	86.8	11.6	14.6
L45ST	t/2	73.6	82.3	12.0	3.6

Table 10. Typical Tensile Properties of 1.85 inch thick 2195-T8 Plate (ref. 16)

Orient.	75°F			-320°F		
	F_{ty} (ksi)	F_{tu} (ksi)	e_T (%)	F_{ty} (ksi)	F_{tu} (ksi)	e_T (%)
L	76	80	9.0	93	101	10.9
LT	76	83	8.1	92	104	7.6
ST	74	86	4.5	81	95	6.4
45	73	81	9.6	87	99	10.2

5. Compression Testing

Compression tests were conducted per ASTM E9-09 (ref. 17) using cylindrical specimens with a diameter of 0.500 inches and a length of 1.5 inches, resulting in a length-to-diameter (L/D) ratio of 3. Specimens were extracted from the 4 inch 2050-T84 temper plate at t/6 and t/2 locations in L, LT and 45° orientations, similar to the tensile specimens shown in Figure 9. Testing was conducted using a servohydraulic test stand at a constant crosshead speed of 0.010 ipm. Strain was measured using two back-to-back extensometers with a 1.000 inch gage length. Specimens were loaded to a plastic strain of approximately 2%, then unloaded. Tests were conducted at ambient temperature (75°F) in laboratory air and at cryogenic temperature (-320°F) immersed in liquid nitrogen. Test data were recorded at 10 Hz.

The A-Basis compressive properties (ref. 2) are shown in Table 11. The average of the three specimens tested is presented in Table 12 for both ambient and cryogenic tests. The individual test results are tabulated in Appendix B and the stress strain curves are included in Appendix D.

The ambient temperature compressive properties exceed the A-Basis properties for 2050 in the L and LT orientations. Through-thickness location dependent variations were noted in the L and LT orientations, with higher strengths and moduli at t/2 than at t/6 for all orientations. The 45° orientation showed no variation in strength or modulus with through-thickness location.

As 2050 was originally intended for use at ambient temperatures, no cryogenic mechanical property data were available for a comparison with the presently reported data. In the present study, all of the specimen orientations exhibited an increase in strength and modulus as temperature was decreased from ambient temperature to -320°F. Variations in through-thickness compressive properties similar to those observed at ambient, were also observed at cryogenic temperatures.

For comparison, the typical compressive properties for 1.85 inch thick 2195-T8 (ref. 16) plate are shown in Table 13. The strength values for the 4 inch 2050-T84 plate are 17% lower than those of 2195-T8 at ambient temperature and 10% lower at cryogenic (-320°F) temperature.

Table 11. A-Basis Compressive Properties of 4 inch thick 2050-T84 Plate (ref. 2)

Orient.	F_{cy} (ksi)	E_c (Msi)
L	66	11.3
LT	64	11.3
ST	59	11.3

Table 12. Average Compression Test Results for 4 inch thick 2050-T84 Plate

Orient.	Plate Location	75°F		-320°F	
		F_{cy} (ksi)	E_c (Msi)	F_{cy} (ksi)	E_c (Msi)
L	t/2	74.9	11.2	86.4	12.3
	t/6	69.6	11.1	76.5	12.5
LT	t/2	77.3	11.3	89.6	12.4
	t/6	71.3	11.2	82.0	12.4
45	t/2	70.5	11.0	81.3	12.2
	t/6	69.6	11.0	81.9	12.3

Table 13. Typical Compression Properties of 1.85 inch thick 2195-T8 Plate (ref. 16)

Orient.	Plate Location	75°F		-320°F	
		F_{cy} (ksi)	E_c (Msi)	F_{cy} (ksi)	E_c (Msi)
L	t/2	84.4	11.1	96.0	12.4
	t/6	83.3	--	92.8	--
LT	t/2	85.5	--	--	--
	t/6	81.2	--	95.0	--
45	t/2	--	--	--	--
	t/6	82.0	11.0	92.0	12.3

6. Fracture Toughness

Fracture toughness tests were carried out per ASTM E1820-09 (ref. 18) using compact tension, C(T), specimens with a width of 2.00 inches and thickness of 0.25 inch, illustrated in Figure 10. Specimens were extracted from the 4 inch 2050 plate at the t/6 and 5t/6 locations in the following orientations: L-T (5t/6), T-L (t/6 and 5t/6) and L-S (t/6), as shown in Figure 11. Precracking was carried out at ambient temperature (75°F) in laboratory air for all specimens. Crack length during precracking was measured using compliance techniques. Fracture toughness tests were conducted at ambient temperature in laboratory air and cryogenic temperature (-320°F) immersed in liquid nitrogen. Crack length during fracture testing was measured using the potential drop method. Physical precrack and fracture lengths were measured in nine locations per ASTM E1820 and used in the determination of toughness.

Results are presented in Table 14 for the average of three tests at the indicated temperatures and orientations. The individual test results are tabulated in Appendix B. Fracture toughness data, J-curves, and images showing fracture path for individual tests are included in Appendix E. All tests failed the validity requirements of ASTM E1820 due to deviations in crack front curvature. However, a comparison can still be made of the trends between the various orientations at ambient and cryogenic temperatures using conditional (K_{QJIC}) fracture toughness values. At ambient temperature, fracture toughness was highest in the L-T orientation and lowest in the T-L orientation. At cryogenic temperature, fracture toughness was highest in the L-S orientation and lowest in the T-L orientation. An increase in fracture toughness from ambient to cryogenic temperature was observed for the T-L and L-S orientations, but not for the L-T orientation. There are limited published plane strain fracture data available for 2195, however the available data (ref. 4) show minimal increase or a decrease in fracture toughness, depending on orientation, for tests conducted at 75°F to -320°F, followed by a significant increase for tests conducted at -423°F.

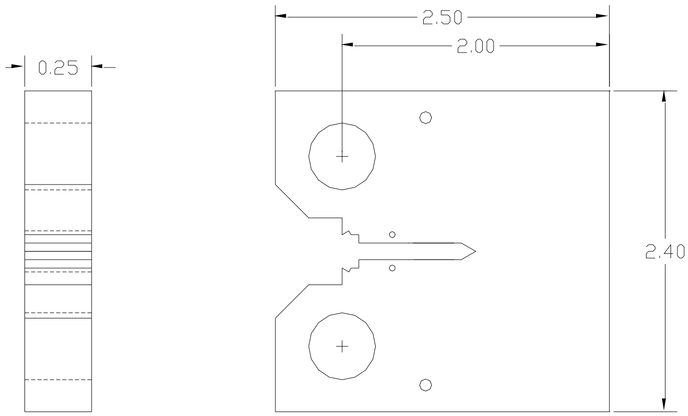

Figure 10. Compact tension specimen (all dimensions in inches).

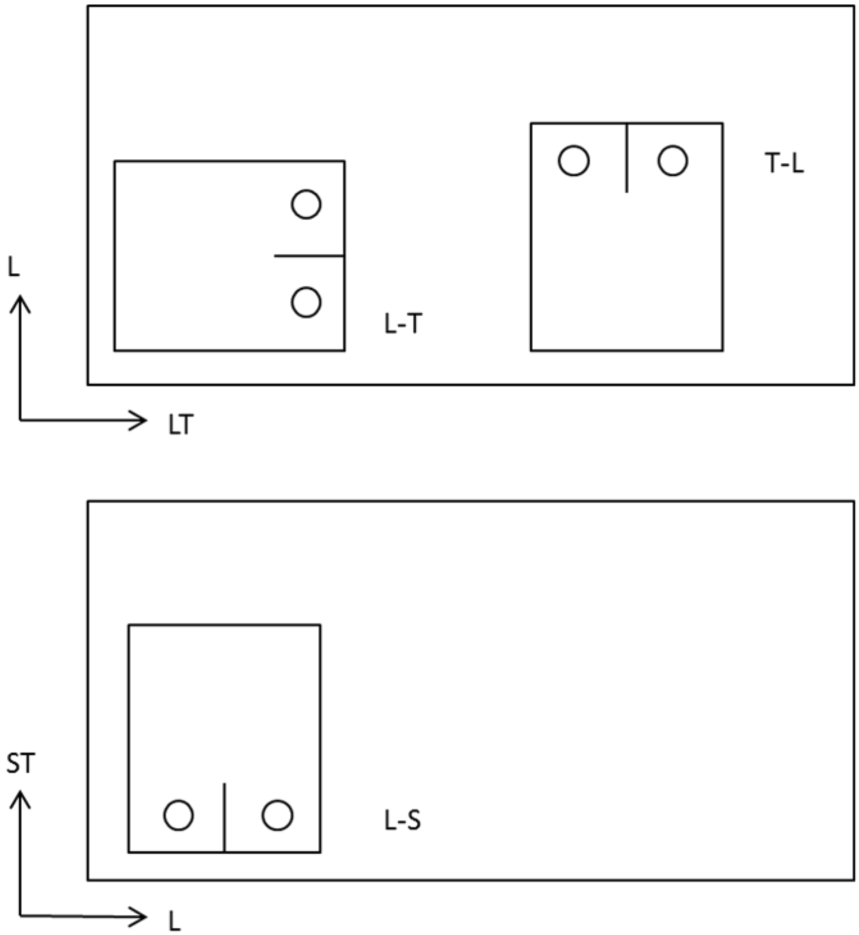

Figure 11. Compact tension specimen orientation with respect to plate.

Table 14. Fracture Toughness of 4 inch thick 2050-T84 Plate at Ambient and Cryogenic Temperatures

Orient.	75°F	-320°F
	K_{QJIC} (ksi√in)	K_{QJIC} (ksi√in)
L-T	38.4	32.4
T-L	24.8	28.2
L-S	37.7	44.4

7. Conclusions

Both the 2 inch and 4 inch plates exhibited elongated, lamellar microstructures typical of Al-Li rolled products. The through-thickness microstructures of both plates were uniform in regard to grain morphology, composition, hardness, and type and volume fraction of strengthening precipitates. Through-thickness variations in texture components observed in the 4 inch plate were rationalized as being due to strain gradients associated with rolling, which produces increased strain at t/2. The texture components correlated well with trends in yield strength. Stronger intensities of the deformation texture components explained the higher yield strength and greater anisotropy at the t/2 plate location in the 4 inch thick 2050-T84 tested. Conversely, at the t/6 plate location, weaker intensities of deformation texture components were associated with lower yield strength but more isotropic properties observed.

This preliminary examination of one lot of 2050 showed no apparent limitations to its potential use as a cryogenic tank alloy. Notwithstanding its yield and tensile strengths being lower than those of the current cryogenic tank alloy 2195, alloy 2050 exhibited similar trends in variations of strength properties versus temperature. The fracture toughness of 2050 showed a general increase as test temperature was decreased from ambient temperature to -320°F. This observation was also corroborated by the temperature-dependent increase observed in its strength and elongation during the tensile tests. In other words, for most sample orientations, both strength and elongation increased with a decrease in temperature from 75°F to -320°F.

In the future, characterization of mechanical properties should be carried out at -423°F to verify the suitability of 2050 for use in liquid hydrogen tank structures. Additional fracture testing of 2050 should include surface flaw fracture specimens to better compare with existing data for 2195.

8. References

1. Lequeu, Ph; Smith, K. P.; and Danielou, A.: Aluminum-Copper-Lithium Alloy 2050 Developed for Medium to Thick Plate. *J. Mat. Eng. and Perf.*, Vol. 19(6), August 2010, pp. 841-847.
2. Federal Aviation Administration: *Metallic Materials Properties Development and Standardization (MMPDS) MMPDS-05*, Battelle Memorial Institute, Columbus, OH, April 2010.

3. SAE Aerospace Material Specification 4413: Aluminum Alloy, Plate 3.5 Cu - 1.0Li - .40Mg - .35 Mn - .45Ag - 0.12Zr (2050-T84) Solution Heat Treated, Stress Relieved, and Artificially Aged, SAE Aerospace, Oct. 2007.
4. Aerospace Structural Metals Handbook, edition 39, CINDAS Handbooks Operation West Lafayette, IN, March 2002.
5. Lovejoy, A.E.; Chunchu, P.B.; Hilburger, M. W.. Ares-V Design Study: The Effects of Buckling Knockdown Factors, Internal Pressure, and Materials. NASA/TM-=2011-217061. February 2011.
6. Metals Handbook, Ninth Edition, Volume 4, Heat Treating, American Society for Metals, November 1981, pp 688-695.
7. J. Bunge: Z. Metallkunde. 56 (1965) No. 12, p. 872/874
8. W.G. Fricke and M.A. Przystupa, “Texture”, in Aluminum Alloys - Contemporary Research and Applications, A.K. Vasudevan and R.D. Doherty (eds.), Treatise on Materials Science and Technology, Academic Press, San Diego, CA, vol.31, 1989, pp. 563-578.
9. F.J. Humphreys and M. Hatherly, "Control of recrystallization", in Recrystallization and Related Annealing Phenomena, Second Edition, Elsevier Ltd., New York, NY, Ch.15, 2004, pp.469-505.
10. Standard Test Method for Determining Specific Heat Capacity by Differential Scanning Calorimetry. ASTM Designation: E1269-05, Volume 14.02 of the *2010 Annual Book of ASTM Standards*, 2010.
11. NASA-STD-(I)-6001B - Flammability, Offgassing, And Compatibility Requirements And Test Procedures, April 2008.
12. NASA-STD-6016 - Standard Materials And Processes Requirements For Spacecraft, July 2008.
13. Standard Test Method for Determining Ignition Sensitivity of Materials to Mechanical Impact in Ambient Liquid Oxygen and Pressurized Liquid and Gaseous Oxygen Environments. ASTM Designation: G86-98, Volume 14.04 of the *2010 Annual Book of ASTM Standards*, 2010.
14. MAPTIS, https://maptis.ndc.nasa.gov/cgi-42/ctcore.exe, Accessed March 30, 2011.
15. Standard Test Methods for Tension Testing of Metallic Materials. ASTM Designation E8-09, Volume 03.01 of the *2010 Annual Book of ASTM Standards*, 2010.
16. Reinmuller, R. E., Al-Li Materials Database Service Order 89818, Lockheed Martin Manned Space Systems, New Orleans, LA, Dec. 1996.
17. Standard Test Methods of Compression Testing of Metallic Materials at Room Temperature. ASTM Designation: E9-09 Volume 03.01 of the *2010 Annual Book of ASTM Standards*, 2010.
18. Standard Test Method for Measurement of Fracture Toughness. ASTM Designation: E1820-09 Volume 03.01 of the *2010 Annual Book of ASTM Standards*, 2010.

Appendix A: Mill Certifications of 2050 Plate Used in this Study

ALCAN ROLLED PRODUCTS

CERTIFIED TEST REPORT
Ravenswood, WV 26164 USA

SHIP TO:
Marcia Domack
NSSC Shared Serveice Center
FMS-Accounts Payable
BLD-1111, C Road
Stennis, MS 39529

SOLD TO:
NSSC Shared Serveice Center
FMS-Accounts Payable
BLD-1111, C Road
Stennis, MS 39529

CUSTOMER PURCHASE ORDER NO. & ITEM			ALCAN ORDER NO.	
NNL08AF41P			100-4861-65	
ALLOY	CLAD	TEMPER	GAUGE	WIDTH	LENGTH
2050		T84	2.0"	40.0"	33.0"

ITEM ORDERED	2050-T84
CUSTOMER SPECIFICATION	AMS 4413
PART NUMBER	
B/L NUMBER	
DATE SHIPPED	10/28/2008
WEIGHT SHIPPED	259 lbs
NO. OF PIECES	1
GOVT. CONTRACT NO.	

CERTIFICATION

"ALCAN Rolled Products, hereby certifies that metal shipped under this order has been inspected and found in conformance with the requirements of the applicable specifications as indicated herein. Any warranty is limited to that shown on ALCAN Rolled Products' standard General Terms and Conditions of Sales. Test reports are on file, subject to examination."

ALCAN ROLLED PRODUCTS
P.O. BOX 68
RAVENSWOOD, WV 26164 USA

LaDonna B. Smith - Quality Manager

LOT NUMBER	TEST DIRECTION	NO. OF TESTS	ULTIMATE STRENGTH K.S.I. MIN	ULTIMATE STRENGTH K.S.I. MAX	YIELD STRENGTH K.S.I. MIN	YIELD STRENGTH K.S.I. MAX	ELONGATION % MIN	ELONGATION % MAX	MIN	MAX
805751	L	2	75.3	75.3	71.4	70.8	14.0	13.5		
	LT	2	75.9	75.5	69.7	69.1	11.5	11.5		
	ST	2	78.1	77.7	69.0	68.1	6.5	6.0		

Fatigue **WMTR 8-29079**
Minimum Fatigue 300.0 KCycles
Maximum Fatigue 300.0 KCycles

Fracture Toughness
T-L (KIC) 30.4 KSI (SQRT. IN.)
L-T (KIC) 42.6 KSI (SQRT. IN.)
S-L (KIC) 28.8 KSI (SQRT. IN.)

Stress Corrosion **WMTR 8-28645**
Pass - WMTR

ALL LOTS ON THIS CERTIFICATION ALSO CONFORM TO THE FOLLOWING REQUIREMENTS
AMS-STD-2154A 100% SOINC MINUS DEAD ZONE CLASS A

CHEM COMP

ALLOY	SILICON MIN	SILICON MAX	IRON MIN	IRON MAX	COPPER MIN	COPPER MAX	MANGANESE MIN	MANGANESE MAX	MAGNESIUM MIN	MAGNESIUM MAX	CHROMIUM MIN	CHROMIUM MAX	ZINC MIN	ZINC MAX	TITANIUM MIN	TITANIUM MAX	OTHERS MIN	OTHERS MAX
	See Actual Composition																	

ALUMINIUM REMAINDER

P-860-155D (1/06)

ALCAN
ROLLED PRODUCTS

CERTIFIED TEST REPORT
Ravenswood, WV 26164 USA

SHIP TO
Marcia Domack
NSSC Shared Serveice Center
FMS-Accounts Payable
BLD-1111, C Road
Stennis, MS 39529

SOLD TO
NSSC Shared Serveice Center
FMS-Accounts Payable
BLD-1111, C Road
Stennis, MS 39529

CUSTOMER PURCHASE ORDER NO. & ITEM				ALCAN ORDER NO.	
NNL08AF41P				100-4861-65	
ALLOY	CLAD	TEMPER	GAUGE	WIDTH	LENGTH
2050		T84	2.0"	40.0"	33.0"
ITEM ORDERED					
2050-T84					
CUSTOMER SPECIFICATION					
AMS 4413					
PART NUMBER		B/L NUMBER		DATE SHIPPED	
N/A Sample Material		N/A		10/28/2008	
WEIGHT SHIPPED	NO. OF PIECES	GOVT. CONTRACT NO.			
259 lbs	1	N/A			

CERTIFICATION

"ALCAN Rolled Products, hereby certifies that metal shipped under this order has been inspected and found in conformance with the requirements of the applicable specifications as indicated herein. Any warranty is limited to that shown on ALCAN Rolled Products' standard General Terms and Conditions of Sales. Test reports are on file, subject to examination."

ALCAN ROLLED PRODUCTS
P.O. BOX 68
RAVENSWOOD, WV 26164 USA

LaDonna B. Smith - Quality Manager

LOT NUMBER	TEST DIRECTION	NO. OF TESTS	ULTIMATE STRENGTH K.S.I.		YIELD STRENGTH K.S.I.		ELONGATION %			
			MIN	MAX	MIN	MAX	MIN	MAX	MIN	MAX
805751	Si = 0.03	Fe = 0.05	Cu = 3.56	Mn = 0.38	Cr = 0.01	Zn = 0.03	Ti = 0.02	Zr = 0.10	Ag = 0.35	Li = 0.88

Others-Each = 0.05 Max Others Total = 0.15 Max Al Remainder

This test report shall note be reproduced except in full, without the written approval of the laboratory or authorized quality delegate. The recording of false, fictitious, or fraudulent statemnts or entries on this certificate may be punished as a felony under federal law.

Chemistry by OES spark.

When fracture toughness test requires, tested per ASTM E399.

When tensile test required, tester per ASTM E8; B557

"End of Certification"

CHEM COMP	SILICON		IRON		COPPER		MANGANESE		MAGNESIUM		CHROMIUM		ZINC		TITANIUM		OTHERS	
ALLOY	MIN	MAX	MIN	MAX	MIN	MAX	MIN	MAX	MIN	MAX	MIN	MAX	MIN	MAX	MIN	MAX	MIN	MAX
	See Actual Composition																	
	ALUMINIUM REMAINDER																	

P-660-155D (1/05)

ALCAN
ROLLED PRODUCTS

CERTIFIED TEST REPORT

RAVENSWOOD, WV 26164 USA

NASA LANGLEY RESEARCH CENTER
ATTN: MARCIA DOMACK
4 SOUTH MARVIN STREET
HAMPTON VA
23681

NSSC SHARED SERVICES CENTER
FMD-ACCOUNTS PAYABLE
BLD-1111, C ROAD
STENNIS, MS
39529

NASA 779803 2413F INCLUSION SERIAL#: 20090814779803 PAGE 1 OF 2

CUSTOMER PURCHASE ORDER NO. & ITEM			ALCAN ORDER NO.	
NNL09AB74P			108-106027	

ALLOY	CLAD.	TEMPER	GAUGE	WIDTH	LENGTH
2050	00	T84	4.00000	64.000	120.000

ITEM ORDERED
LITHIUM - AEROSPACE
LITHIUM MILL

CUSTOMER SPECIFICATION
AMS 4413

PART NUMBER	B/L NUMBER	DATE SHIPPED
	779800	08/14/09

WEIGHT SHIPPED	NO. OF PIECES	GOVT. CONTRACT NO.
3,030	1	

CERTIFICATION

"ALCAN Rolled Products, hereby certifies that metal shipped under this order has been inspected and found in conformance with the requirements of the applicable specifications as indicated herein. Any warranty is limited to that shown on ALCAN Rolled Products' standard General Terms and Conditions of Sales. Test reports are on file, subject to examination."

ALCAN ROLLED PRODUCTS
Rt 2 South, Century Road
P.O. BOX 68
RAVENSWOOD, WV 26164 USA

LaDonna B. Smith - Quality Manager

LOT NUMBER	TEST DIRECTION	NO. OF TESTS	ULTIMATE STRENGTH K.S.I. MIN.	ULTIMATE STRENGTH K.S.I. MAX.	YIELD STRENGTH K.S.I. MIN.	YIELD STRENGTH K.S.I. MAX.	ELONGATION % MIN.	ELONGATION % MAX.	MIN	MAX
278111			***** T84				*****			
	L	2	73.7	73.9	70.0	70.3	13.5	14.0		
	LT	2	75.0	75.6	68.1	69.0	10.5	11.0		
	ST	2	74.0	74.1	63.3	64.7	5.0	5.0		

FRACTURE TOUGHNESS
L-T (KIC) 32.8 KSI (SQRT.IN.)
T-L (KIC) 26.8 KSI (SQRT.IN.)
S-L (KIC) 23.5 KSI (SQRT.IN.)

ALL LOTS ON THIS CERTIFICATION ALSO CONFORM TO THE FOLLOWING REQUIREMENTS

ASTM B594(LITHIUM) 100% SONIC MINUS DEAD ZONE CLASS A

CHEM COMP	ALLOY	SILICON MIN.	SILICON MAX.	IRON MIN.	IRON MAX.	COPPER MIN.	COPPER MAX.	MANGANESE MIN.	MANGANESE MAX.	MAGNESIUM MIN.	MAGNESIUM MAX.	CHROMIUM MIN.	CHROMIUM MAX.	ZINC MIN.	ZINC MAX.	TITANIUM MIN.	TITANIUM MAX.	OTHERS EACH MAX.	OTHERS TOTAL MAX.
	SEE ACTUAL CHEMICAL COMPOSITION																		

ALUMINUM REMAINDER

P-860-155D (1/05)

Appendix B: Individual Tensile, Compression and Fracture Toughness Test Data for 4 inch thick 2050-T84 Plate

Table B1. 2050-T84 Ambient Temperature (75°F) Tensile Results

Specimen #	Orientation	Through Thickness Location	F_{ty} (ksi)	F_{tu} (ksi)	E (Msi)	e_T (%)
1	L	t/6	70.6	73.9	10.8	13.81
2	L	t/6	70.5	73.9	10.8	13.73
3	L	t/6	70.7	74.0	10.8	13.87
		Average	70.6	73.9	10.8	13.80
1	L	t/2	74.8	79.2	10.9	6.69*
2	L	t/2	74.8	79.3	10.9	8.53
3	L	t/2	74.5	79.1	10.9	9.07
		Average	74.7	79.2	10.9	8.80
1	LT	t/6	68.8	75.6	10.9	7.04*
2	LT	t/6	68.9	75.7	10.9	11.51
3	LT	t/6	70.6	75.8	10.8	11.03
		Average	69.4	75.7	10.9	11.27
1	LT	t/2	67.8	74.8	11.0	6.98*
2	LT	t/2	67.9	74.7	11.0	8.83
3	LT	t/2	68.3	74.9	11.0	8.11
		Average	68.0	74.8	11.0	8.47
1	ST	t/2	64.3	73.3	10.7	4.72
2	ST	t/2	64.3	73.2	10.7	4.68
3	ST	t/2	64.1	73.5	10.7	4.98
		Average	64.2	73.3	10.7	4.79
1	L45ST	t/2	63.7	68.7	10.9	2.36
2	L45ST	t/2	62.8	67.8	10.9	2.60
3	L45ST	t/2	62.8	67.8	10.9	2.60
		Average	63.1	68.1	10.9	2.52
1	45	t/6	65.6	72.9	10.7	11.66
2	45	t/6	65.4	72.9	10.7	12.23
3	45	t/6	65.2	72.6	10.7	12.11
		Average	65.4	72.8	10.7	12.00
1	45	t/2	65.9	72.7	10.7	9.63
2	45	t/2	65.6	72.4	10.7	9.71
4	45	t/2	65.4	72.3	10.7	10.31
		Average	65.6	72.4	10.7	9.88

*Specimen broke outside extensometer knife edge, not included in average elongation

Table B2. 2050-T84 Cryogenic Temperature (-320°F) Tensile Results

Specimen #	Orientation	Through Thickness Location	F_{ty} (ksi)	F_{tu} (ksi)	E (Msi)	e_T (%)
4	L	t/6	81.4	88.5	12.0	14.98*
5	L	t/6	81.7	88.8	12.0	14.98*
6	L	t/6	81.5	88.8	11.7	16.70**
7	L	t/6	81.4	88.9	11.8	17.10**
		Average	81.5	88.8	11.9	16.90
4	L	t/2	—	95.9	12.1	—***
5	L	t/2	86.1	95.8	12.1	11.05
6	L	t/2	85.7	95.5	12.3	10.41
		Average	85.9	95.7	12.2	10.73
4	LT	t/6	79.4	91.5	12.1	12.00
5	LT	t/6	79.5	91.6	11.9	12.25
6	LT	t/6	80.6	91.6	12.1	12.33
		Average	79.9	91.6	12.0	12.29
4	LT	t/2	79.1	91.7	12.3	8.39
5	LT	t/2	78.7	91.4	12.2	8.85
6	LT	t/2	78.9	91.2	12.2	6.75
		Average	78.9	91.4	12.2	7.80
4	ST	t/2	73.1	87.6	11.9	5.45
5	ST	t/2	73.0	87.0	11.9	4.84***
6	ST	t/2	73.1	87.4	11.9	5.23
		Average	73.1	87.3	11.9	5.34
4	L45ST	t/2	72.9	81.4	12.0	3.48
5	L45ST	t/2	71.8	80.7	11.9	4.08
6	L45ST	t/2	76.1	84.8	11.9	3.19
		Average	73.6	82.3	11.9	3.58
4	45	t/6	74.5	86.7	11.6	14.63**
5	45	t/6	74.5	86.8	11.5	14.55**
6	45	t/6	74.6	87.0	11.8	14.65**
		Average	74.5	86.8	11.6	14.61
5	45	t/2	74.7	87.0	11.7	11.06
6	45	t/2	73.9	86.0	11.8	11.48
7	45	t/2	74.0	86.2	11.8	11.10
		Average	74.2	86.4	11.8	11.21

*Extensometer off scale, not included in average elongation; **Used 0.9 inch gage length extensometer; ***Extensometer slipped, not included in average elongation

Table B3. 2050-T84 Ambient Temperature (75°F) Compression Results

Specimen #	Orientation	Through Thickness Location	F_{cy} (ksi)	E_c (Msi)
1	L	t/2	74.6	11.1
2	L	t/2	74.6	11.1
3	L	t/2	75.3	11.2
		Average	74.9	11.2
1	L	t/6	69.3	11.1
3	L	t/6	69.5	11.1
4	L	t/6	69.9	11.1
		Average	69.6	11.1
1	LT	t/2	77.4	11.3
2	LT	t/2	77.3	11.3
3	LT	t/2	77.3	11.3
		Average	77.3	11.3
1	LT	t/6	71.4	11.2
2	LT	t/6	71.6	11.2
3	LT	t/6	71.0	11.2
		Average	71.3	11.2
1	45	t/2	70.2	11.0
2	45	t/2	70.1	11.0
3	45	t/2	71.1	11.0
		Average	70.5	11.0
1	45	t/6	69.6	11.0
2	45	t/6	69.9	11.0
3	45	t/6	69.2	11.0
		Average	69.6	11.0

Table B4. 2050-T84 Cryogenic Temperature (-320°F) Compression Results

Specimen #	Orientation	Through Thickness Location	F_{cy} (ksi)	E_c (Msi)
4	L	t/2	86.7	12.3
5	L	t/2	86.3	12.3
6	L	t/2	86.2	12.3
		Average	86.4	12.3
5	L	t/6	75.5	12.4
6	L	t/6	78.7	12.5
2	L	t/6	75.2	12.7
		Average	76.5	12.5
4	LT	t/2	90.1	12.2
5	LT	t/2	89.8	12.5
6	LT	t/2	88.8	12.5
		Average	89.6	12.4
4	LT	t/6	82.1	12.4
5	LT	t/6	81.7	12.3
6	LT	t/6	82.1	12.4
		Average	82.0	12.4
4	45	t/2	80.4	12.1
5	45	t/2	81.1	12.2
6	45	t/2	82.5	12.2
		Average	81.3	12.2
4	45	t/6	86.8	12.3
5	45	t/6	79.7	12.2
6	45	t/6	79.3	12.3
		Average	81.9	12.3

Table B5. 2050-T84 Ambient Temperature (75°F) Fracture Toughness Results

Specimen #	Orientation	Through Thickness Location	K_{QJIC} (ksi√in)
4	L-T	5t/6	37.6
5	L-T	5t/6	39.1
		Average	38.4
1	T-L	5t/6	22.4
2	T-L	5t/6	26.3
4	T-L	5t/6	25.7
		Average	24.8
1	L-S	t/6	38.7
2	L-S	t/6	36.3
3	L-S	t/6	38.0
		Average	37.7

Table B6. 2050-T84 Cryogenic Temperature (-320°F) Fracture Toughness Results

Specimen #	Orientation	Through Thickness Location	K_{QJIC} (ksi√in)
6	L-T	5t/6	34.1
7	L-T	5t/6	34.4
9	L-T	5t/6	28.8
		Average	32.4
5	T-L	5t/6	27.2
6	T-L	5t/6	28.0
8	T-L	t/6	29.5
		Average	28.2
4	L-S	t/6	43.7
5	L-S	t/6	45.3
6	L-S	t/6	44.1
		Average	44.4

Appendix C: Individual Stress-Strain Curves for Tensile Tests on 4 inch thick 2050-T84 Plate

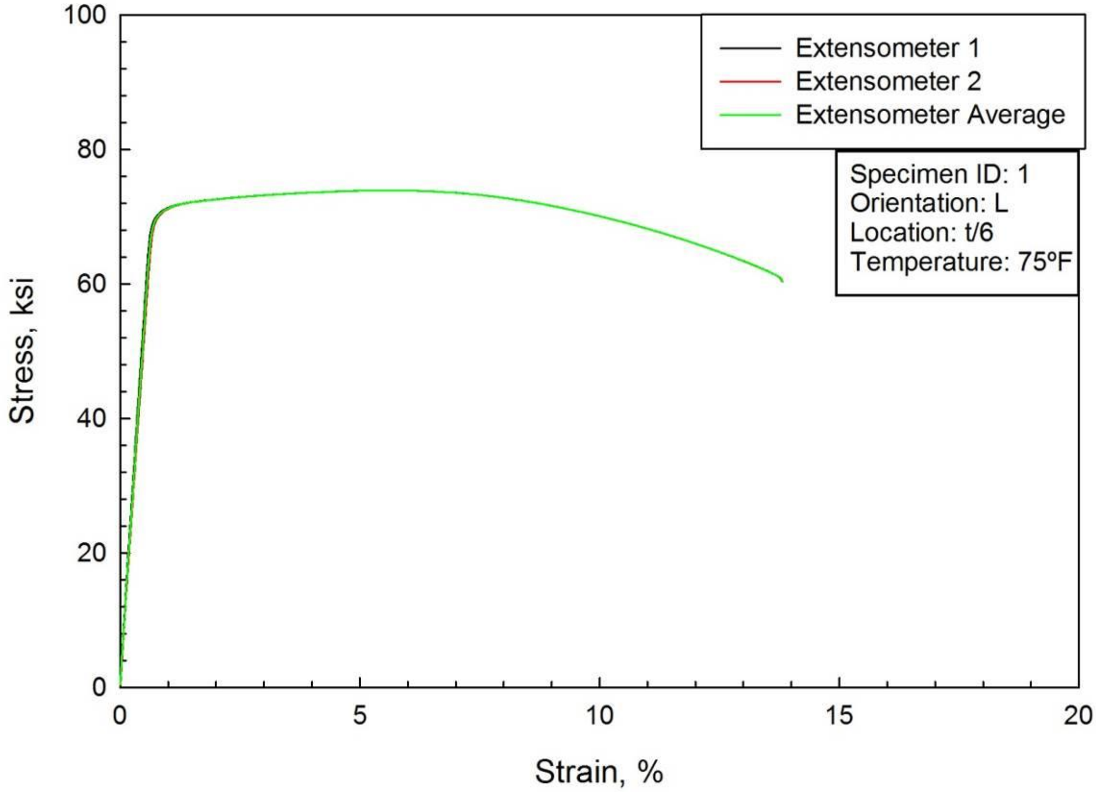

Figure C1. Tensile data for 2050-T84, L orientation, t/6, specimen 1, tested at 75ºF.

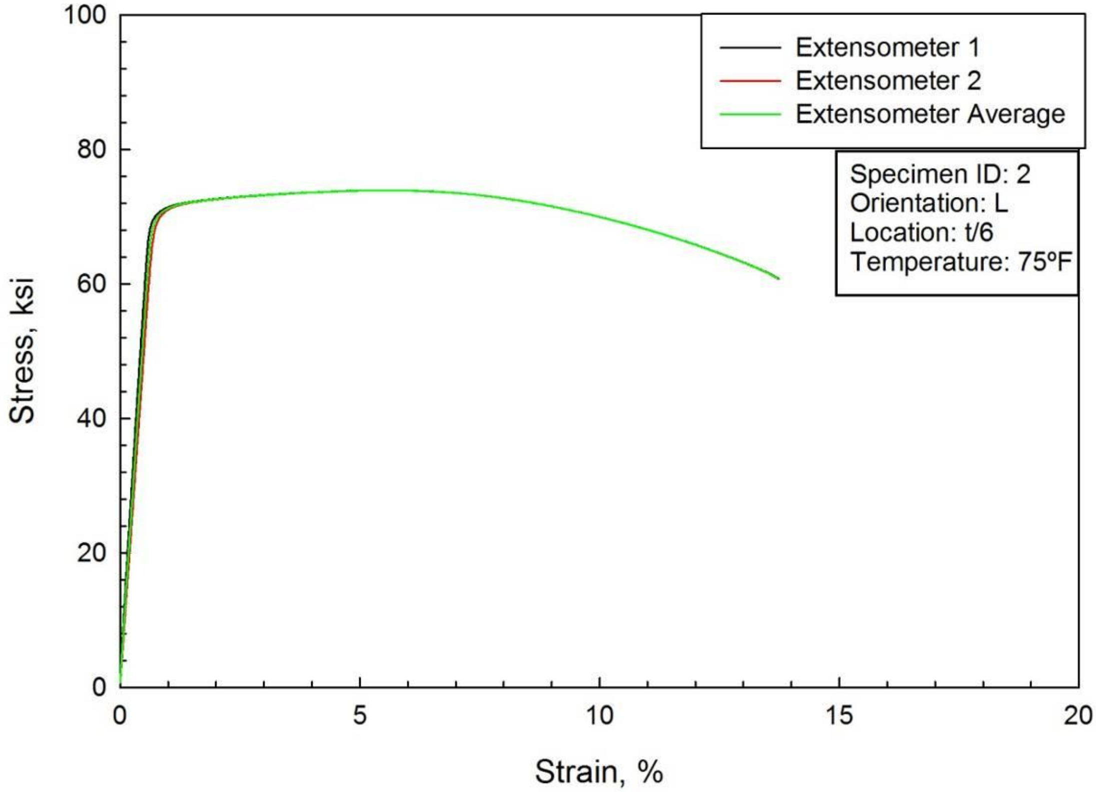

Figure C2. Tensile data for 2050-T84, L orientation, t/6, specimen 2, tested at 75ºF.

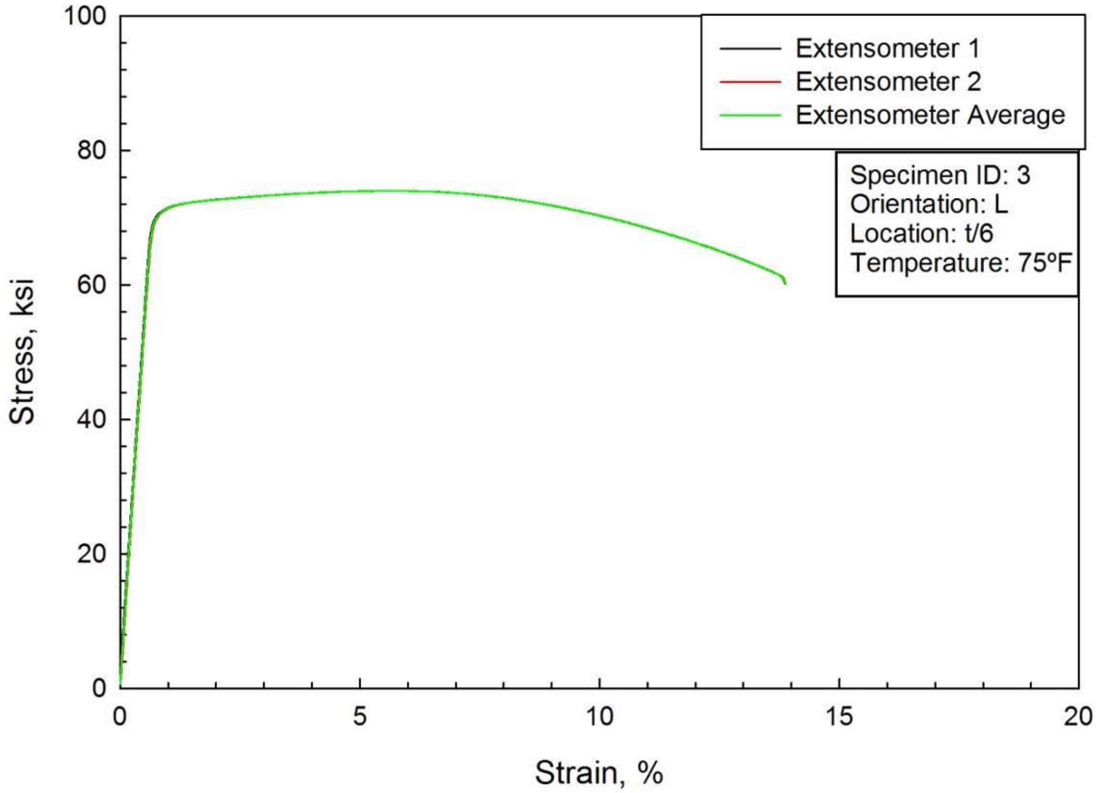

Figure C3. Tensile data for 2050-T84, L orientation, t/6, specimen 3, tested at 75ºF.

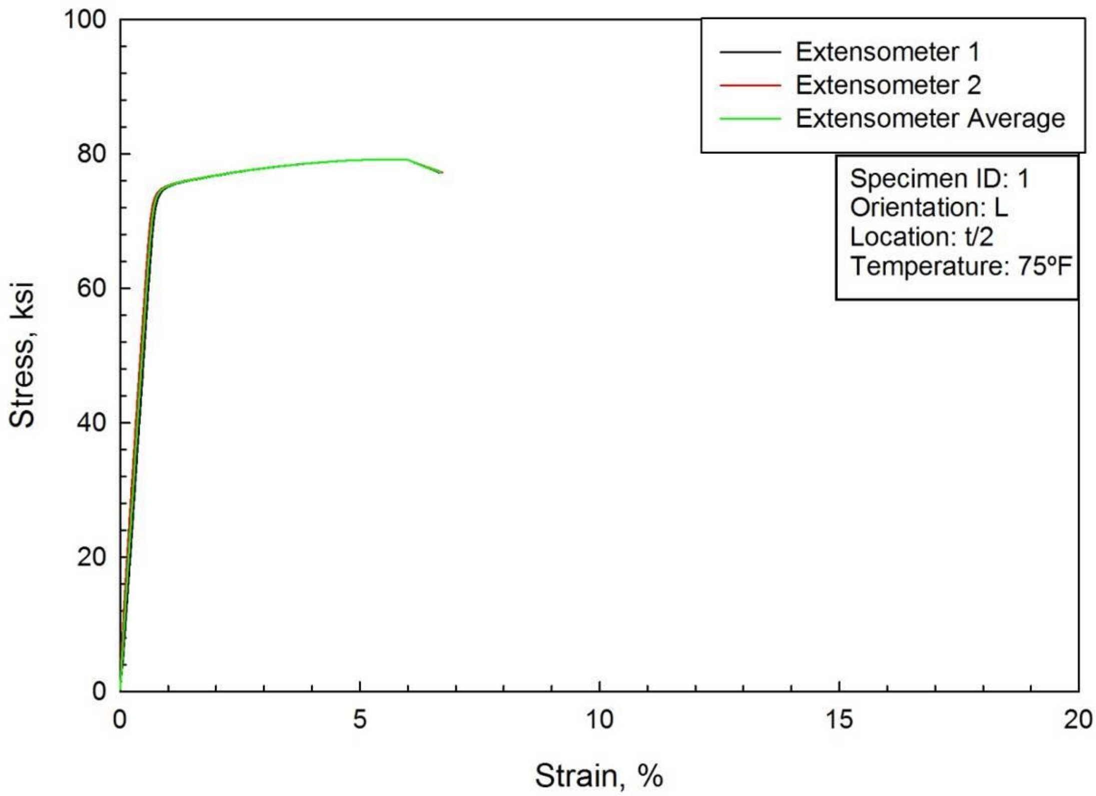

Figure C4. Tensile data for 2050-T84, L orientation, t/2, specimen 1, tested at 75ºF.

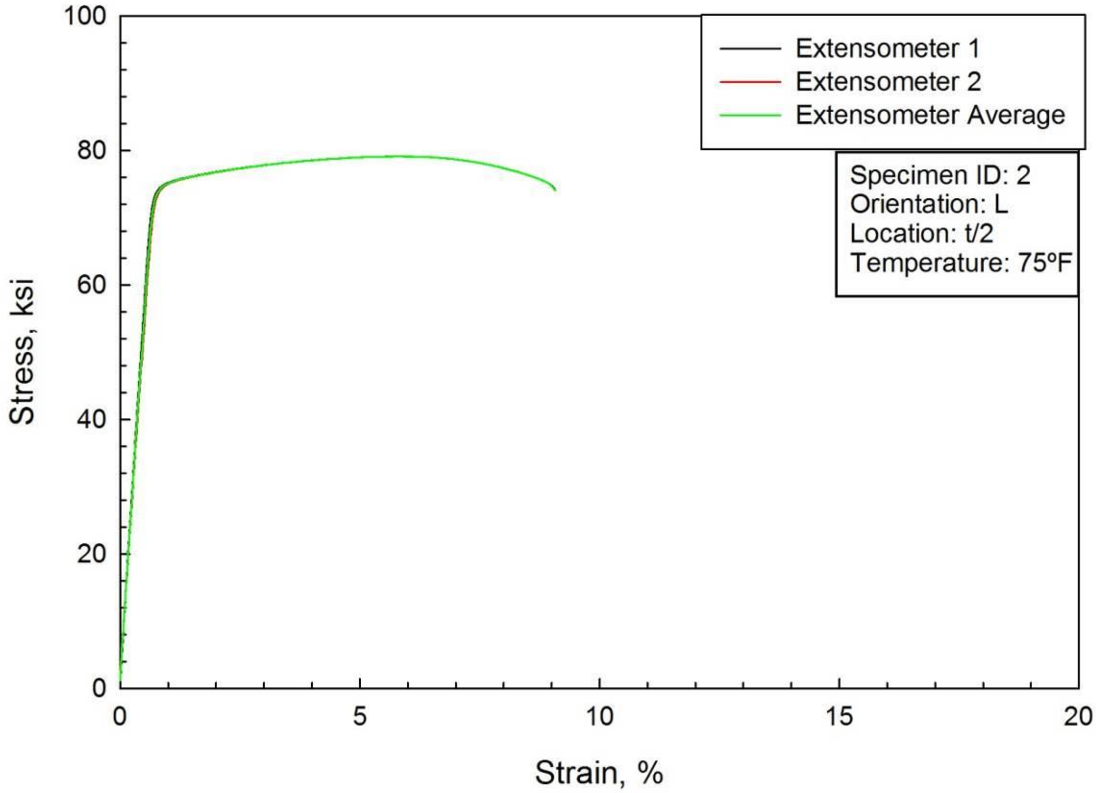

Figure C5. Tensile data for 2050-T84, L orientation, t/2, specimen 2, tested at 75ºF.

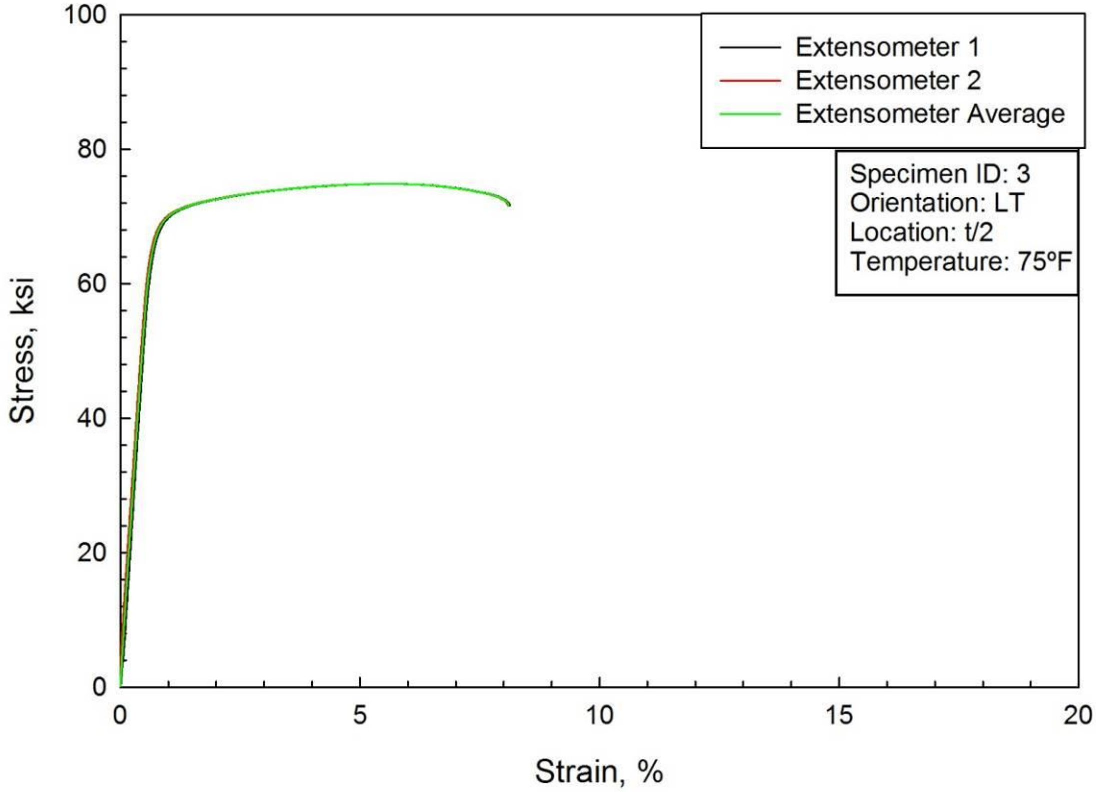

Figure C6. Tensile data for 2050-T84, L orientation, t/2, specimen 3, tested at 75ºF.

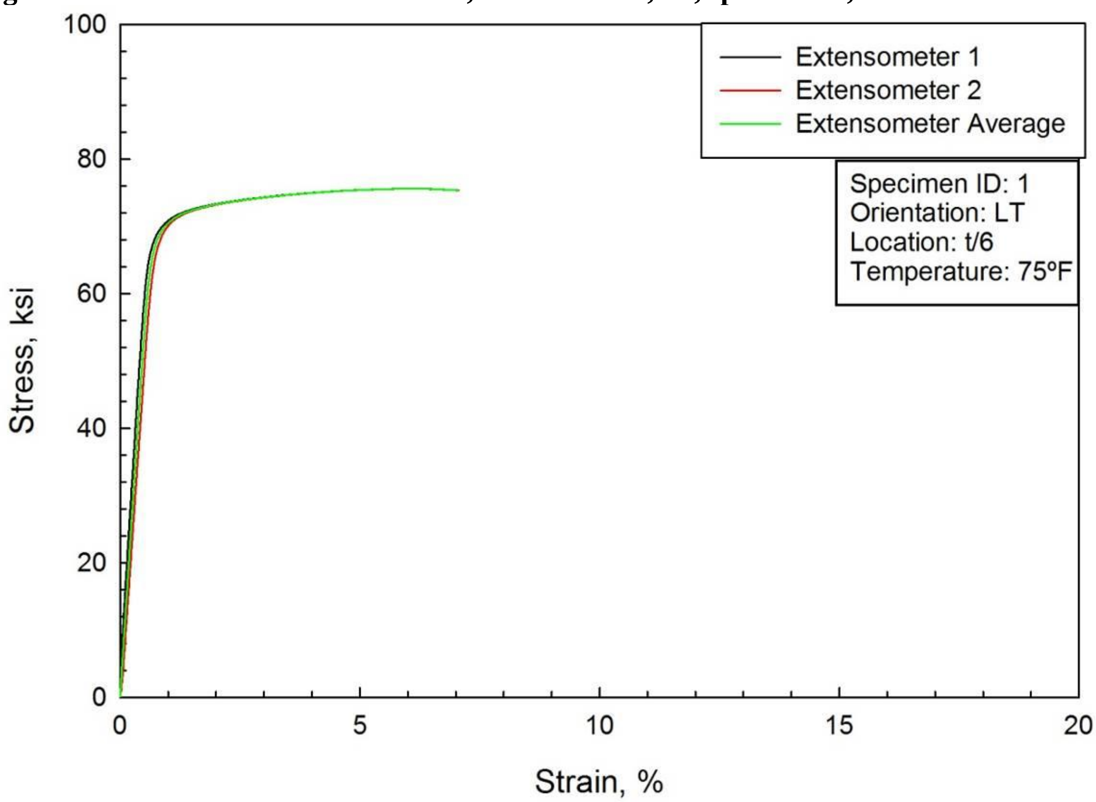

Figure C7. Tensile data for 2050-T84, LT orientation, t/6, specimen 1, tested at 75ºF.

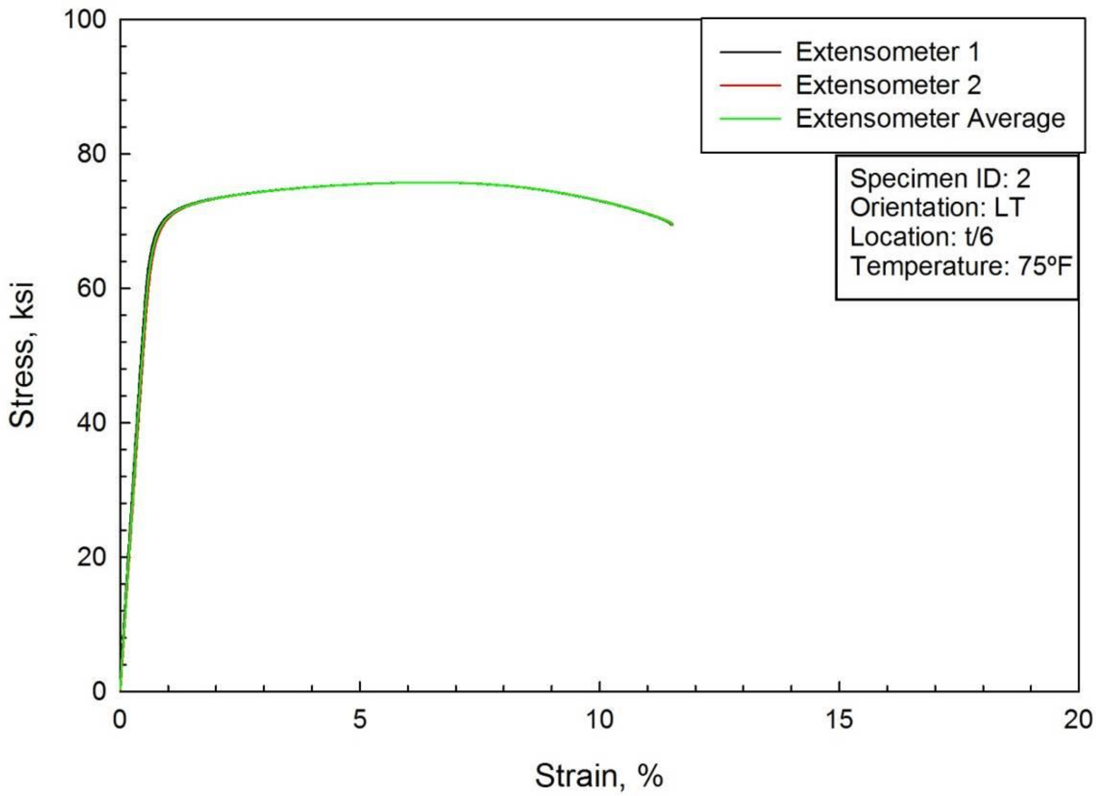

Figure C8. Tensile data for 2050-T84, LT orientation, t/6, specimen 2, tested at 75ºF.

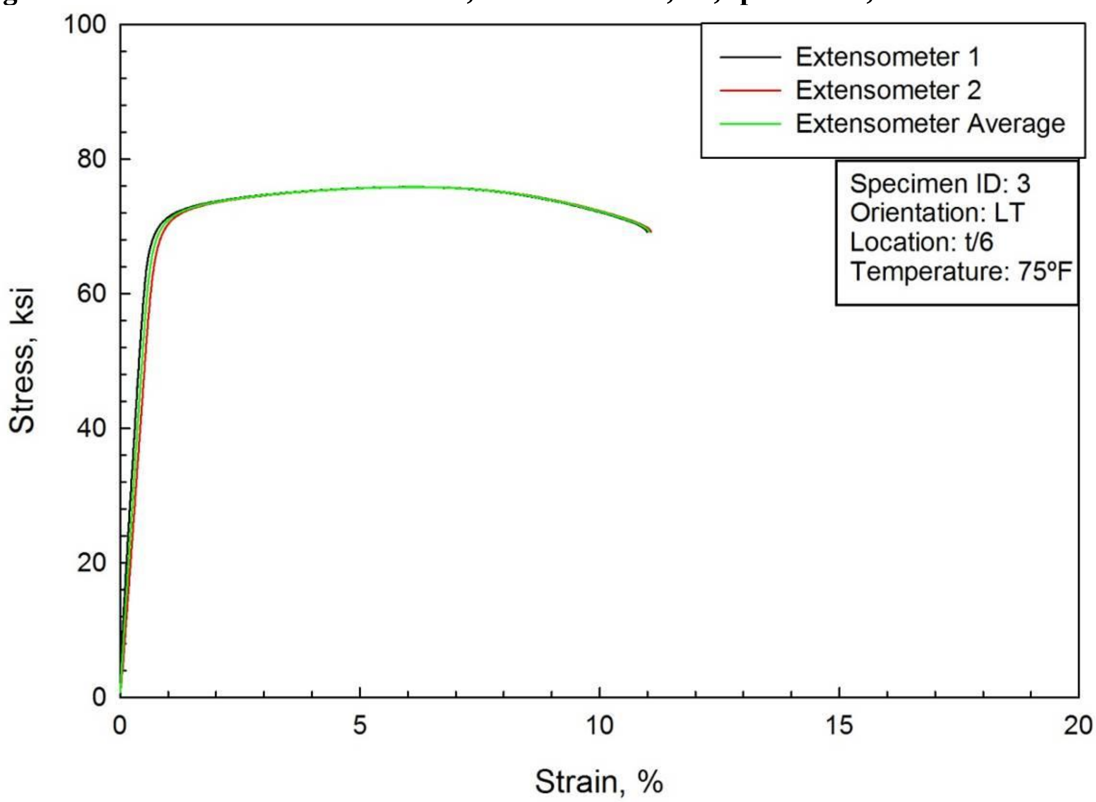

Figure C9. Tensile data for 2050-T84, LT orientation, t/6, specimen 3, tested at 75ºF.

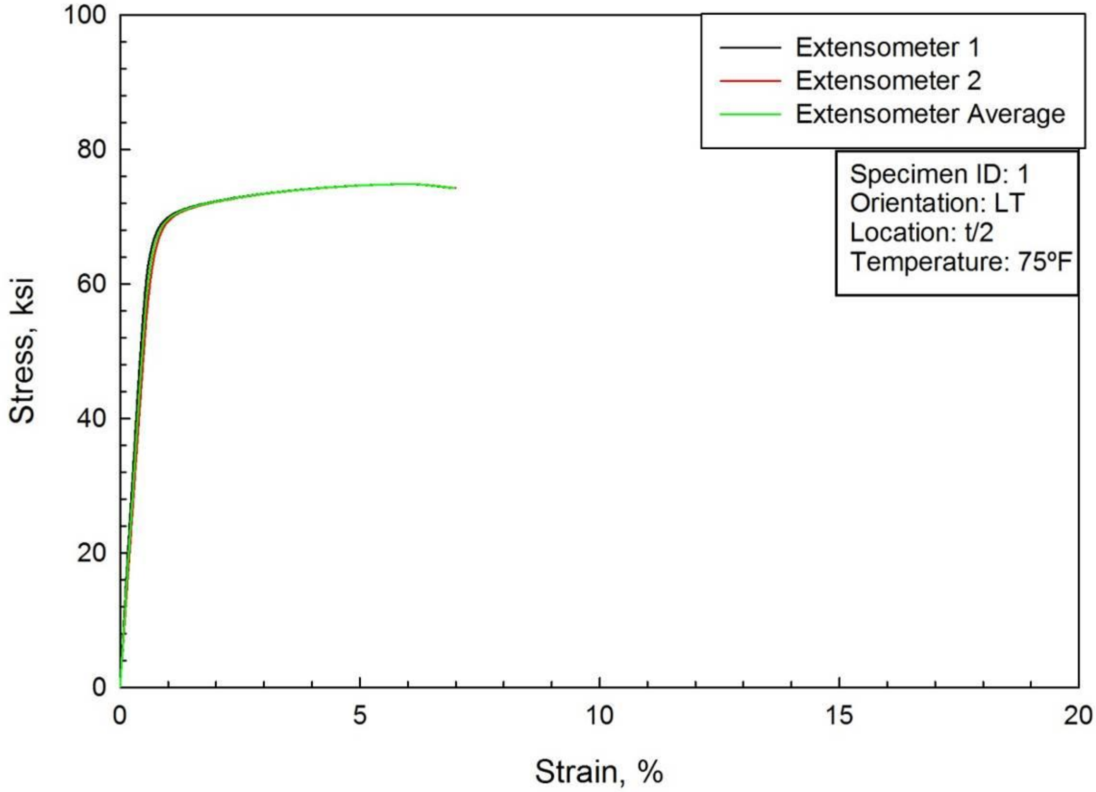

Figure C10. Tensile data for 2050-T84, LT orientation, t/2, specimen 1, tested at 75ºF.

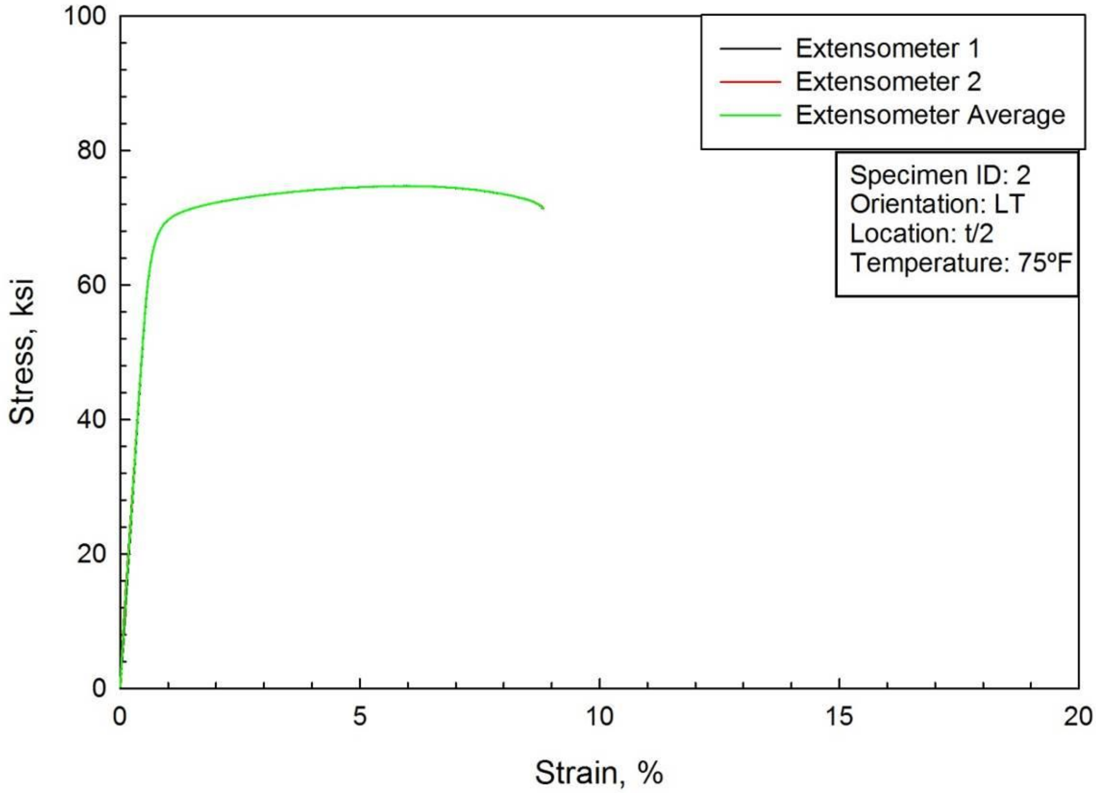

Figure C11. Tensile data for 2050-T84, LT orientation, t/2, specimen 2, tested at 75ºF.

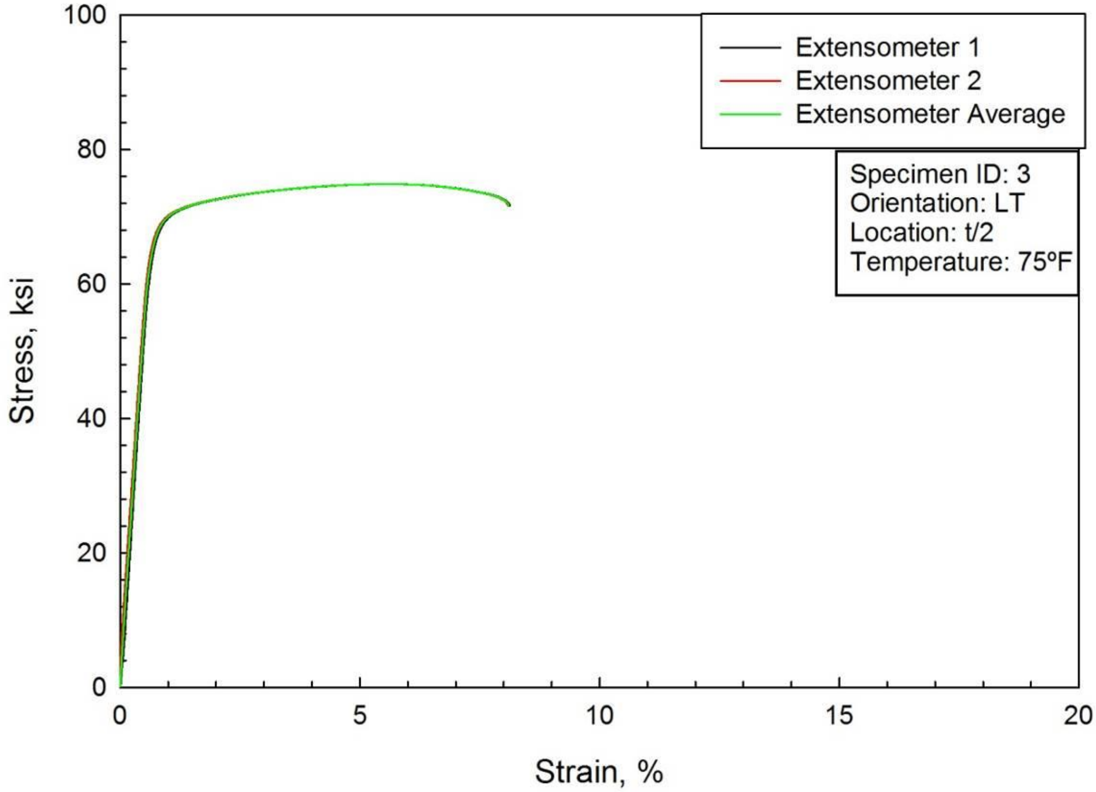

Figure C12. Tensile data for 2050-T84, LT orientation, t/2, specimen 3, tested at 75ºF.

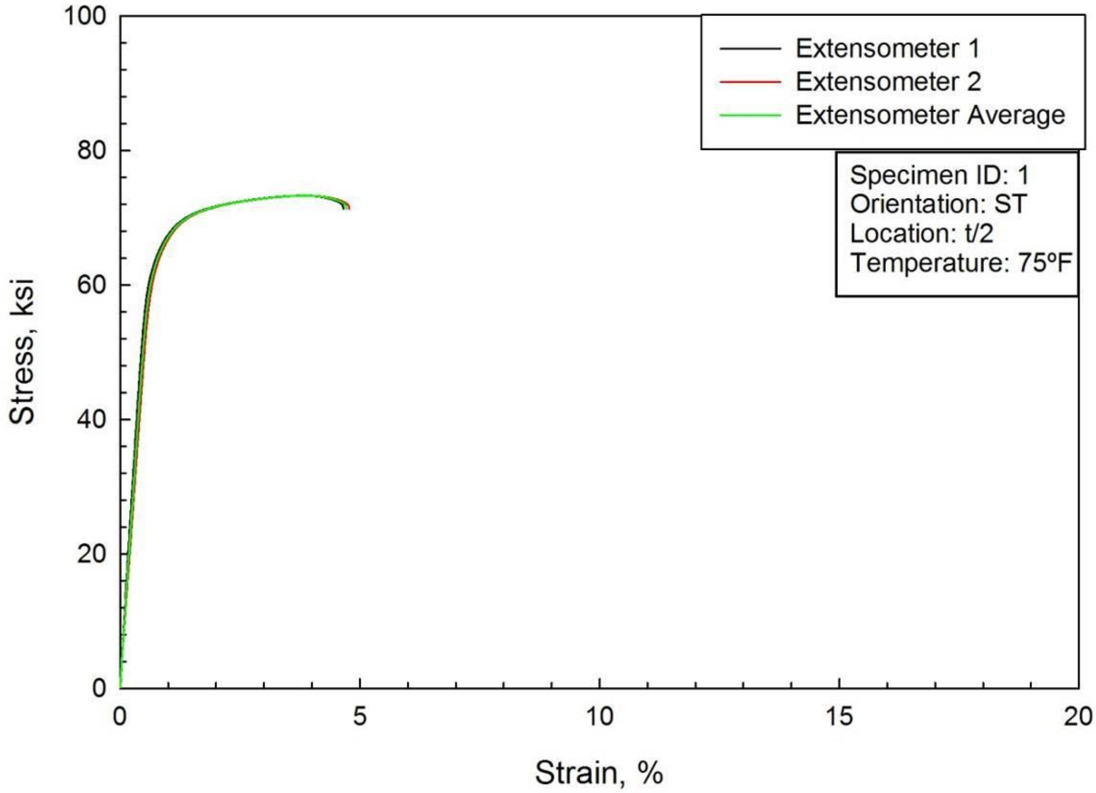

Figure C13. Tensile data for 2050-T84, ST orientation, t/2, specimen 1, tested at 75ºF.

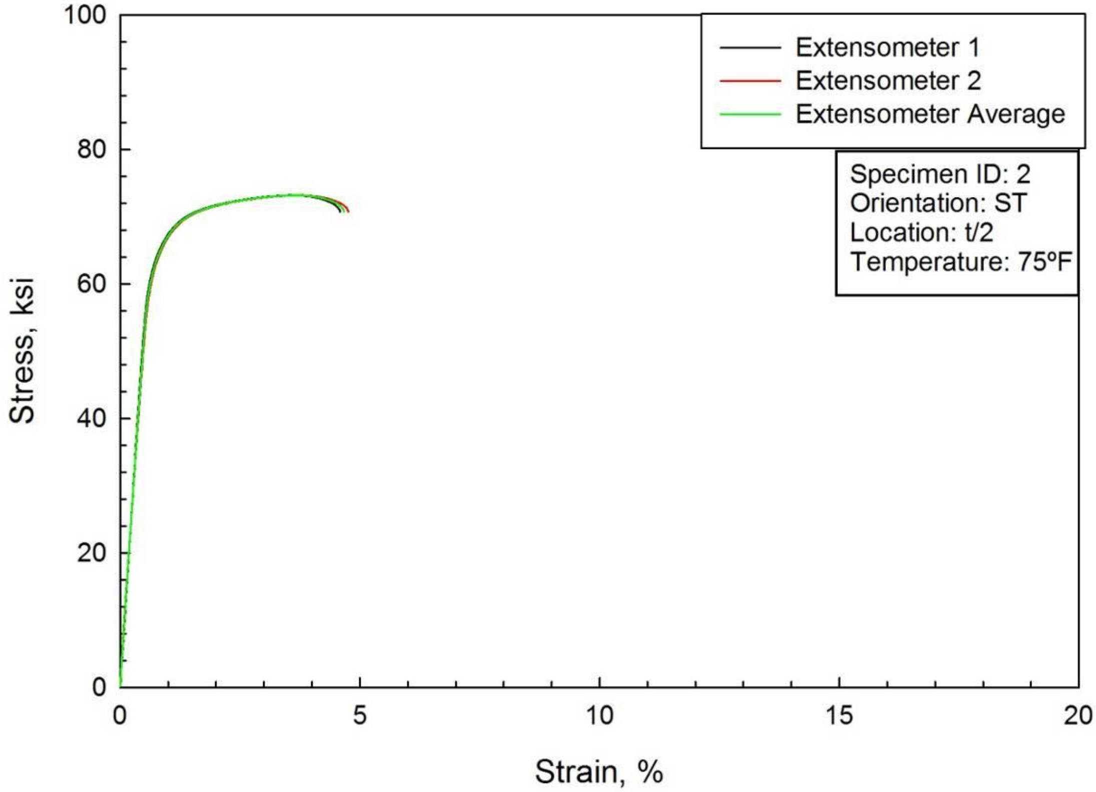

Figure C14. Tensile data for 2050-T84, ST orientation, t/2, specimen 2, tested at 75ºF.

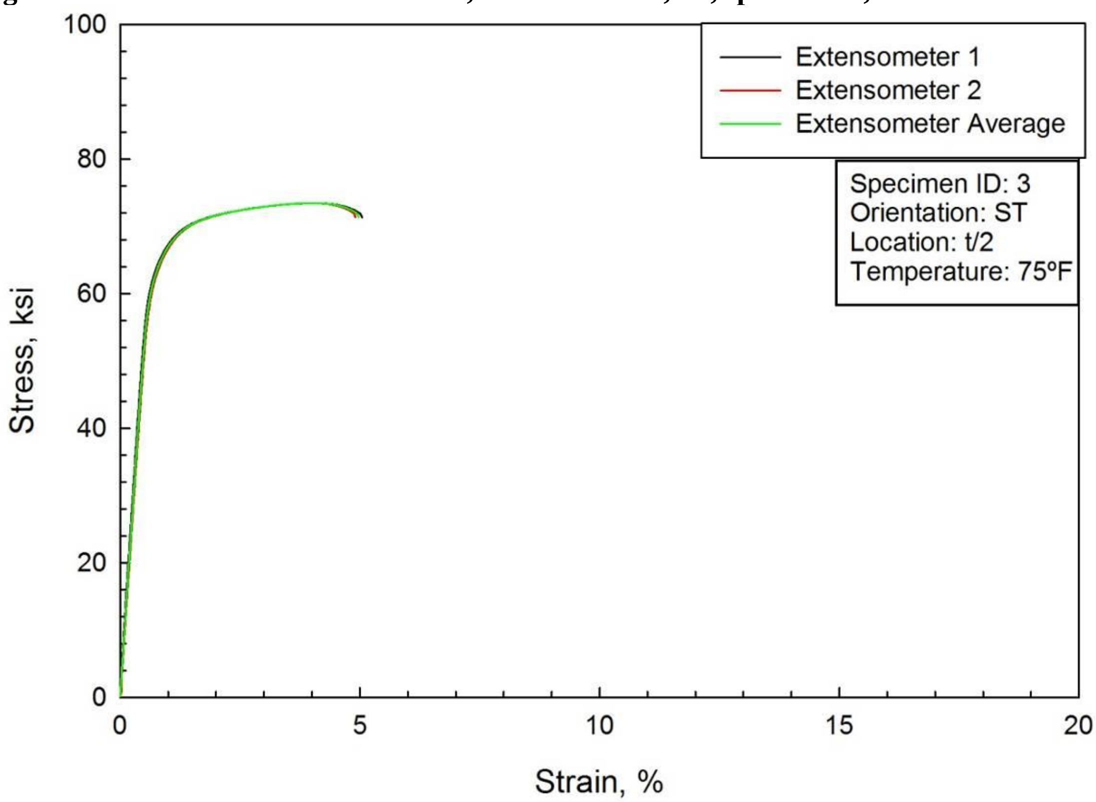

Figure C15. Tensile data for 2050-T84, ST orientation, t/2, specimen 3, tested at 75ºF.

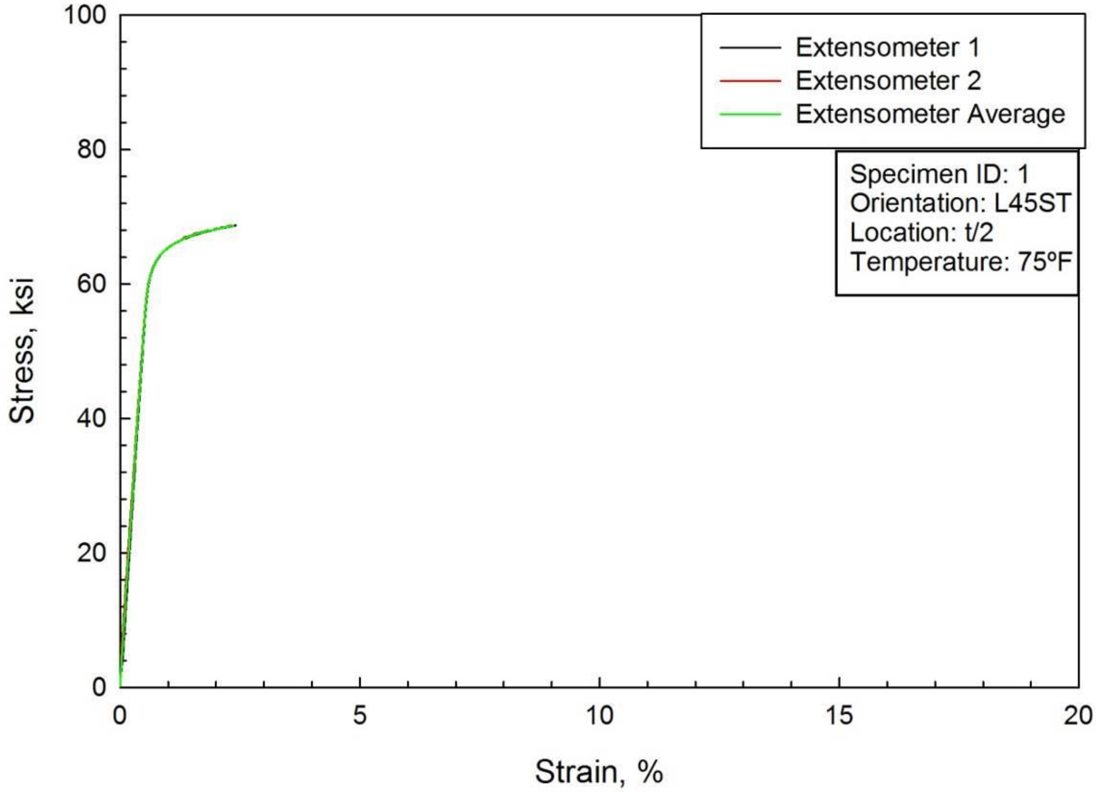

Figure C16. Tensile data for 2050-T84, L45ST orientation, t/2, specimen 1, tested at 75ºF.

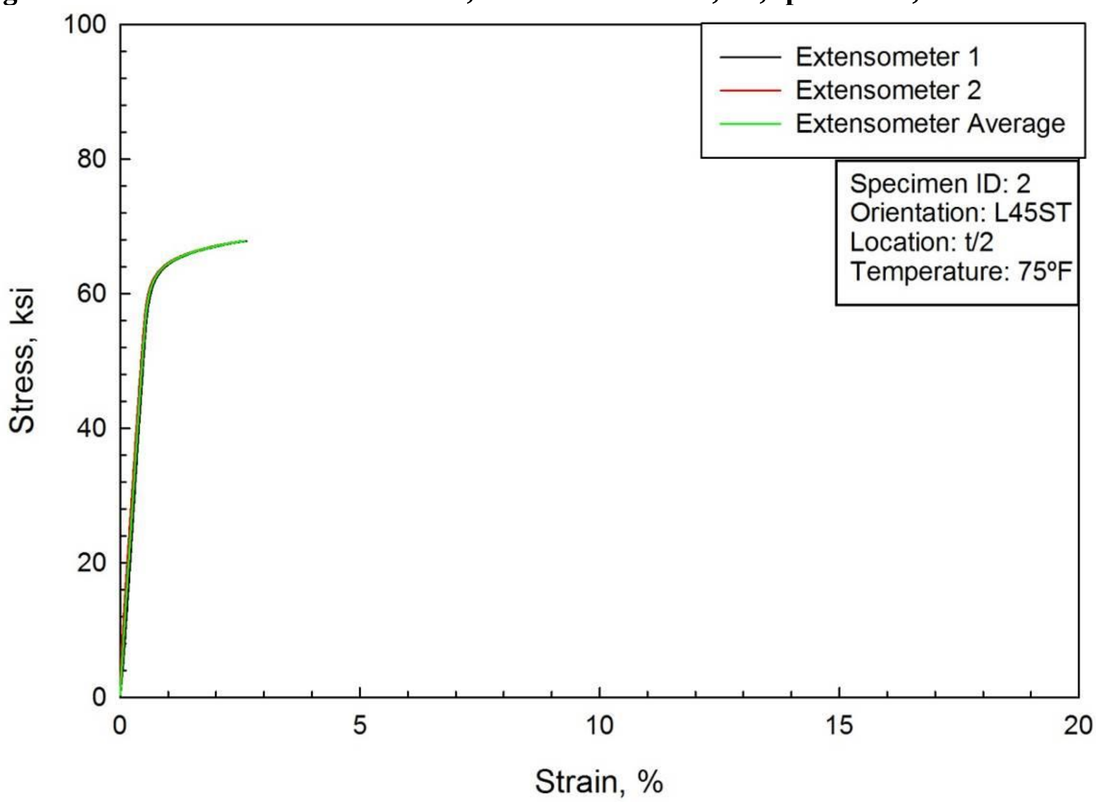

Figure C17. Tensile data for 2050-T84, L45ST orientation, t/2, specimen 2, tested at 75ºF.

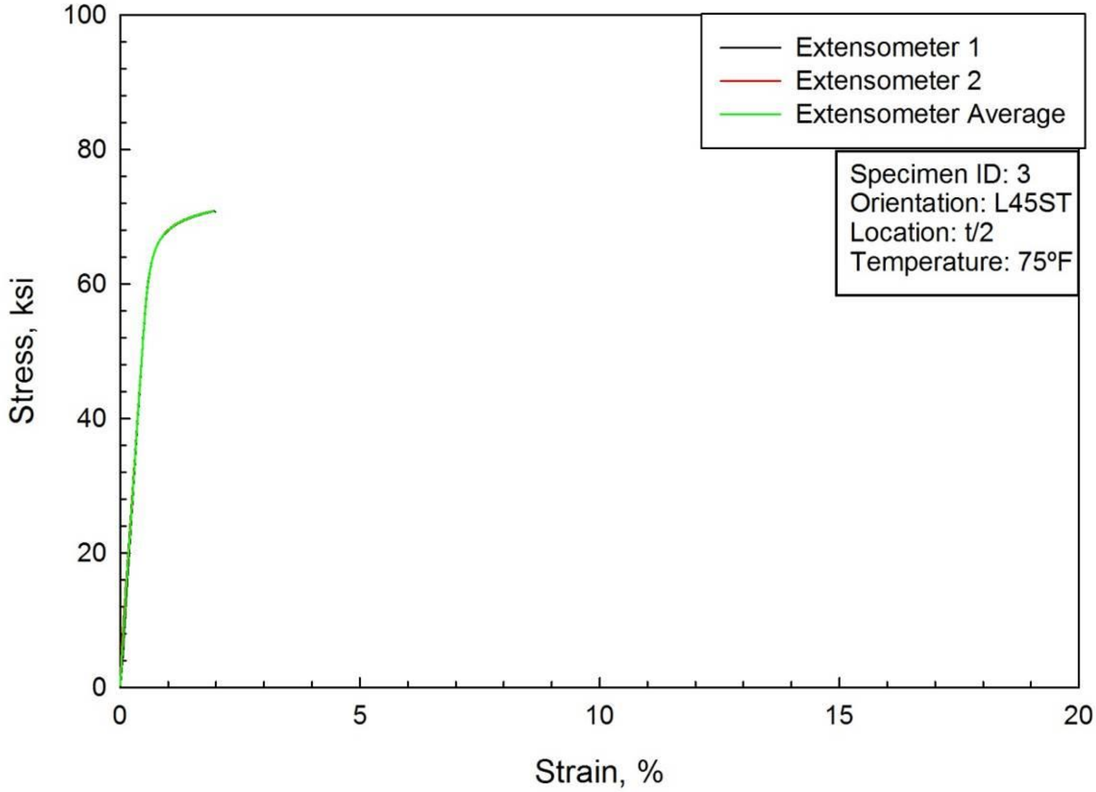

Figure C18. Tensile data for 2050-T84, L45ST orientation, t/2, specimen 3, tested at 75ºF.

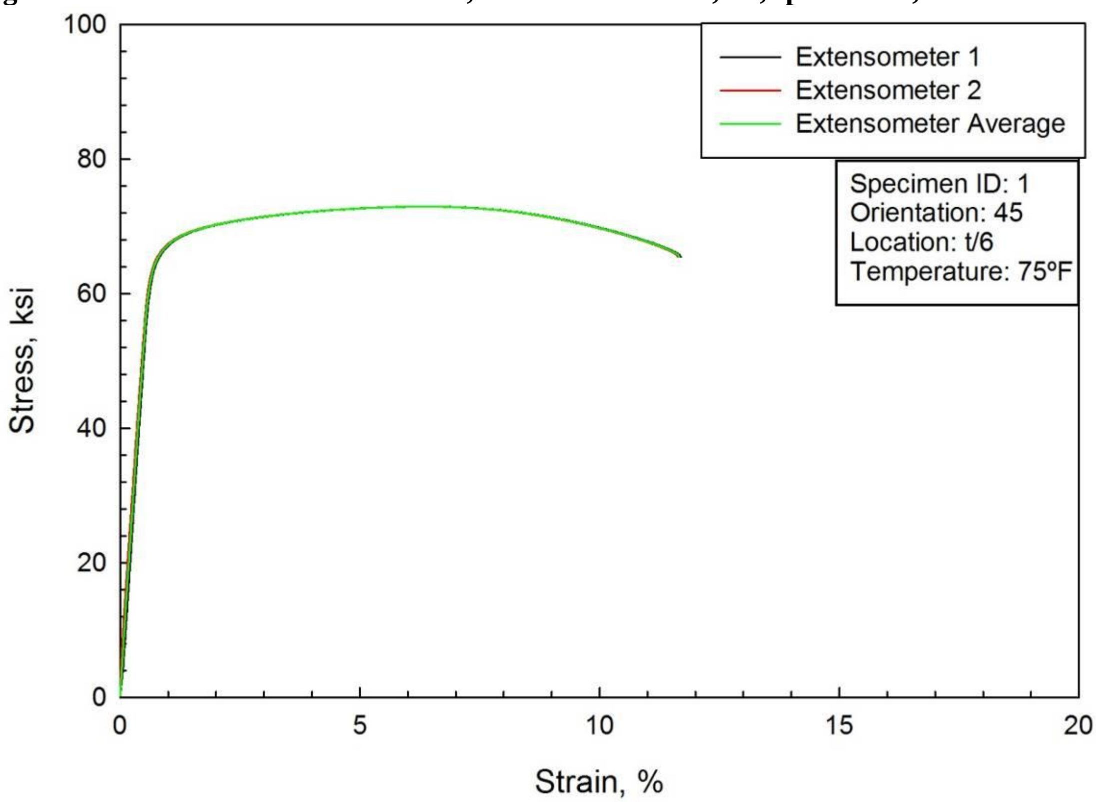

Figure C19. Tensile data for 2050-T84, 45º orientation, t/6, specimen 1, tested at 75ºF.

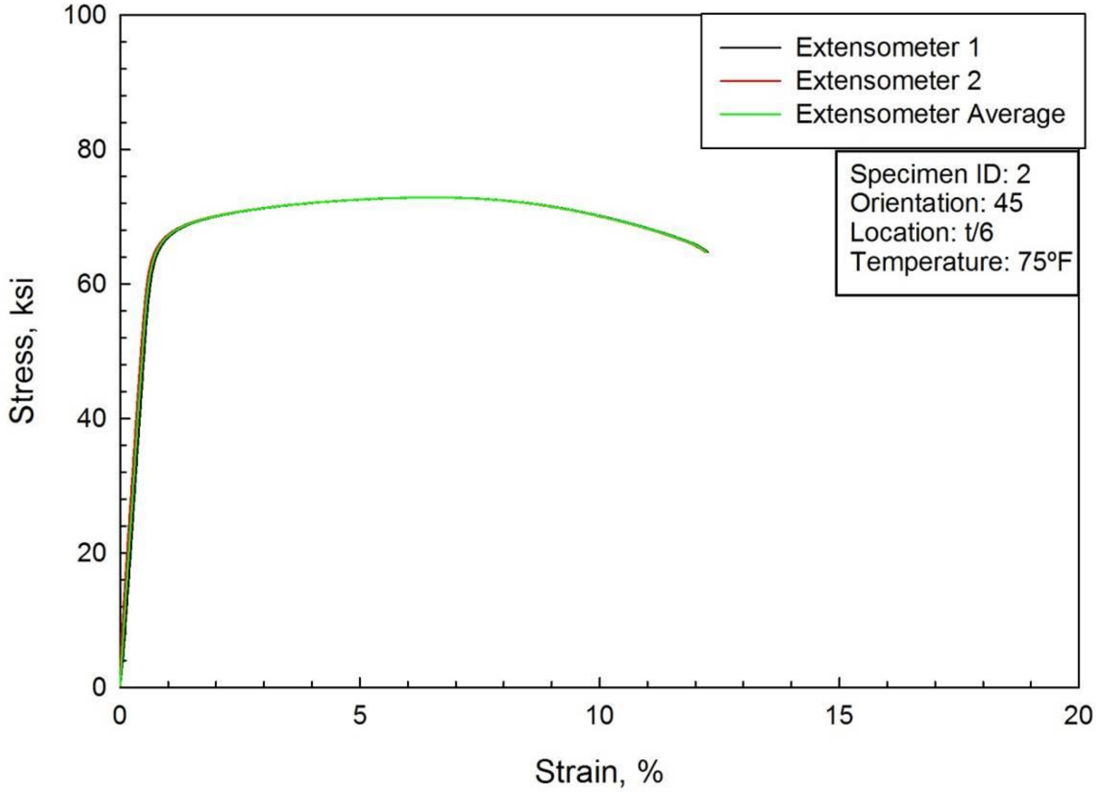

Figure C20. Tensile data for 2050-T84, 45º orientation, t/6, specimen 2, tested at 75ºF.

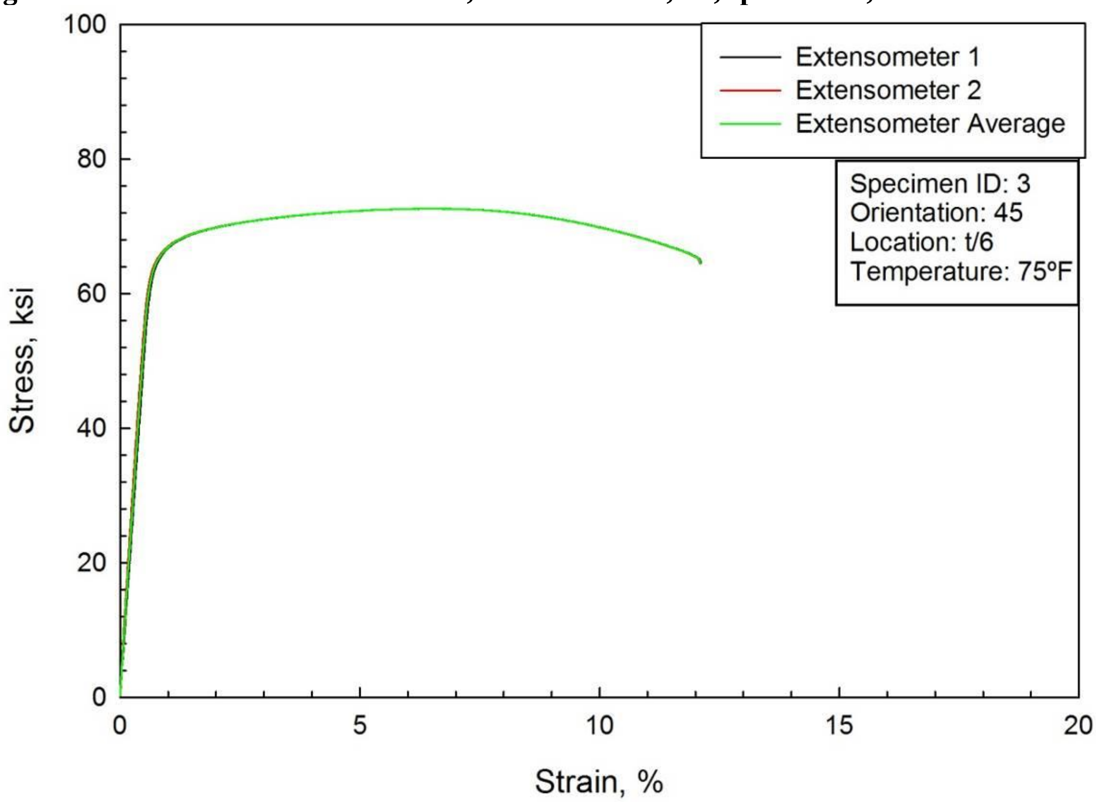

Figure C21. Tensile data for 2050-T84, 45º orientation, t/6, specimen 3, tested at 75ºF.

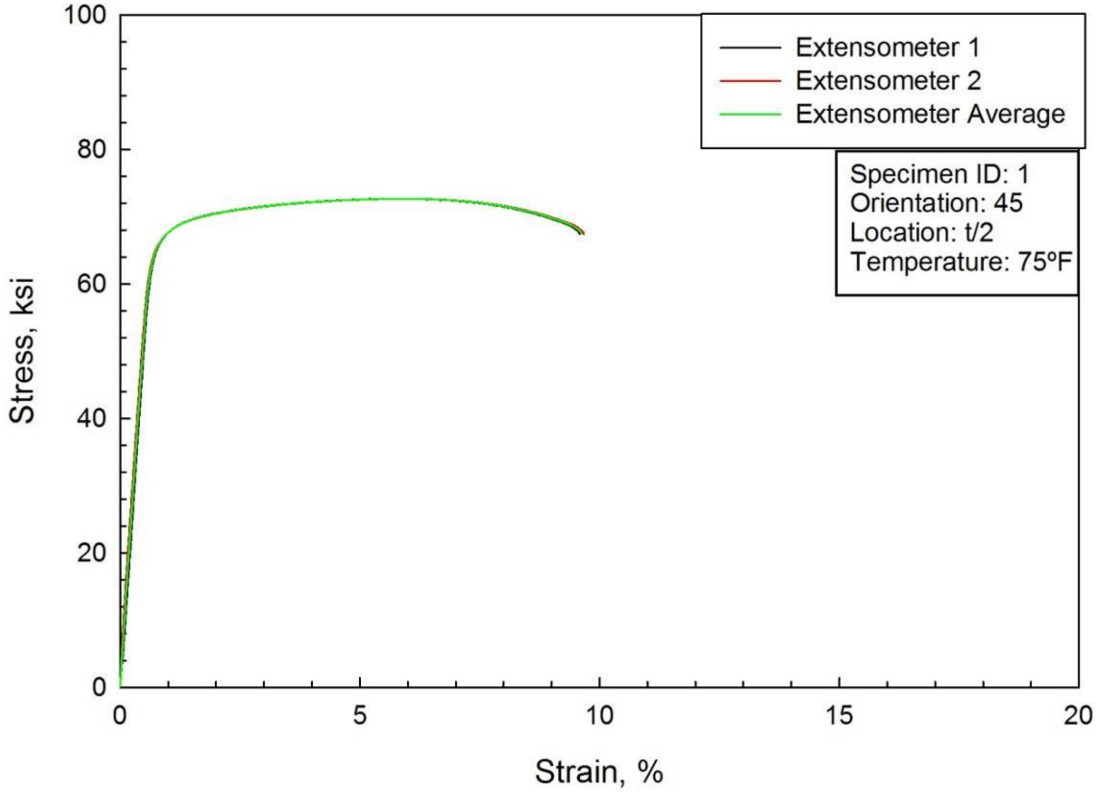

Figure C22. Tensile data for 2050-T84, 45º orientation, t/2, specimen 1, tested at 75ºF.

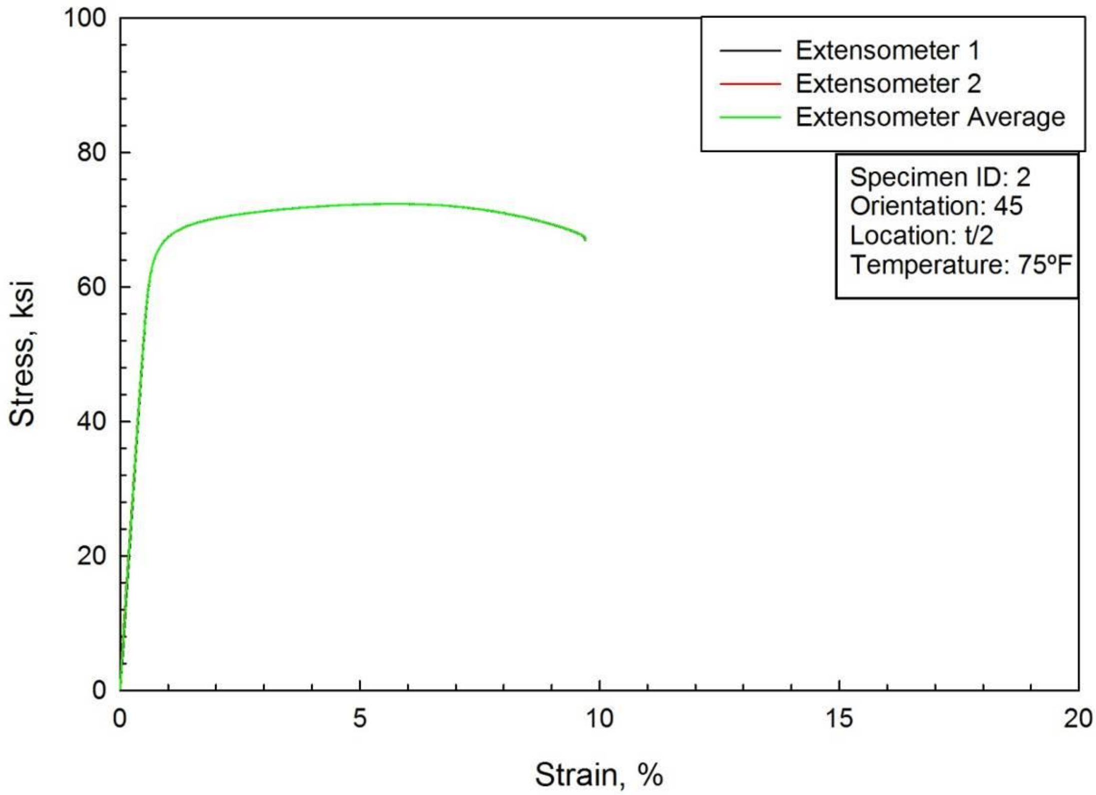

Figure C23. Tensile data for 2050-T84, 45º orientation, t/2, specimen 2, tested at 75ºF.

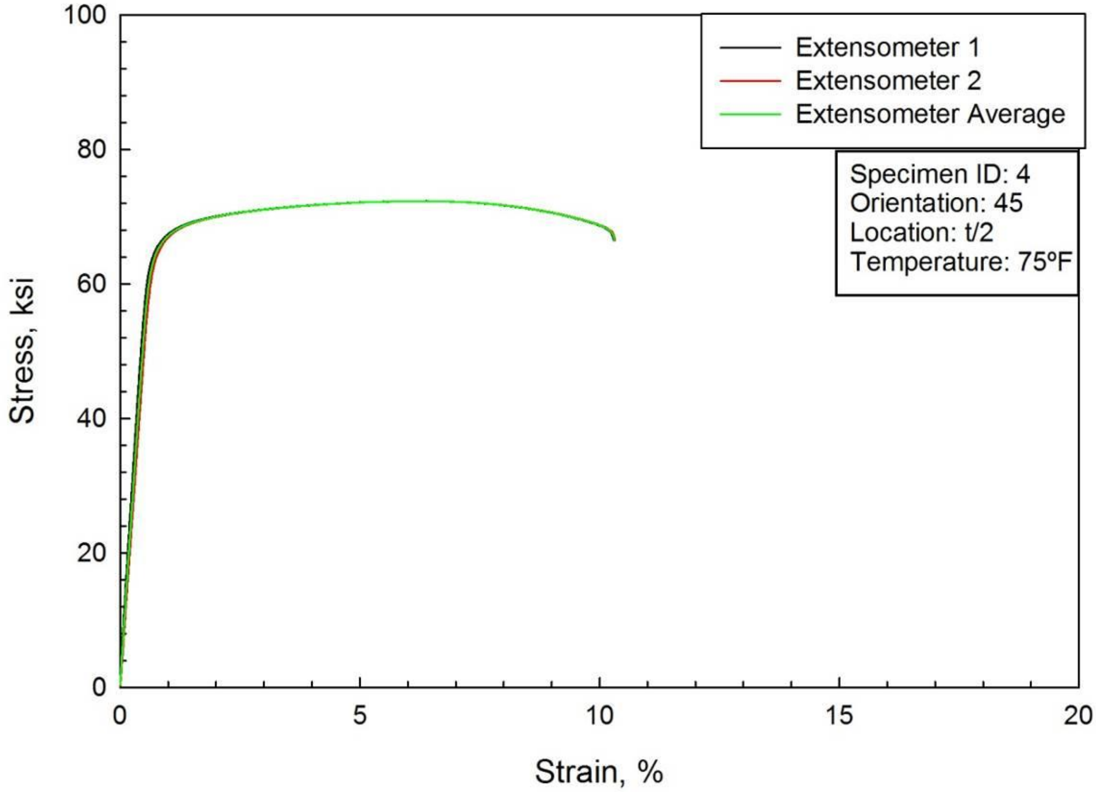

Figure C24. Tensile data for 2050-T84, 45º orientation, t/2, specimen 3, tested at 75ºF.

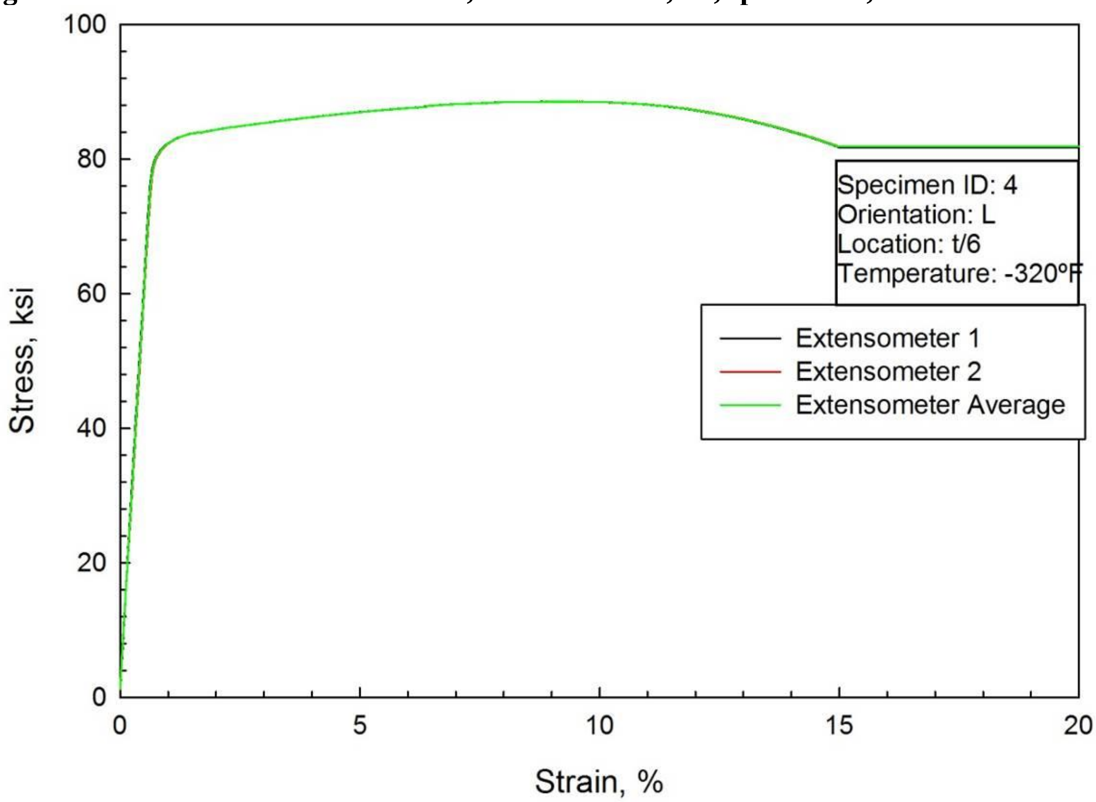

Figure C25. Tensile data for 2050-T84, L orientation, t/6, specimen 4, tested at -320ºF.

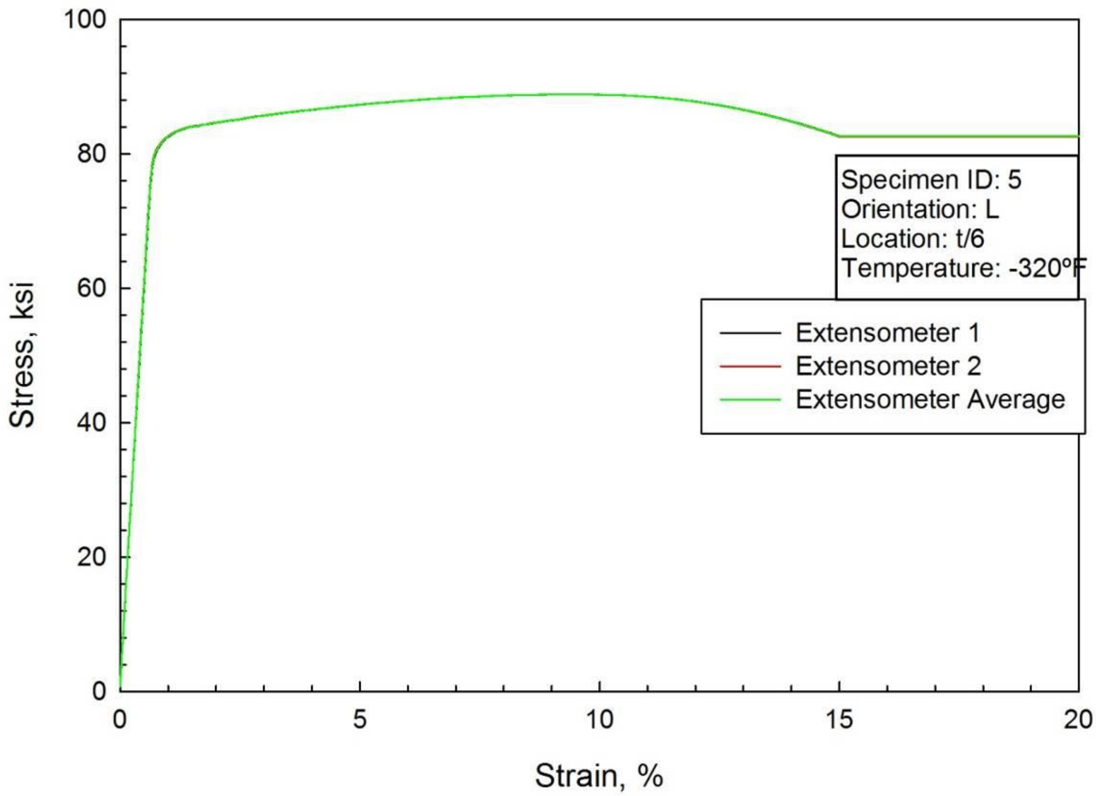

Figure C26. Tensile data for 2050-T84, L orientation, t/6, specimen 5, tested at -320ºF.

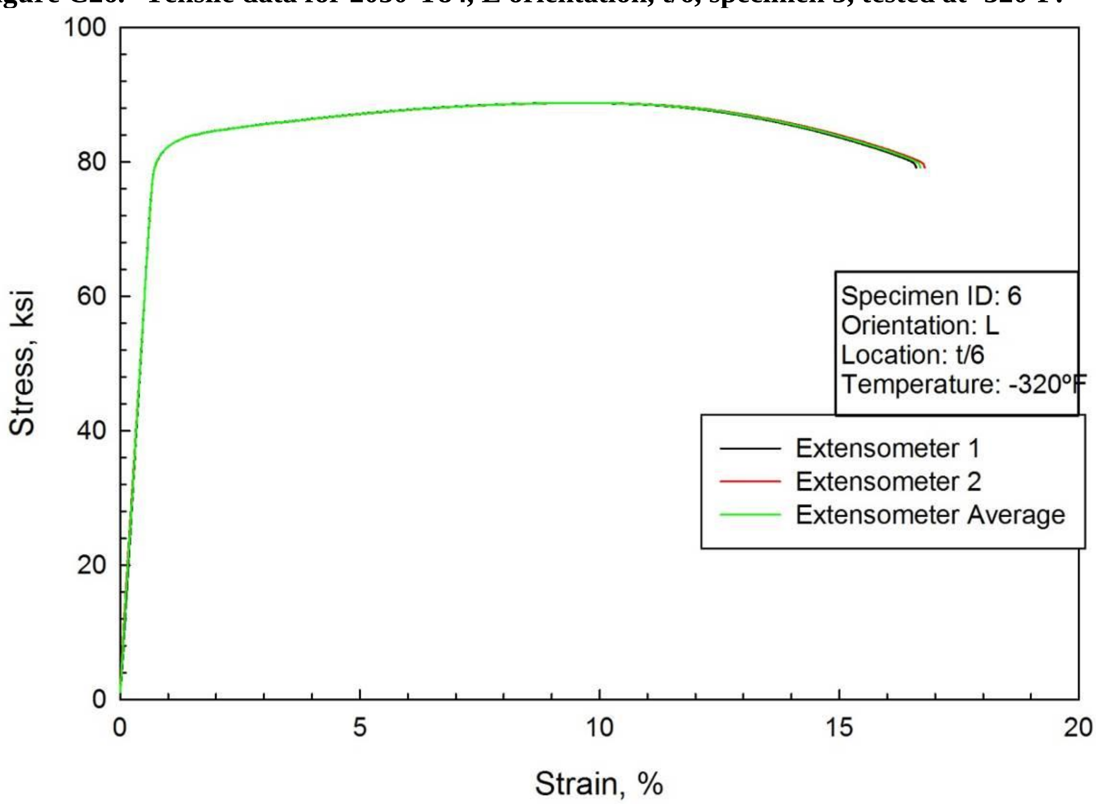

Figure C27. Tensile data for 2050-T84, L orientation, t/6, specimen 6, tested at -320ºF.

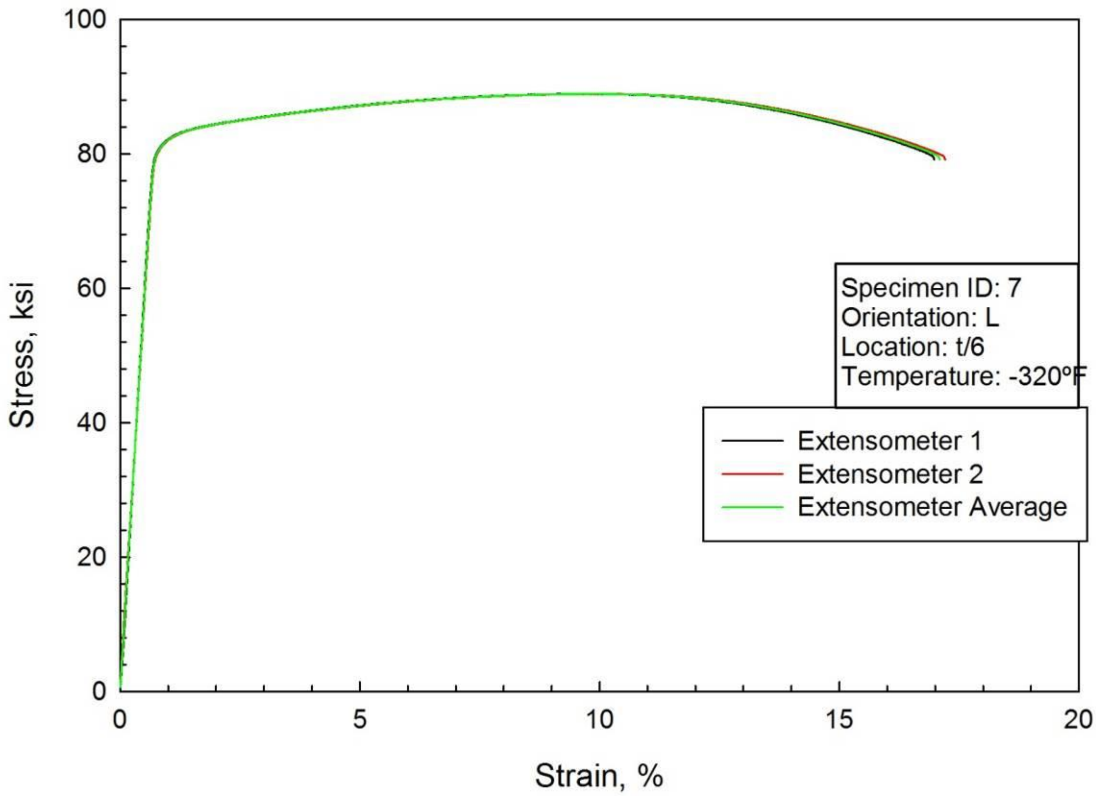

Figure C28. Tensile data for 2050-T84, L orientation, t/6, specimen 7, tested at -320ºF.

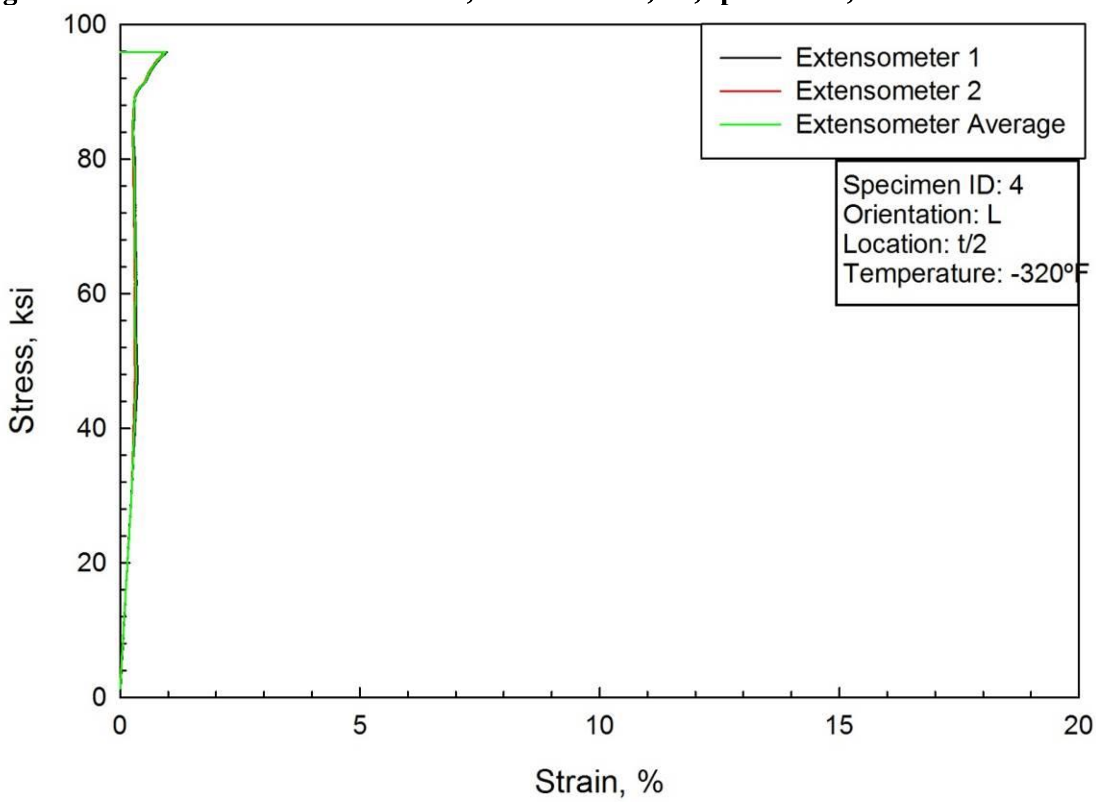

Figure C29. Tensile data for 2050-T84, L orientation, t/2, specimen 4, tested at -320ºF.

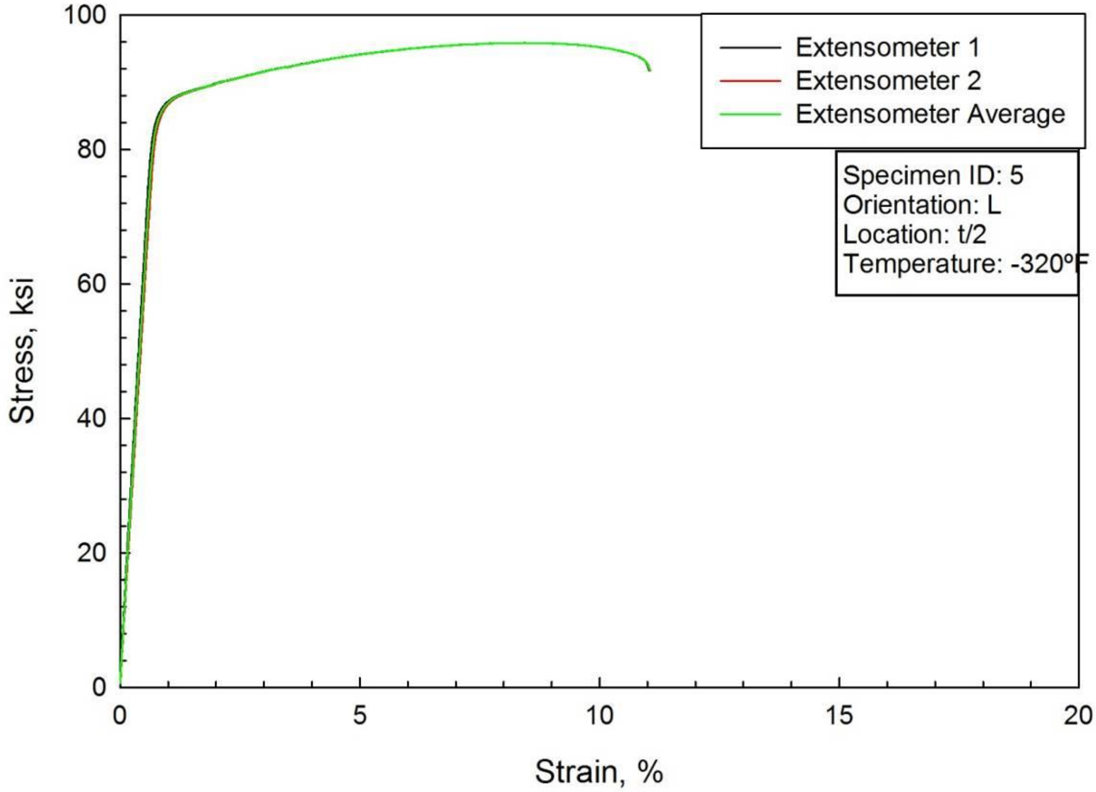

Figure C30. Tensile data for 2050-T84, L orientation, t/2, specimen 5, tested at -320ºF.

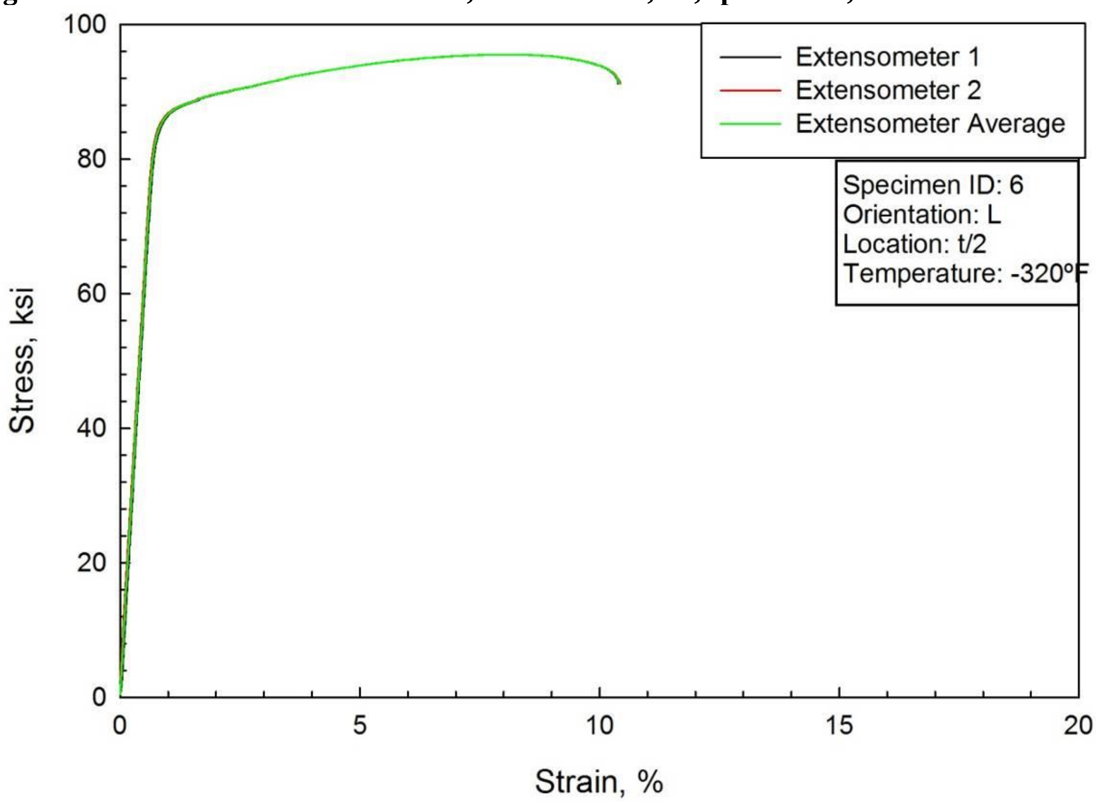

Figure C31. Tensile data for 2050-T84, L orientation, t/2, specimen 6, tested at -320ºF.

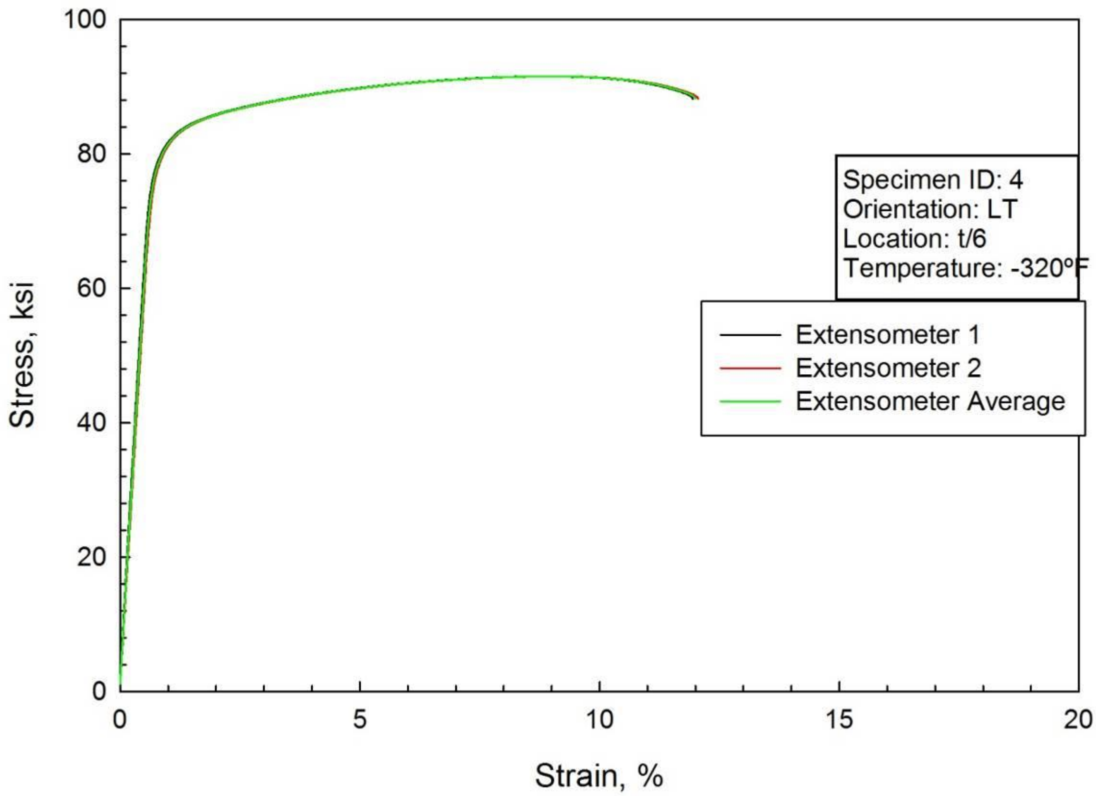

Figure C32. Tensile data for 2050-T84, LT orientation, t/6, specimen 4, tested at -320ºF.

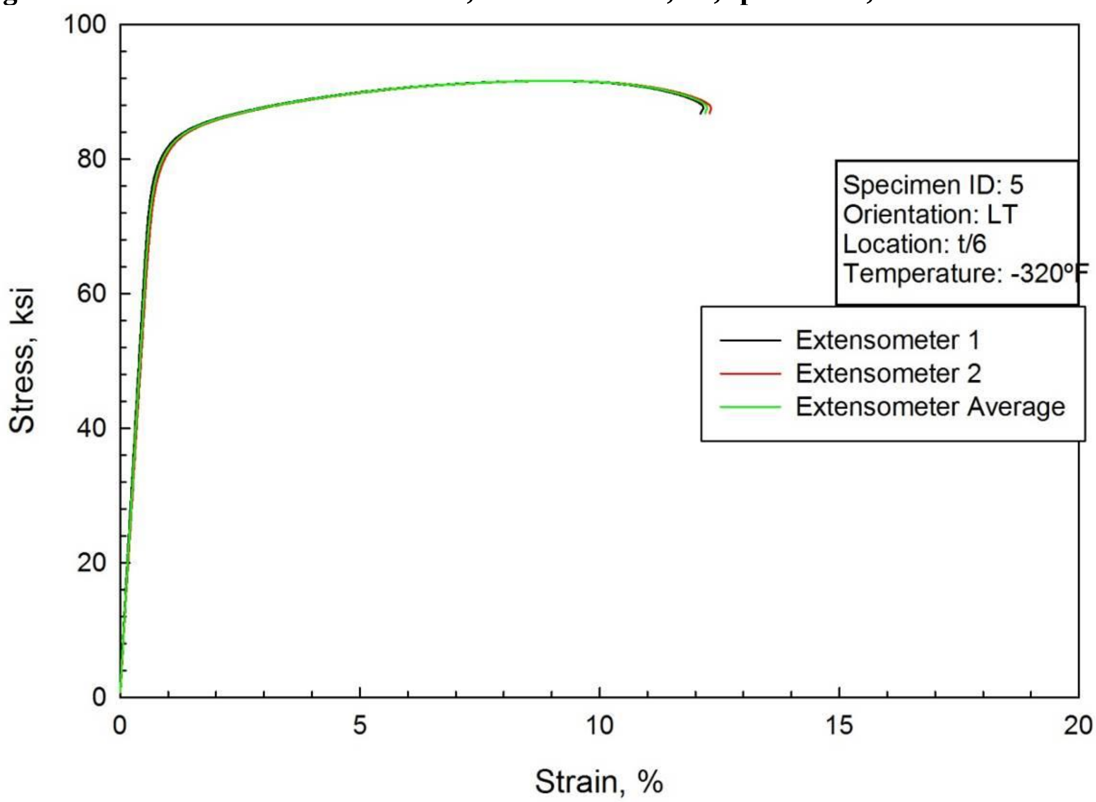

Figure C33. Tensile data for 2050-T84, LT orientation, t/6, specimen 5, tested at -320ºF.

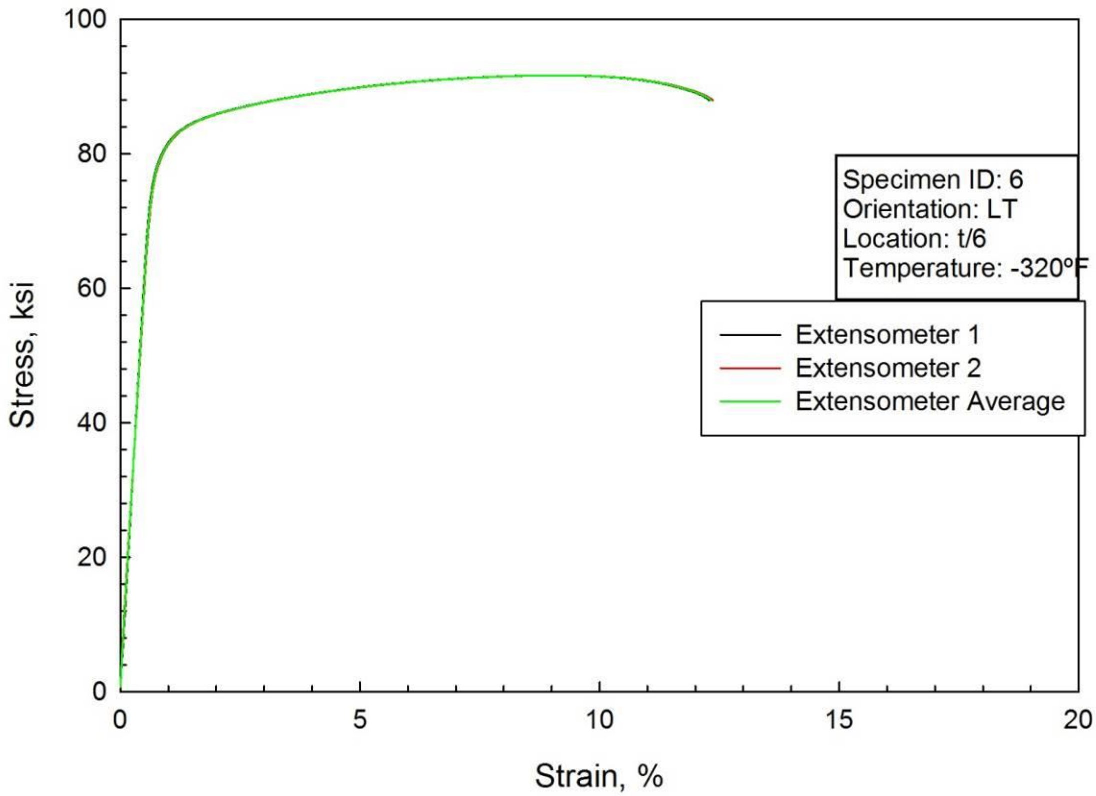

Figure C34. Tensile data for 2050-T84, LT orientation, t/6, specimen 6, tested at -320ºF.

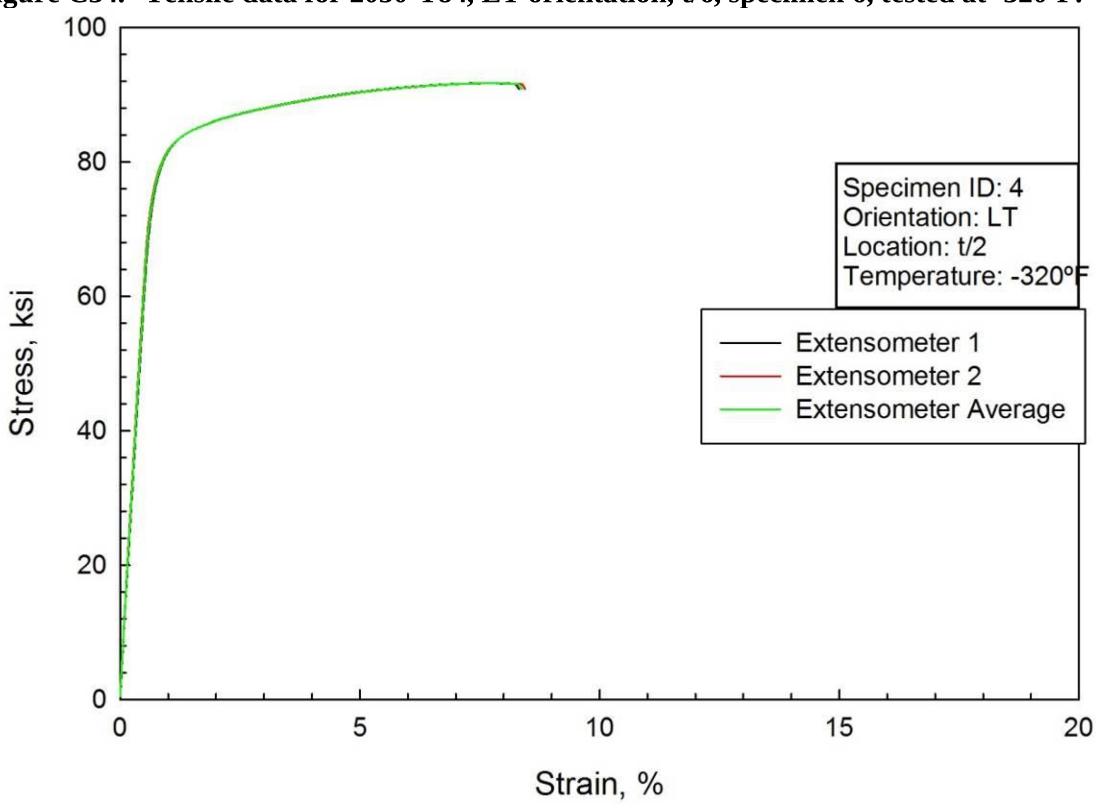

Figure C35. Tensile data for 2050-T84, LT orientation, t/2, specimen 4, tested at -320ºF.

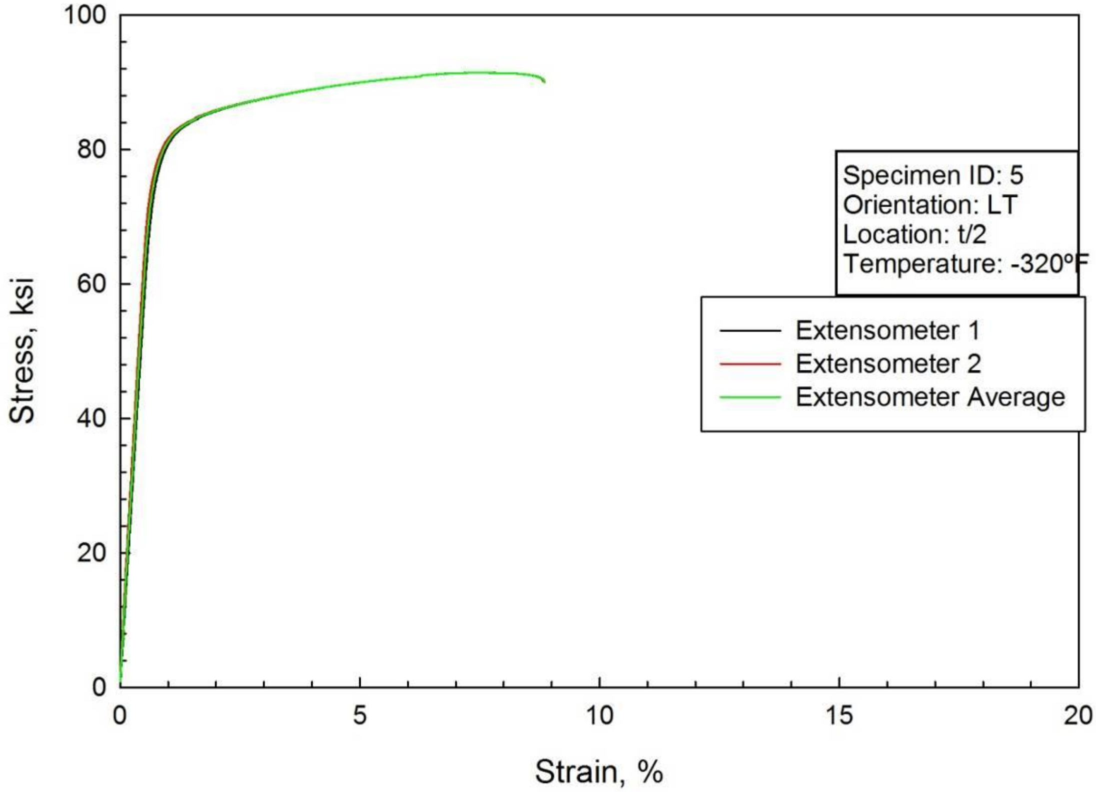

Figure C36. Tensile data for 2050-T84, LT orientation, t/2, specimen 5, tested at -320ºF.

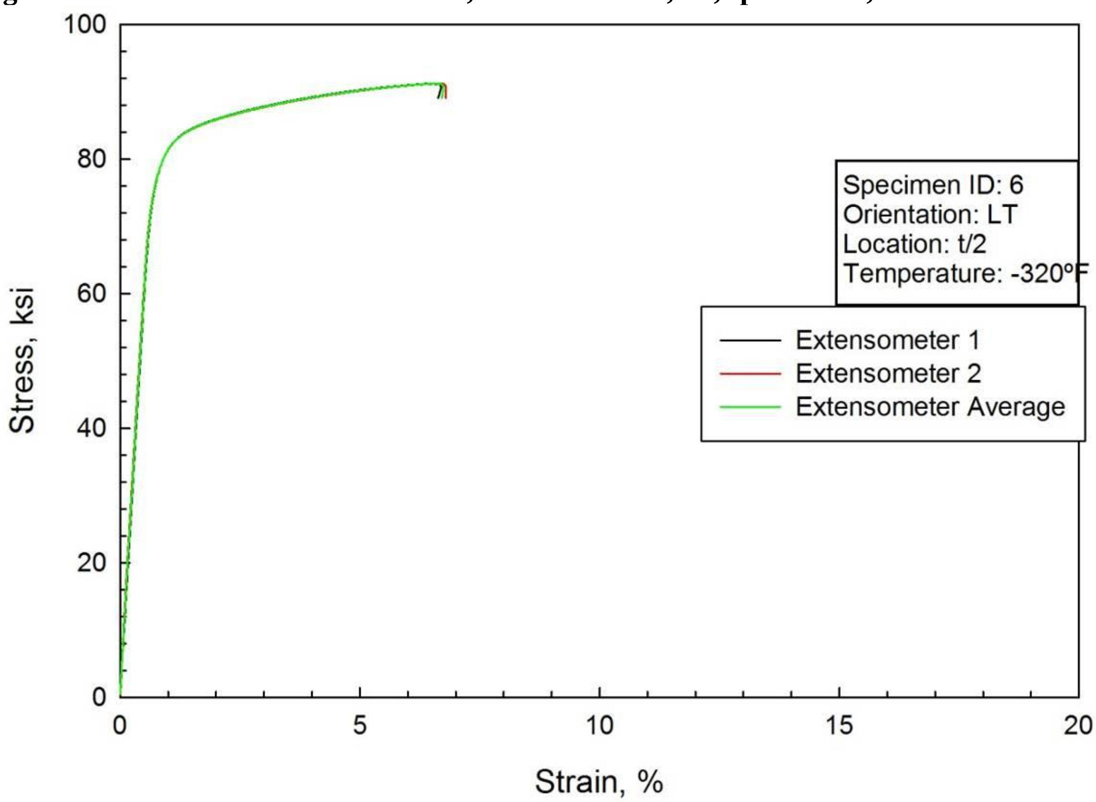

Figure C37. Tensile data for 2050-T84, LT orientation, t/2, specimen 6, tested at -320ºF.

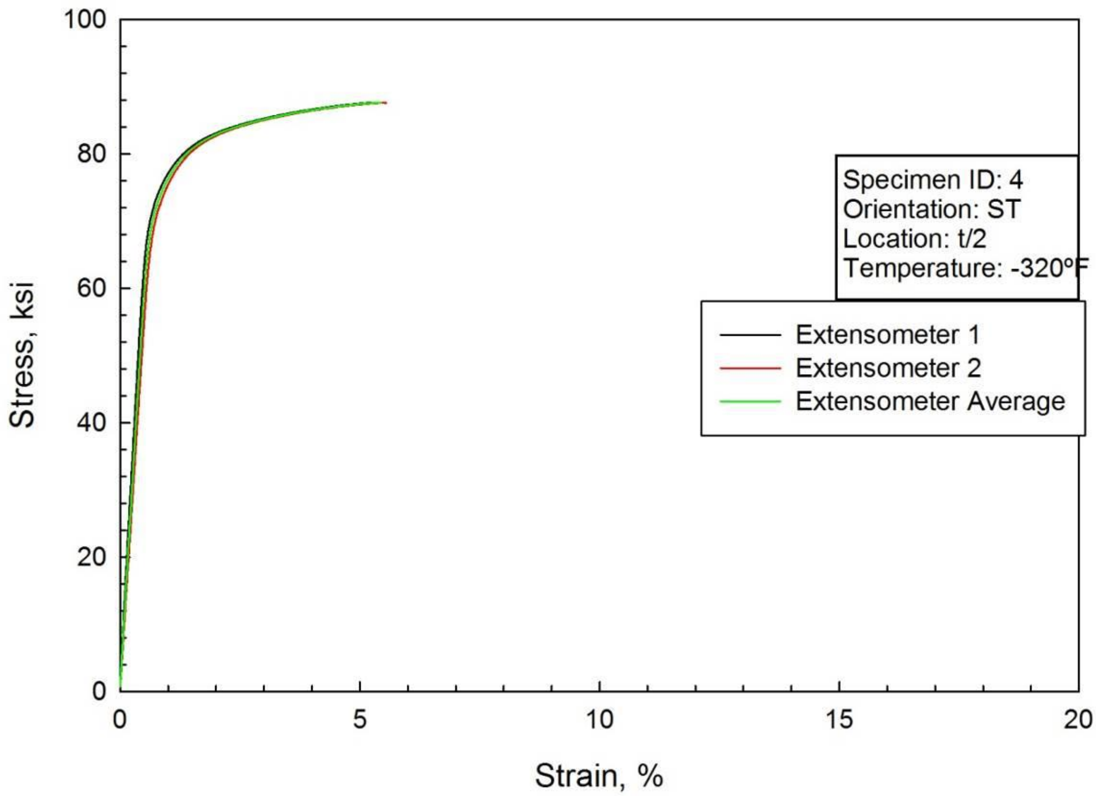

Figure C38. Tensile data for 2050-T84, ST orientation, t/2, specimen 4, tested at -320ºF.

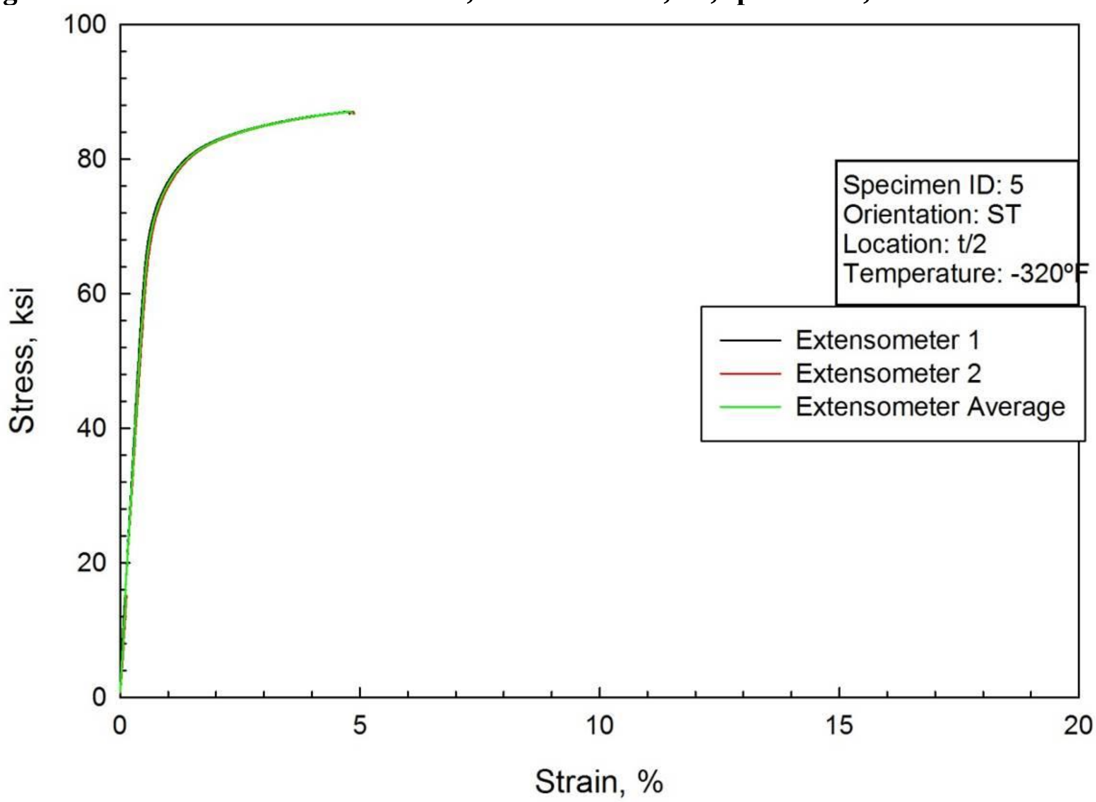

Figure C39. Tensile data for 2050-T84, ST orientation, t/2, specimen 5, tested at -320ºF.

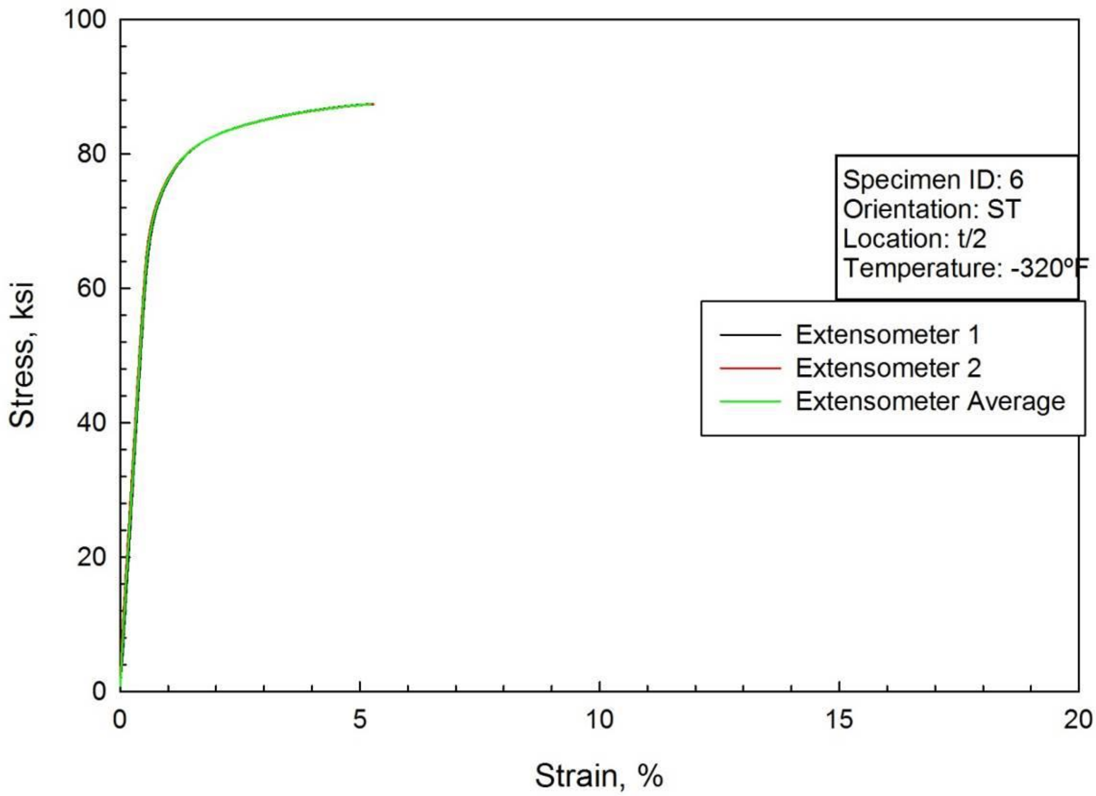

Figure C40. Tensile data for 2050-T84, ST orientation, t/2, specimen 6, tested at -320ºF.

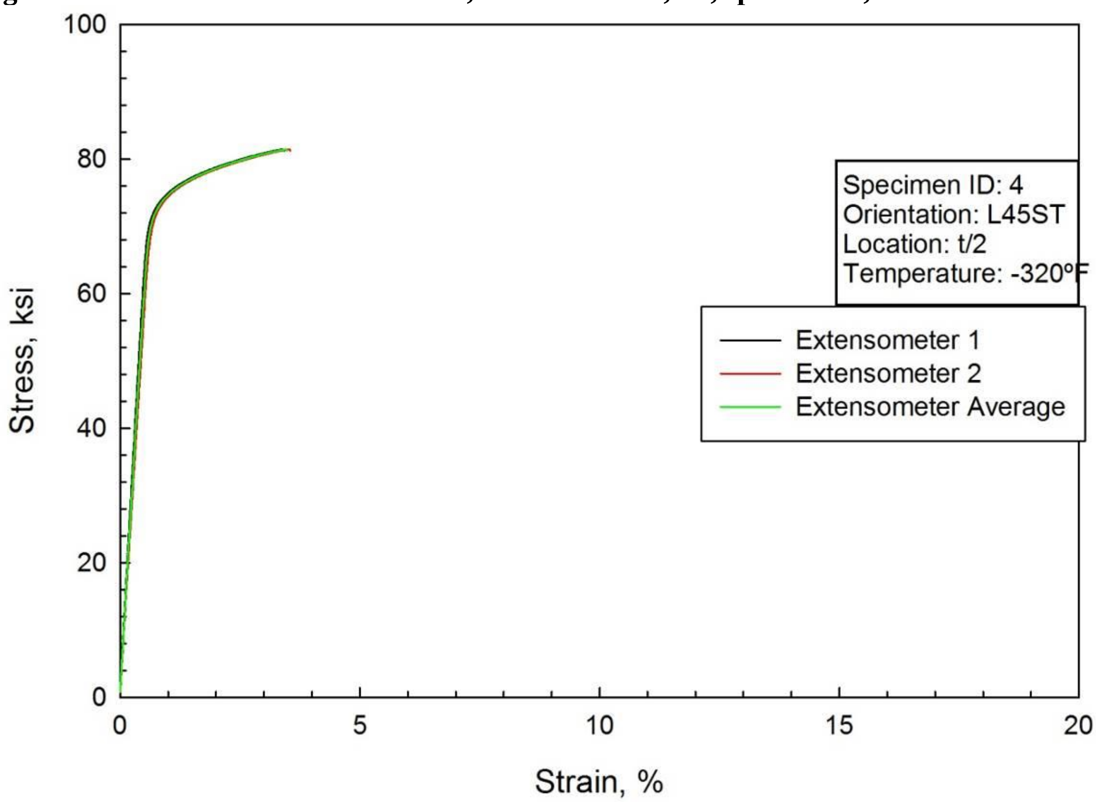

Figure C41. Tensile data for 2050-T84, L45ST orientation, t/2, specimen 4, tested at -320ºF.

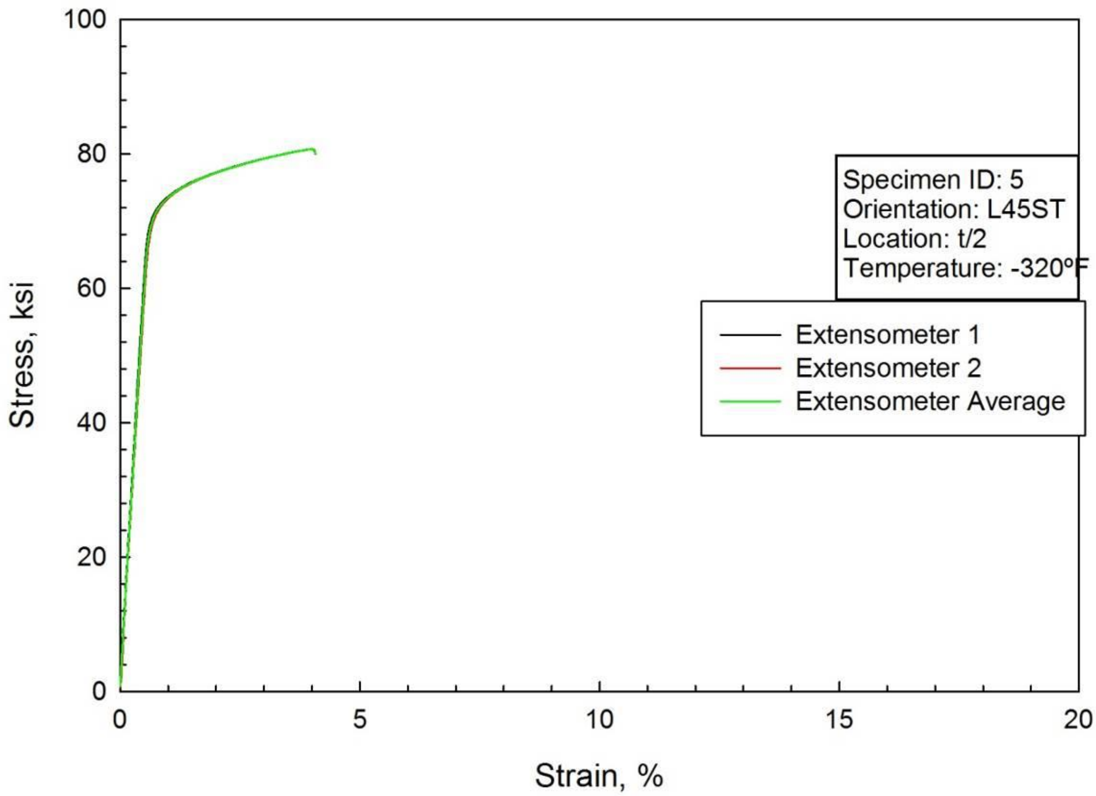

Figure C42. Tensile data for 2050-T84, L45ST orientation, t/2, specimen 5, tested at -320ºF.

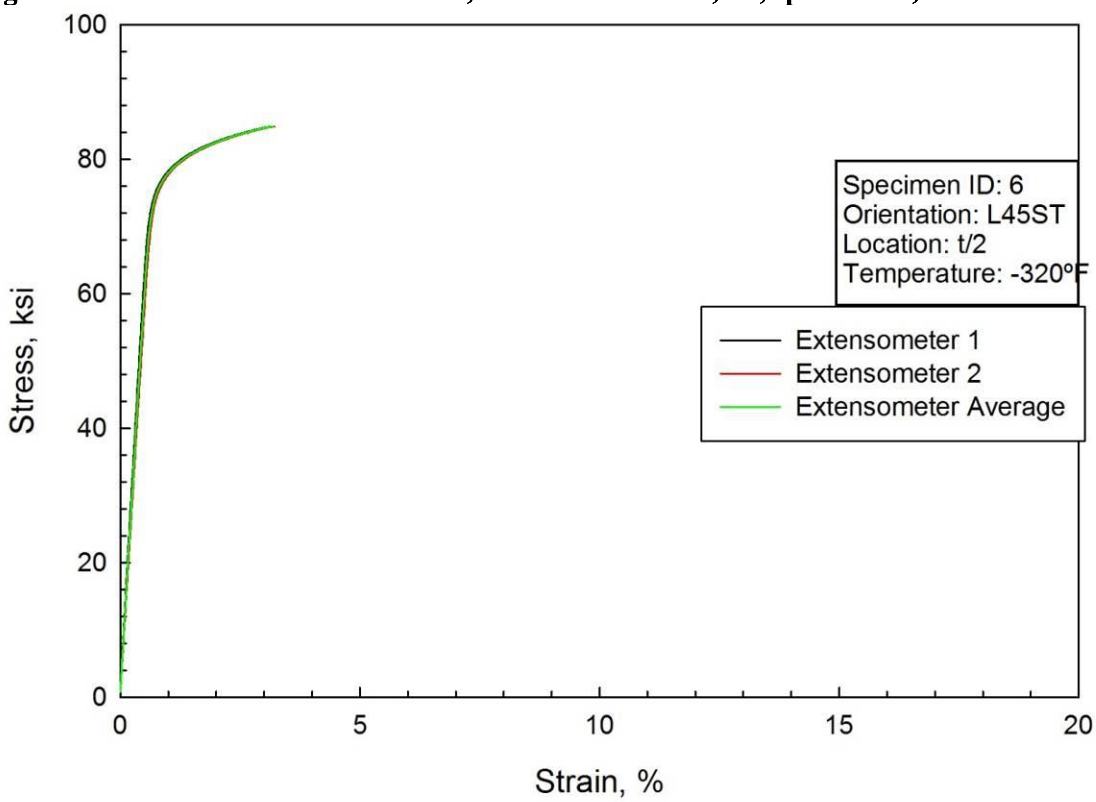

Figure C43. Tensile data for 2050-T84, L45ST orientation, t/2, specimen 6, tested at -320ºF.

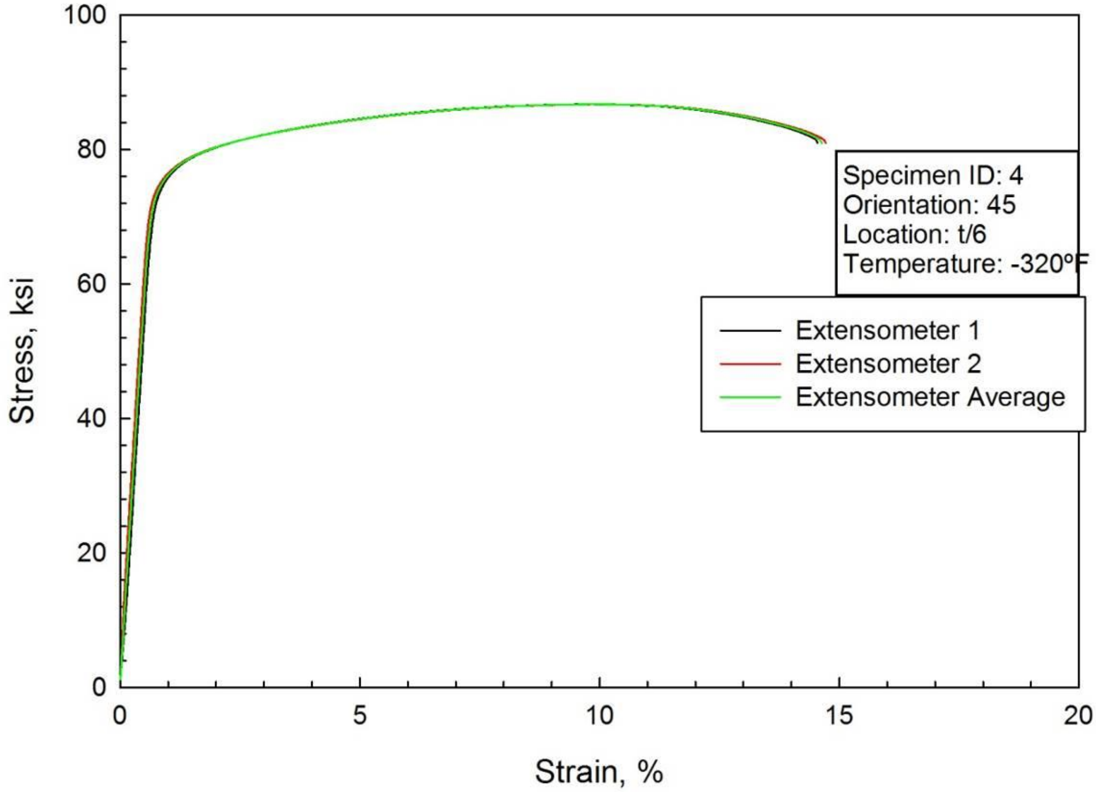

Figure C44. Tensile data for 2050-T84, 45º orientation, t/6, specimen 4, tested at -320ºF.

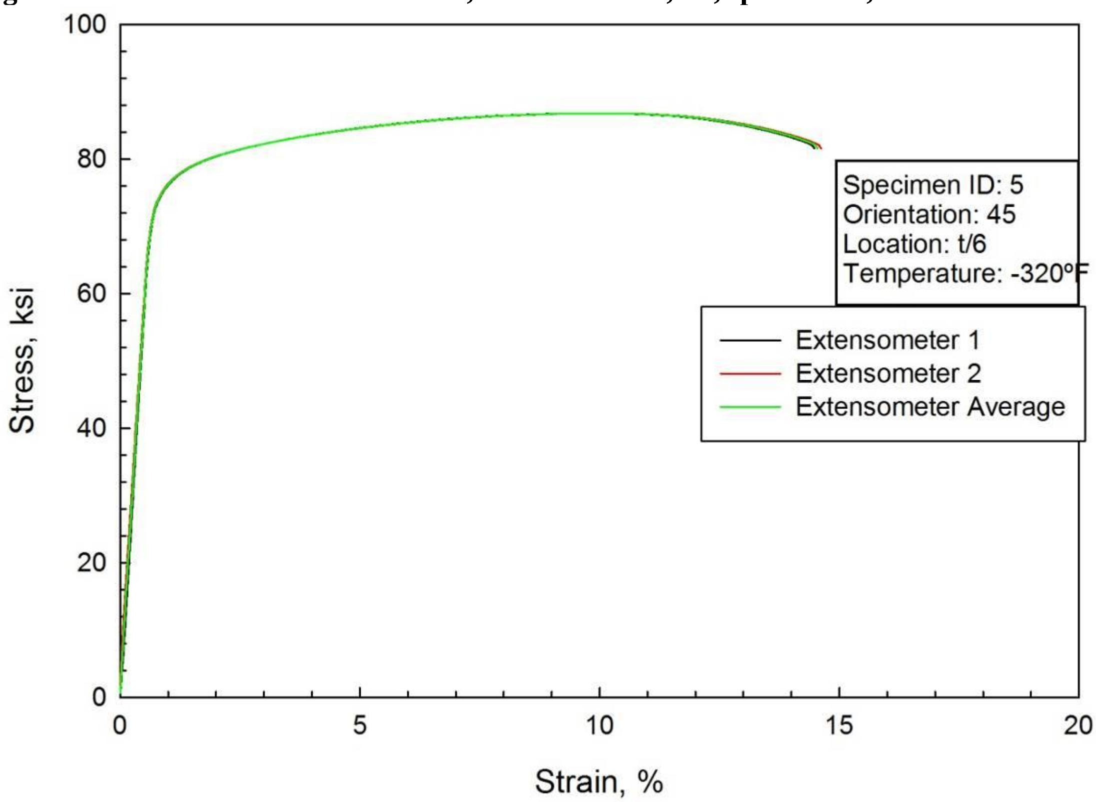

Figure C45. Tensile data for 2050-T84, 45º orientation, t/6, specimen 5, tested at -320ºF.

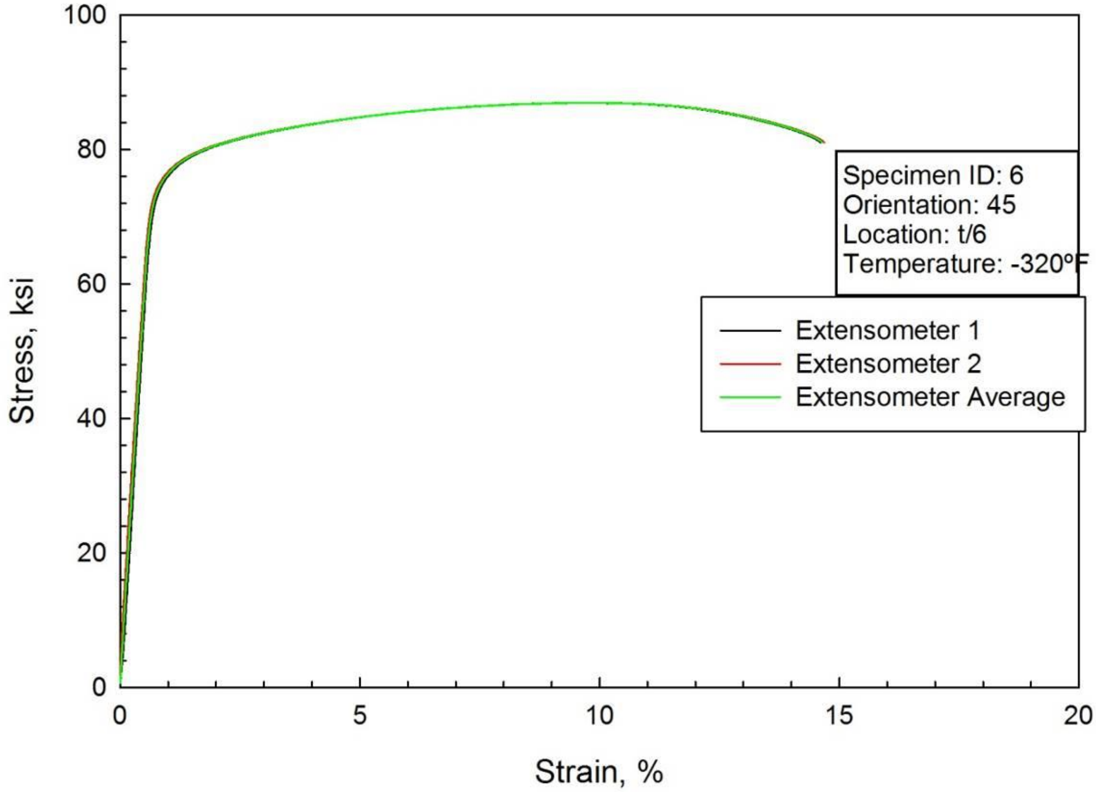

Figure C46. Tensile data for 2050-T84, 45º orientation, t/6, specimen 6, tested at -320ºF.

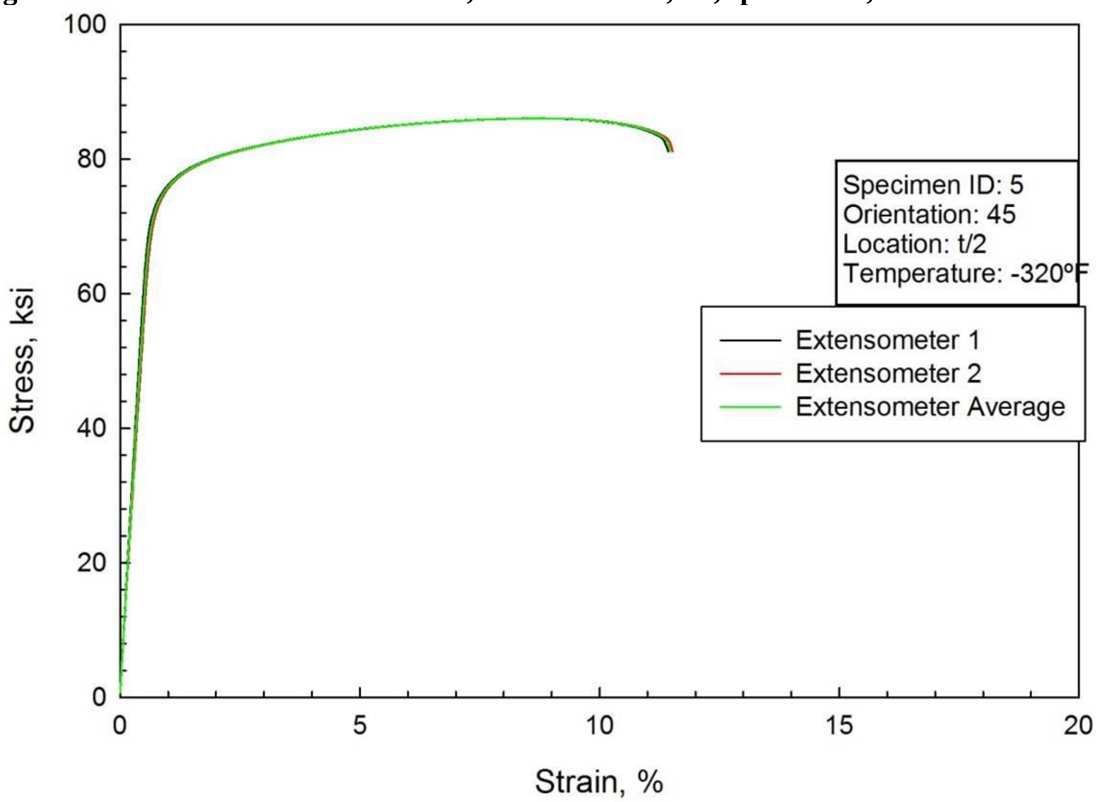

Figure C47. Tensile data for 2050-T84, 45º orientation, t/2, specimen 5, tested at -320ºF.

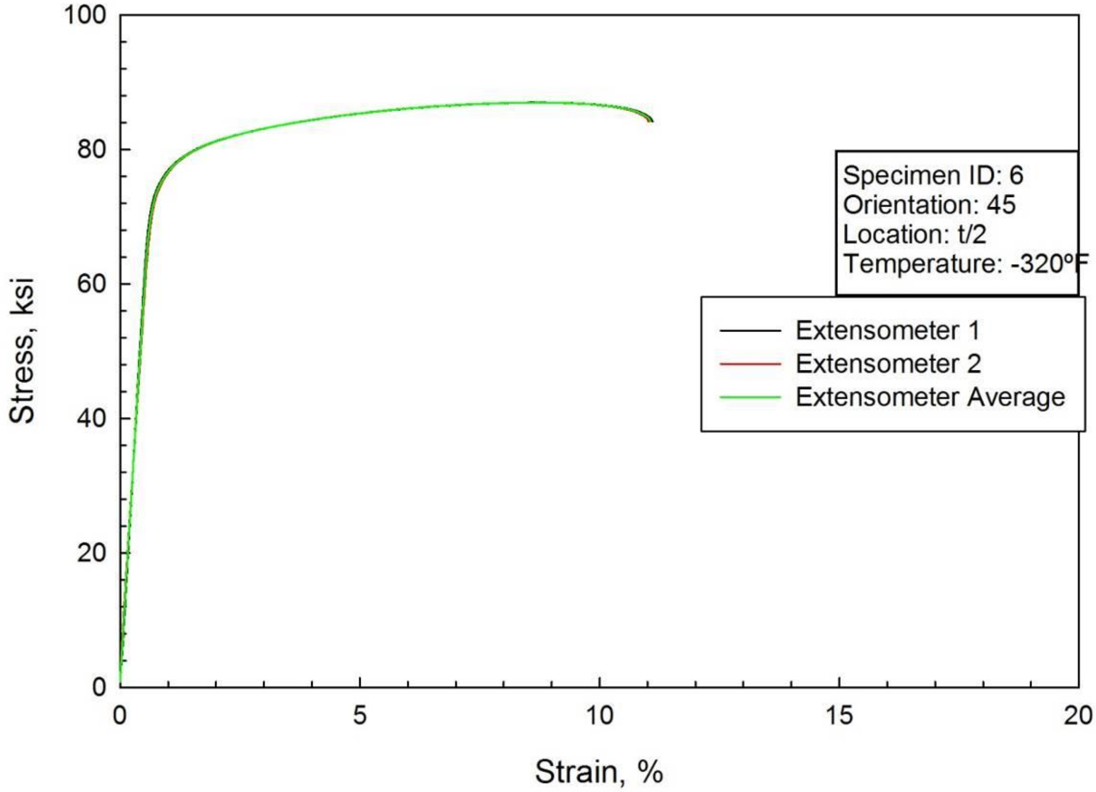

Figure C48. Tensile data for 2050-T84, 45º orientation, t/2, specimen 6, tested at -320ºF.

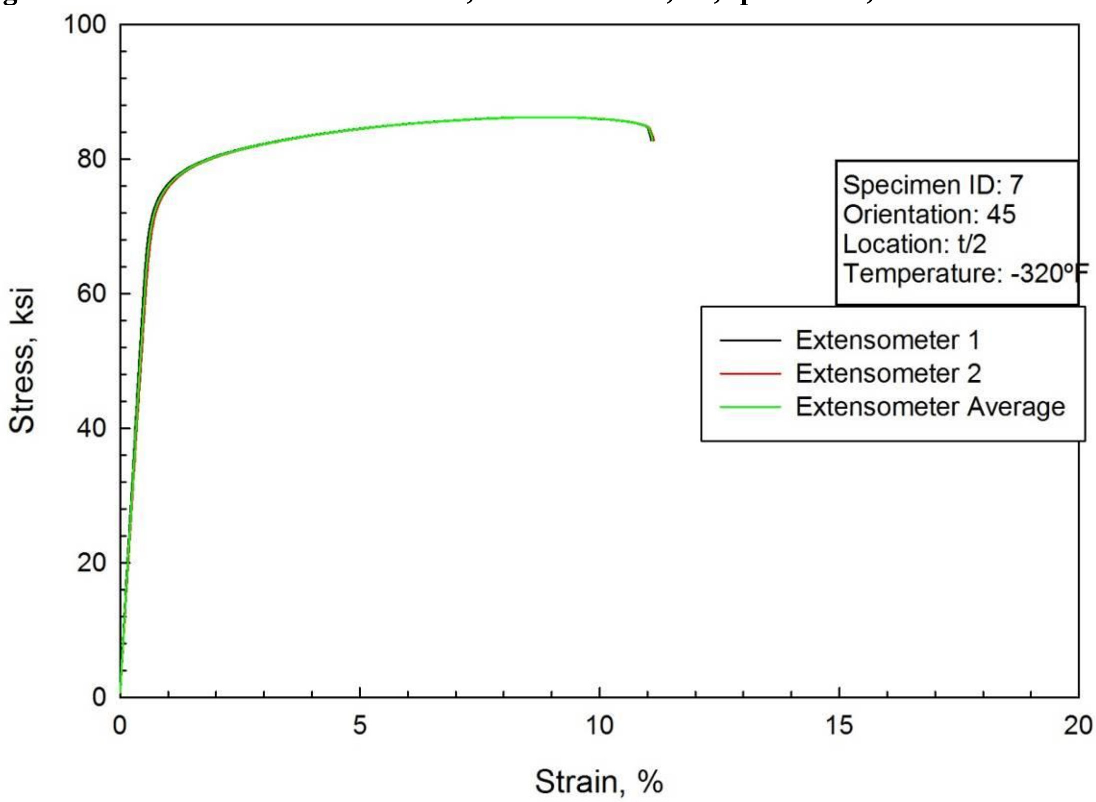

Figure C49. Tensile data for 2050-T84, 45º orientation, t/2, specimen 7, tested at -320ºF.

Appendix D: Individual Stress-Strain Curves for Compression Tests on 4 inch thick 2050-T84 Plate

Absolute value of stress and strain plotted for all tests.

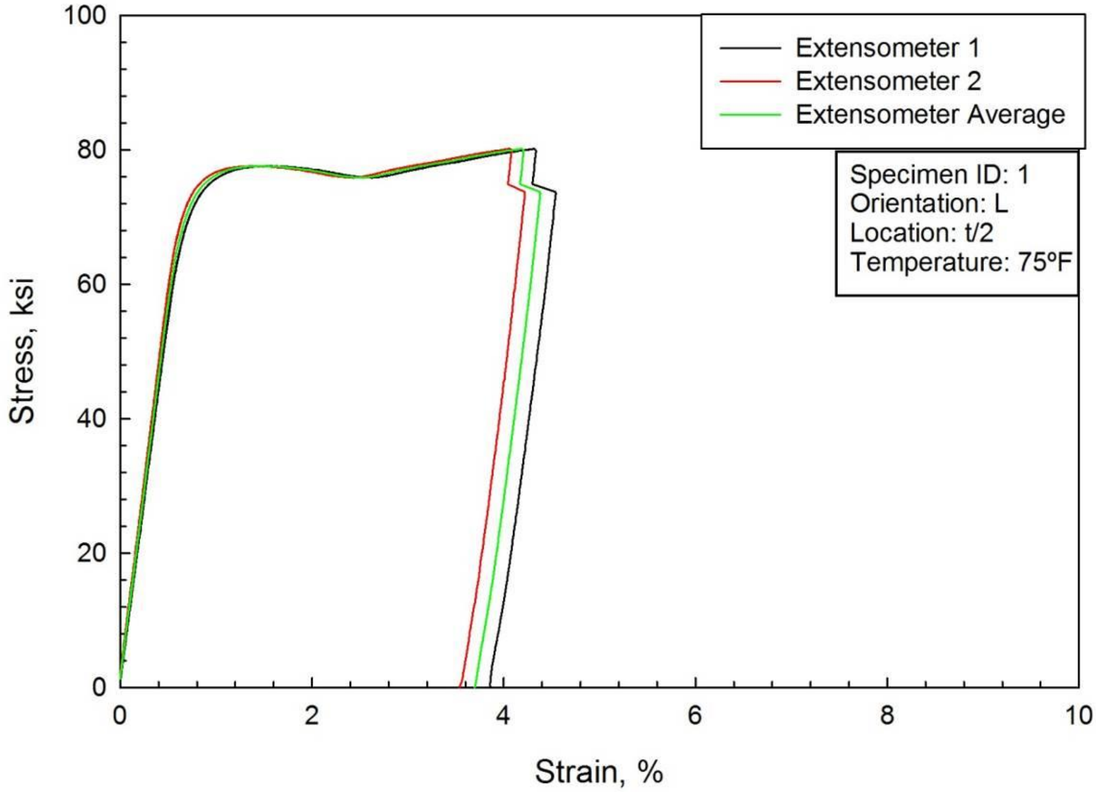

Figure D1. Compression data for 2050-T84, L orientation, t/2, specimen 1, tested at 75ºF.

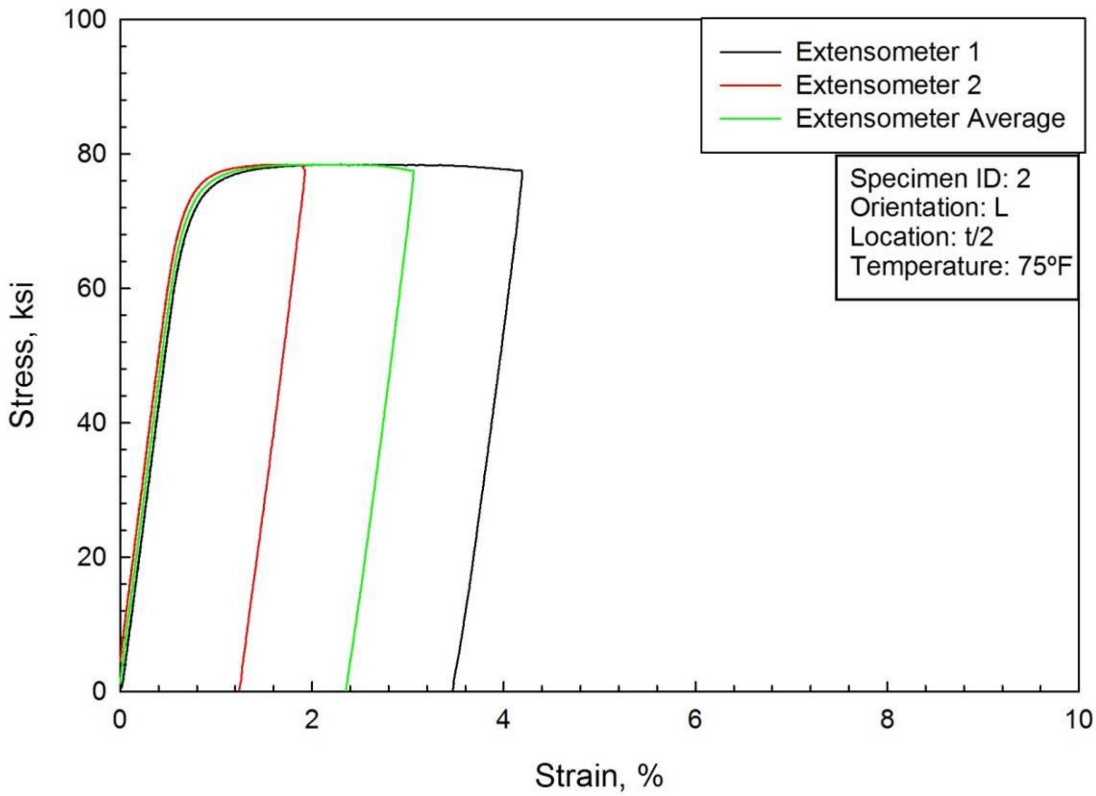

Figure D2. **Compression data for 2050-T84, L orientation, t/2, specimen 2, tested at 75ºF.**

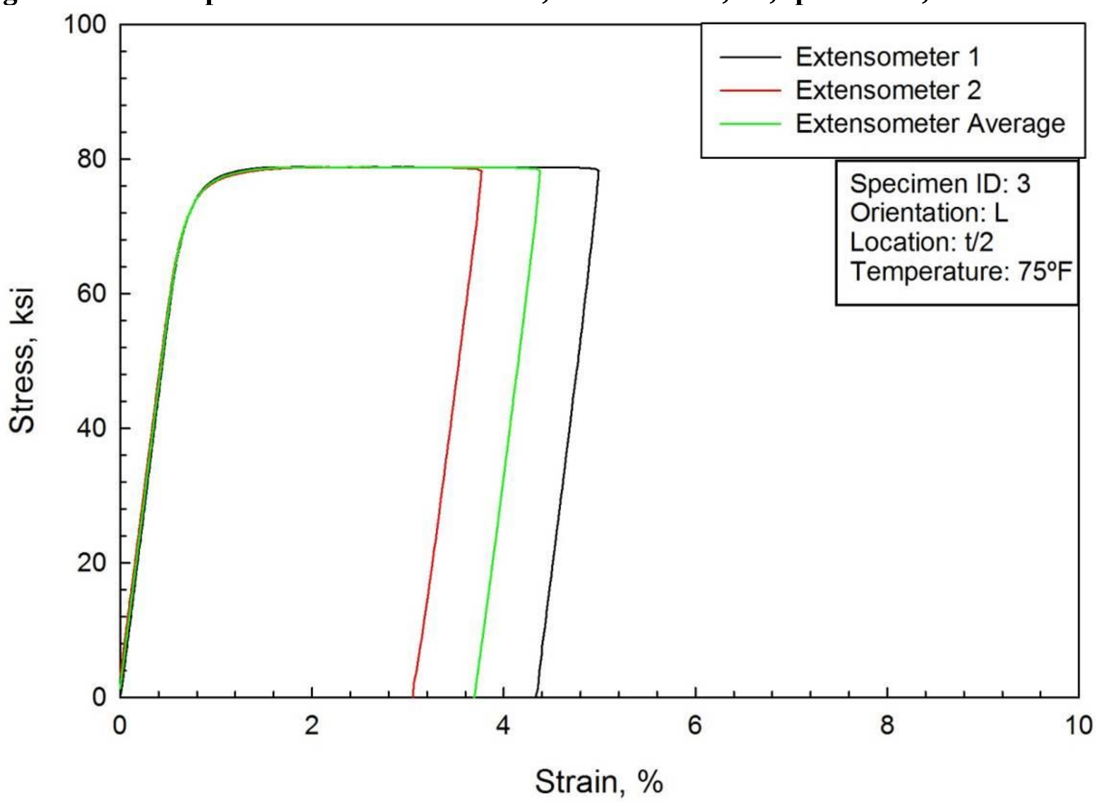

Figure D3. **Compression data for 2050-T84, L orientation, t/2, specimen 3, tested at 75ºF.**

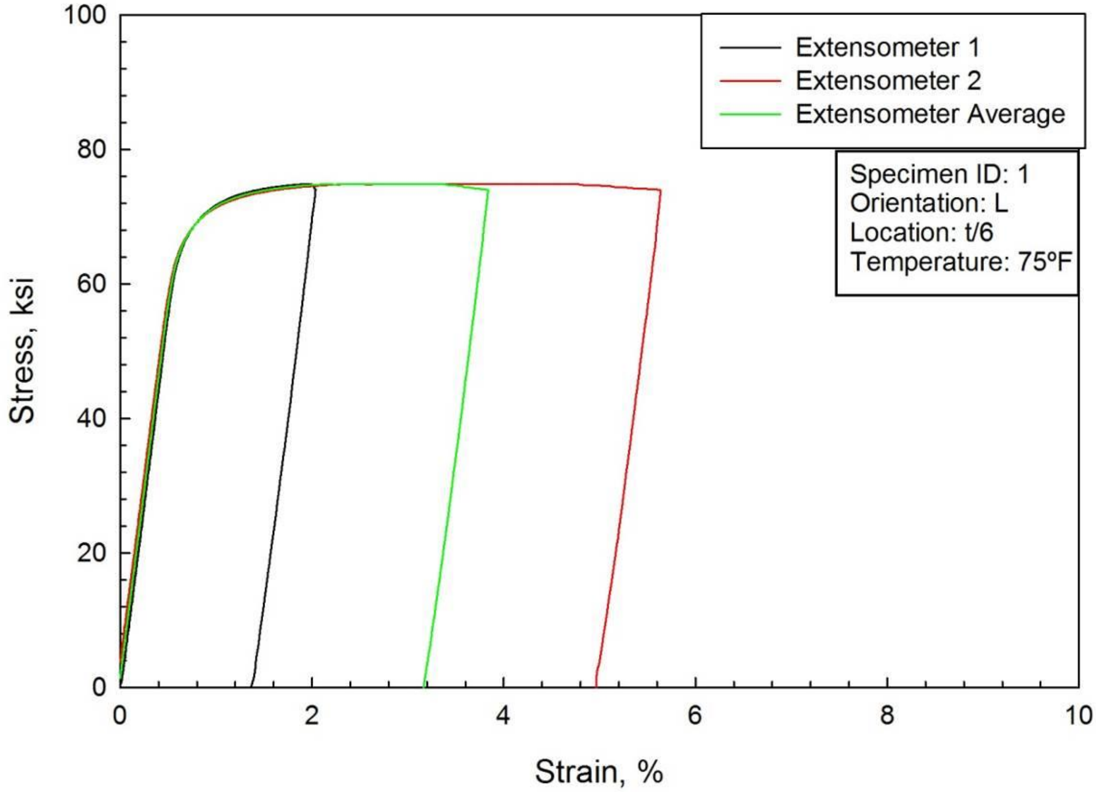

Figure D4. **Compression data for 2050-T84, L orientation, t/6, specimen 1, tested at 75ºF.**

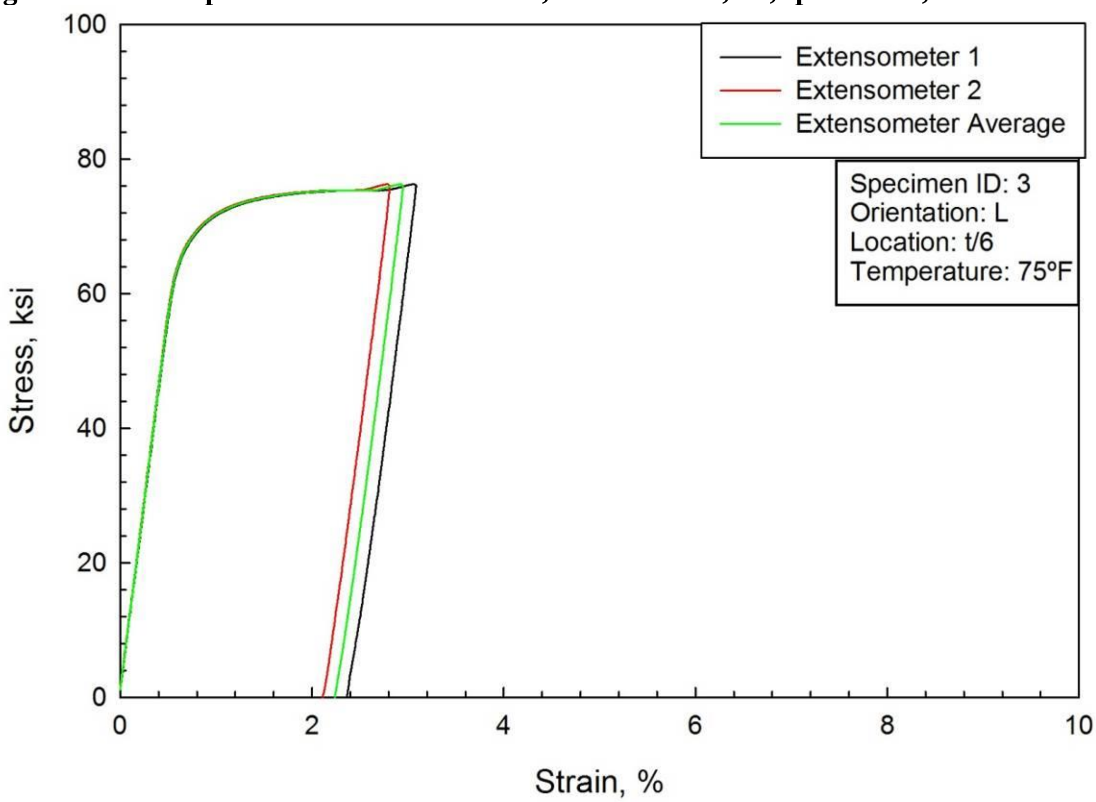

Figure D5. **Compression data for 2050-T84, L orientation, t/6, specimen 3, tested at 75ºF.**

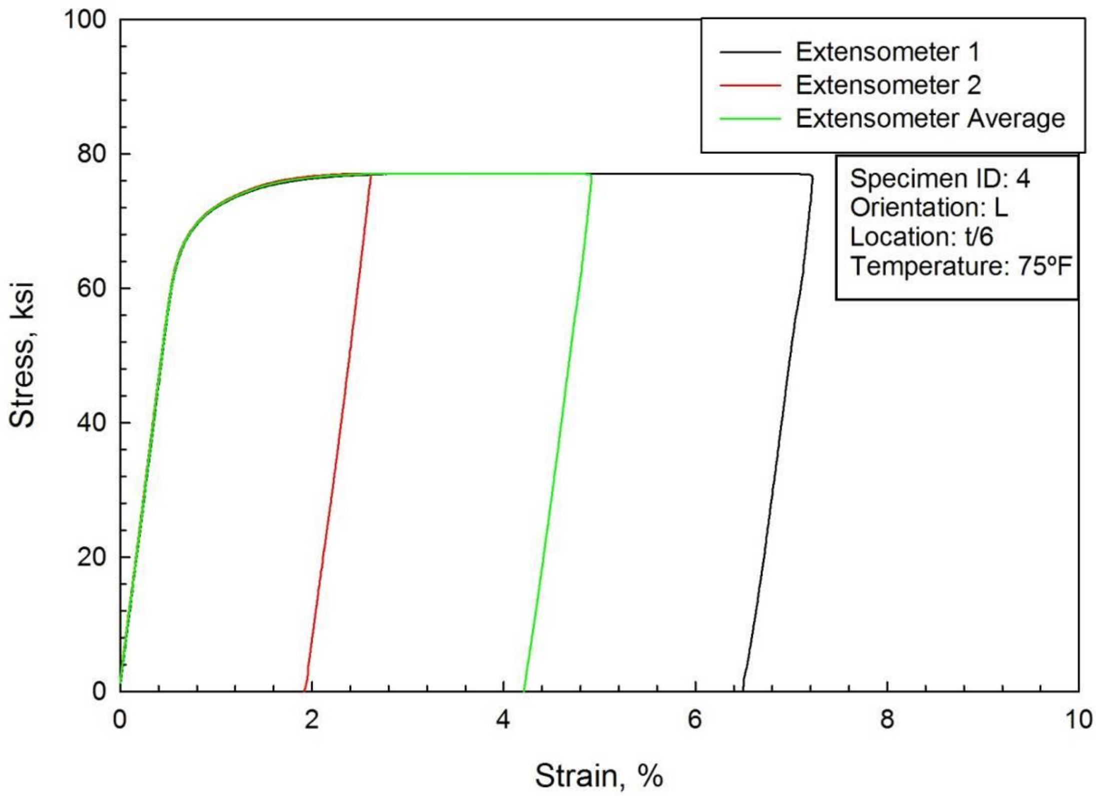

Figure D6. **Compression data for 2050-T84, L orientation, t/6, specimen 4, tested at 75ºF.**

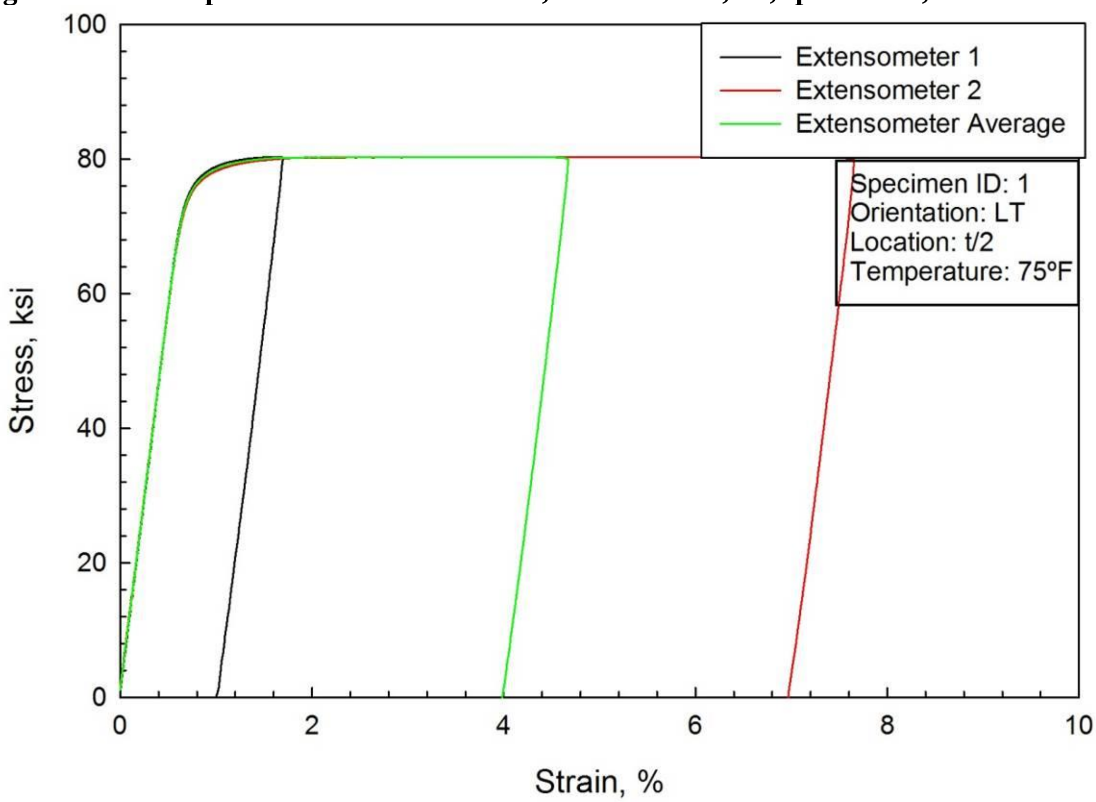

Figure D7. **Compression data for 2050-T84, LT orientation, t/2, specimen 1, tested at 75ºF.**

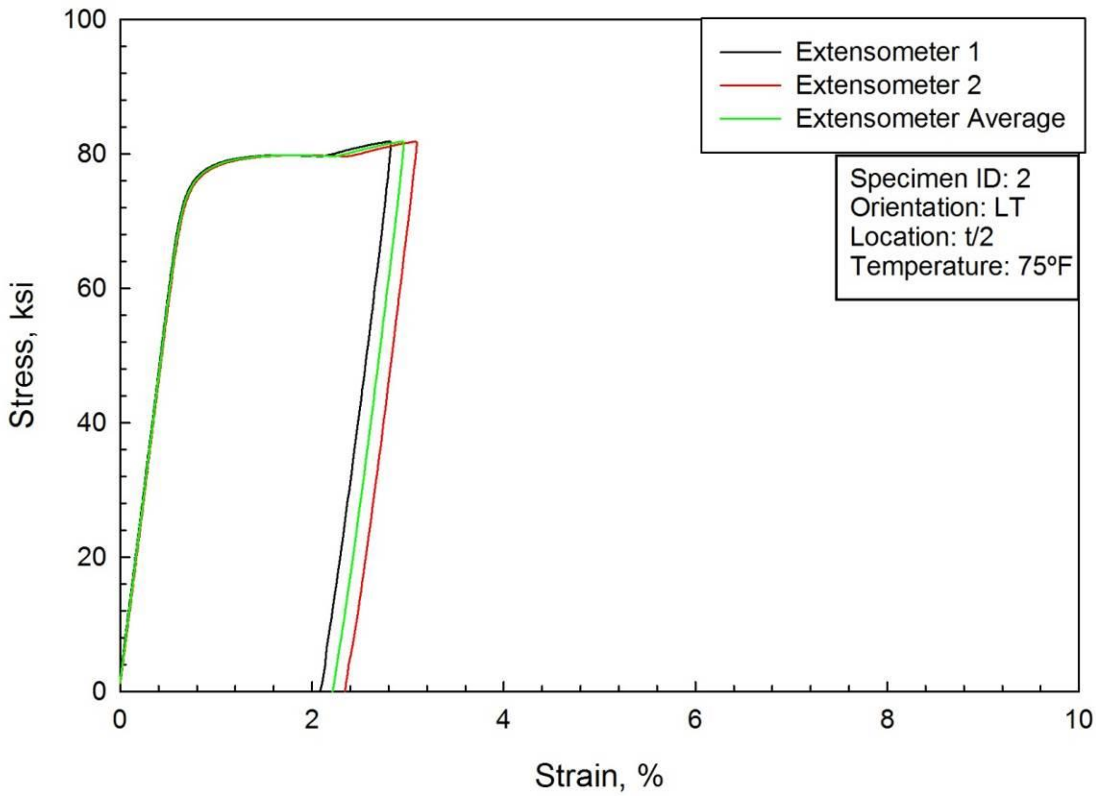

Figure D8. **Compression data for 2050-T84, LT orientation, t/2, specimen 2, tested at 75ºF.**

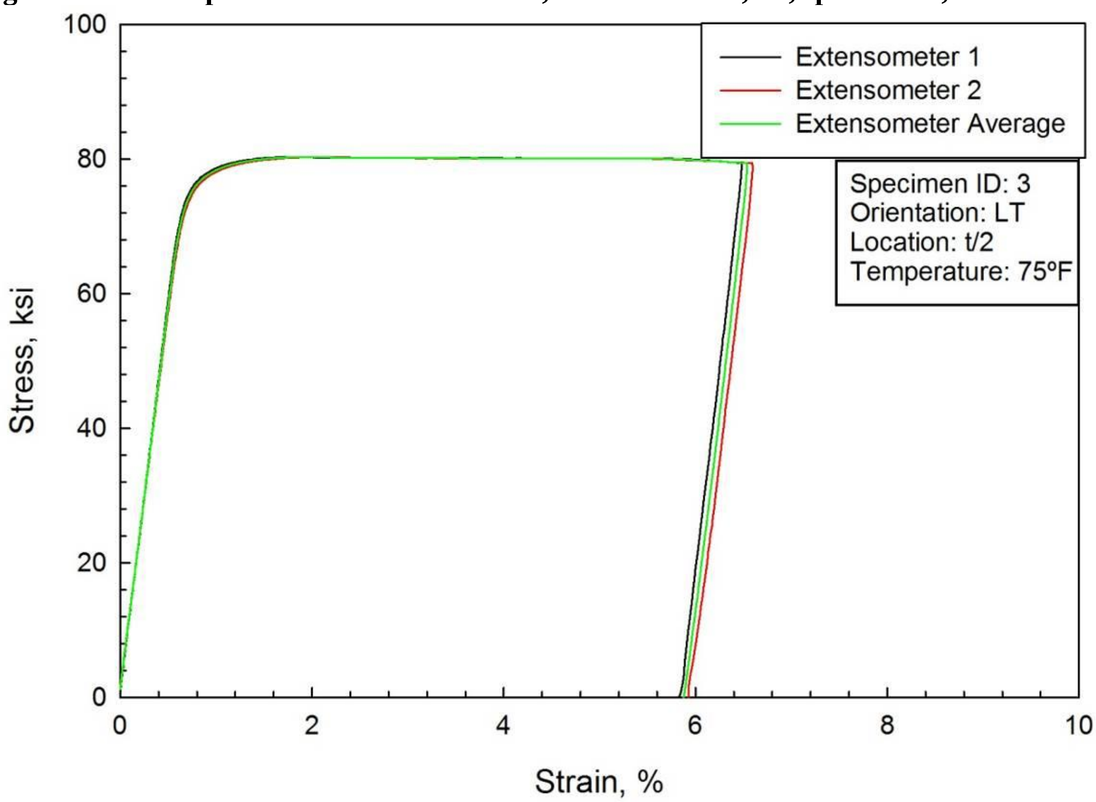

Figure D9. **Compression data for 2050-T84, LT orientation, t/2, specimen 3, tested at 75ºF.**

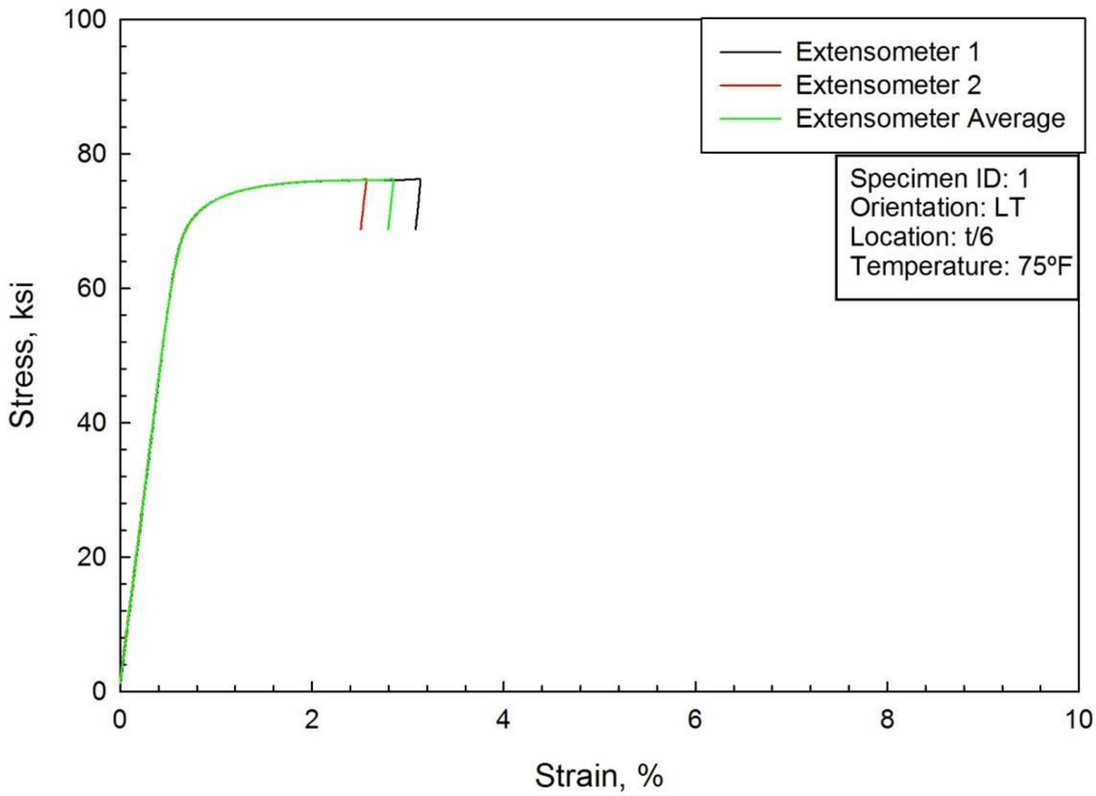

Figure D10. Compression data for 2050-T84, LT orientation, t/6, specimen 1, tested at 75ºF.

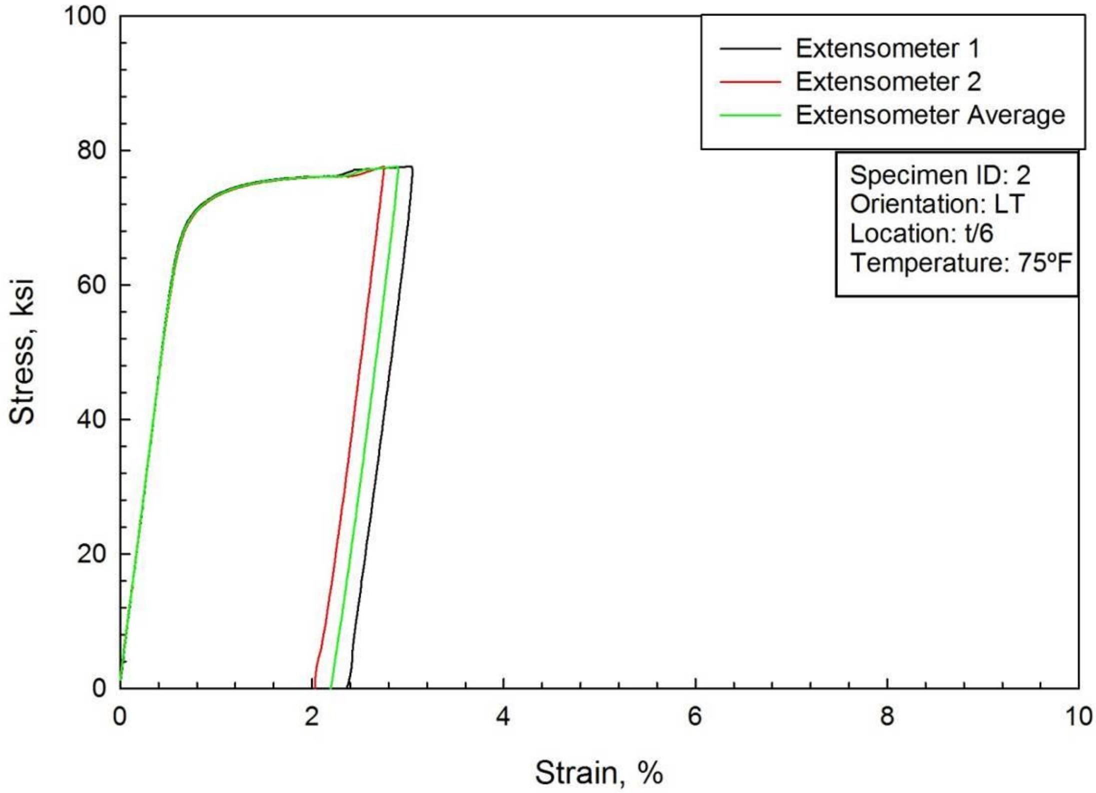

Figure D11. Compression data for 2050-T84, LT orientation, t/6, specimen 2, tested at 75ºF.

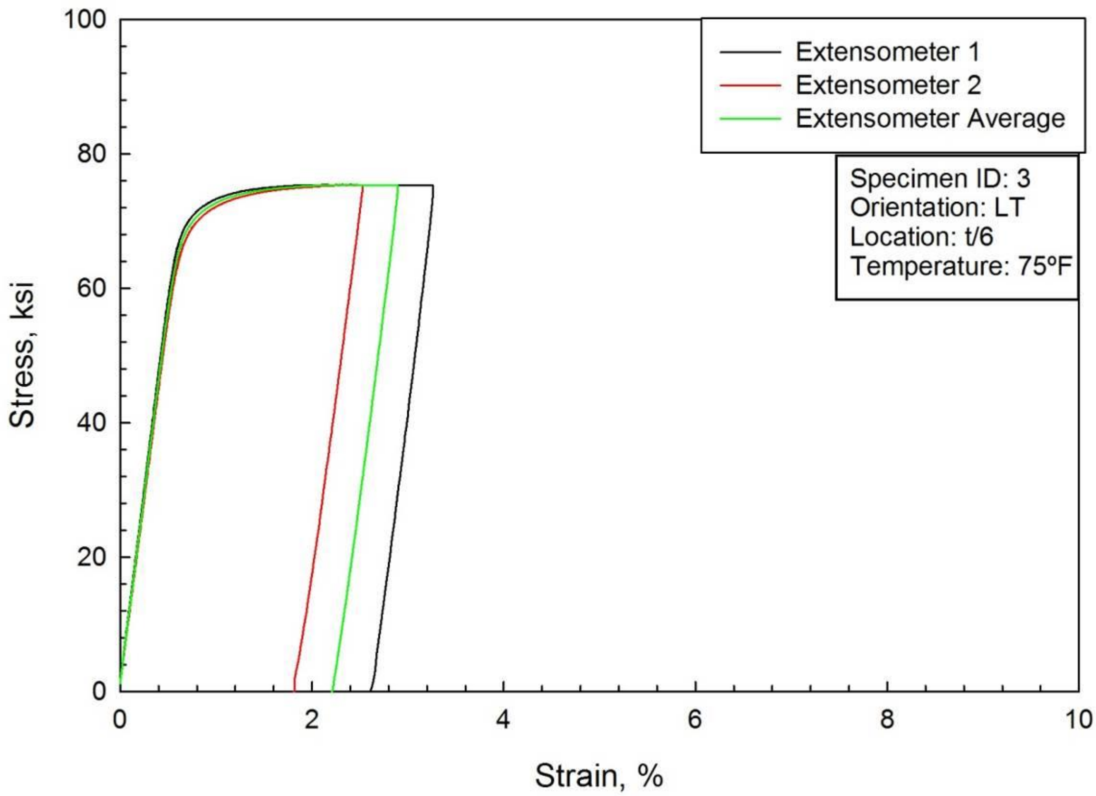

Figure D12. Compression data for 2050-T84, LT orientation, t/6, specimen 3, tested at 75ºF.

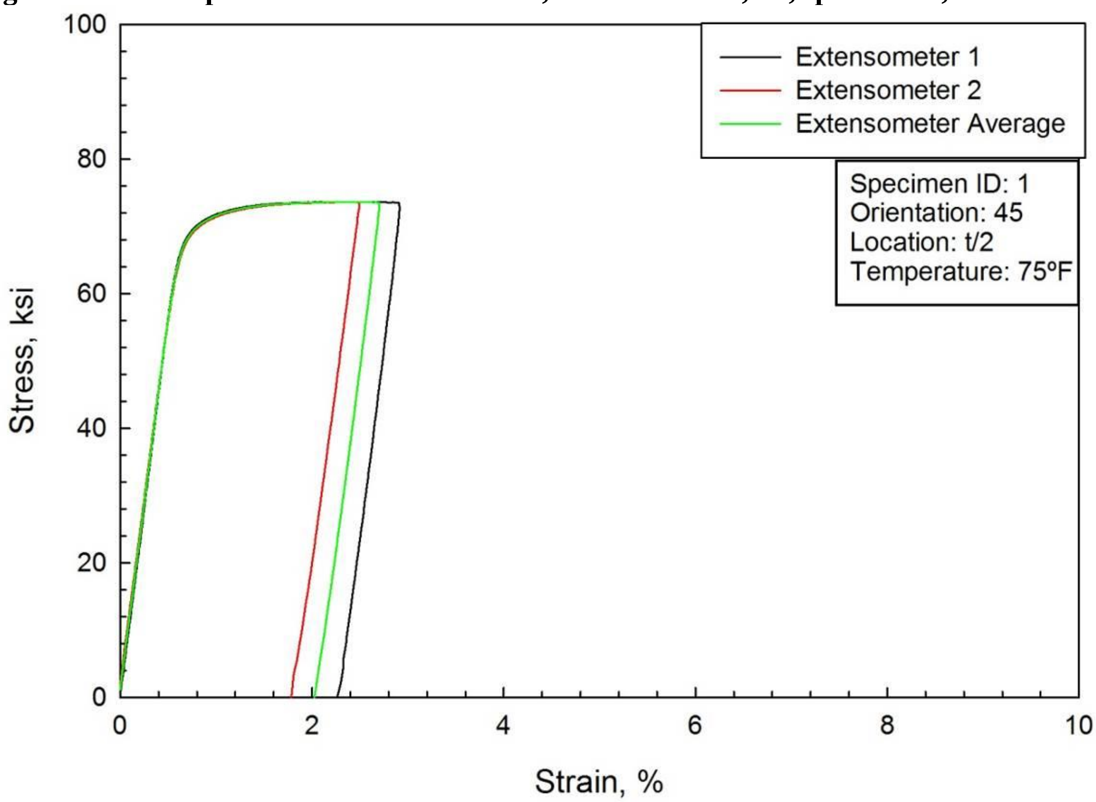

Figure D13. Compression data for 2050-T84, 45º orientation, t/2, specimen 1, tested at 75ºF.

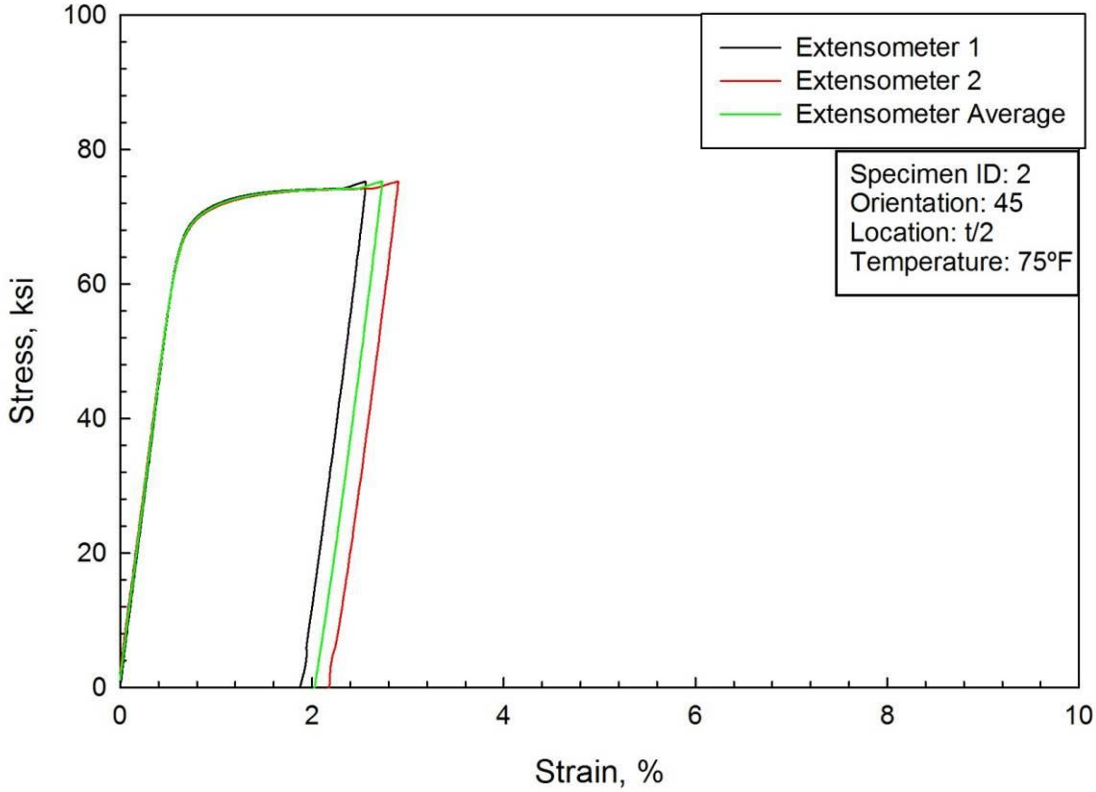

Figure D14. Compression data for 2050-T84, 45º orientation, t/2, specimen 2, tested at 75ºF.

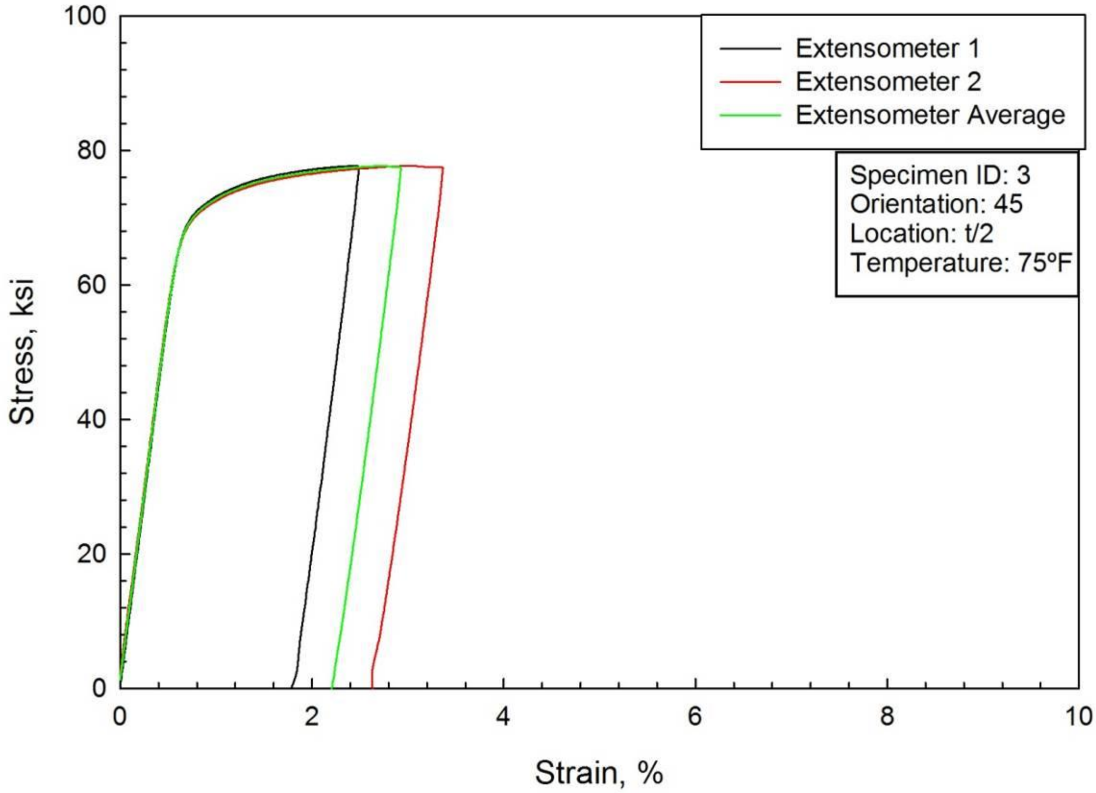

Figure D15. Compression data for 2050-T84, 45º orientation, t/2, specimen 3, tested at 75ºF.

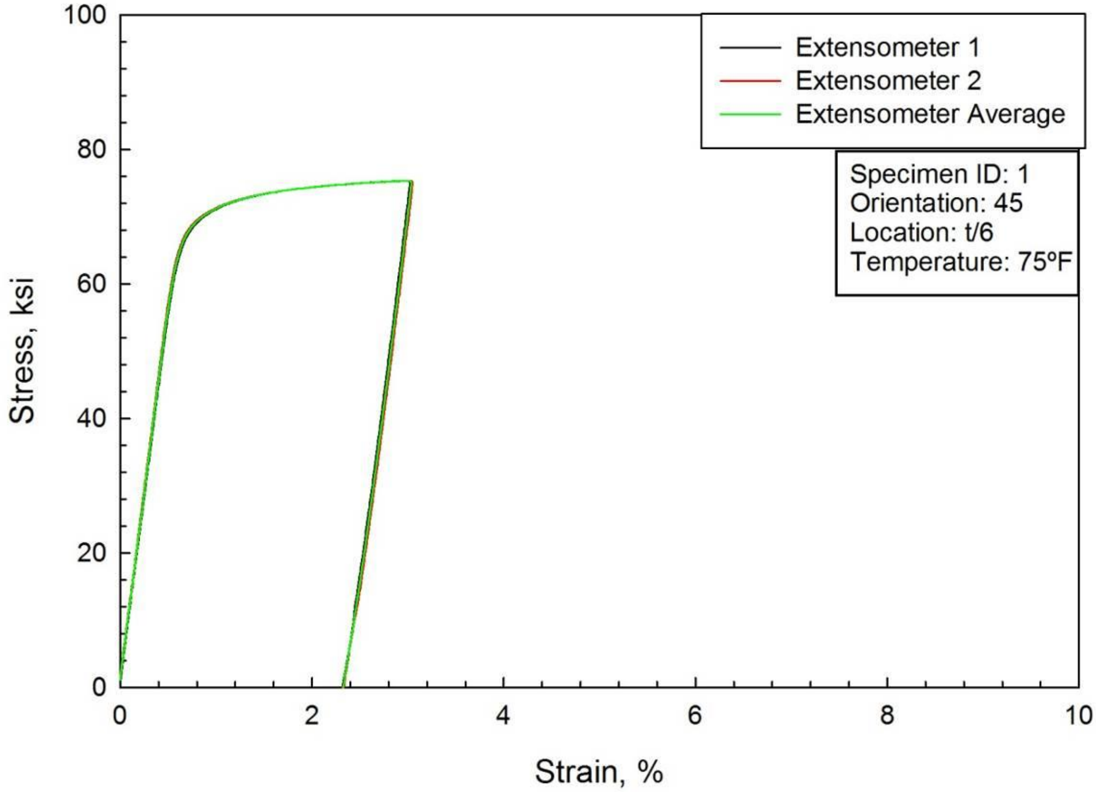

Figure D16. Compression data for 2050-T84, 45º orientation, t/6, specimen 1, tested at 75ºF.

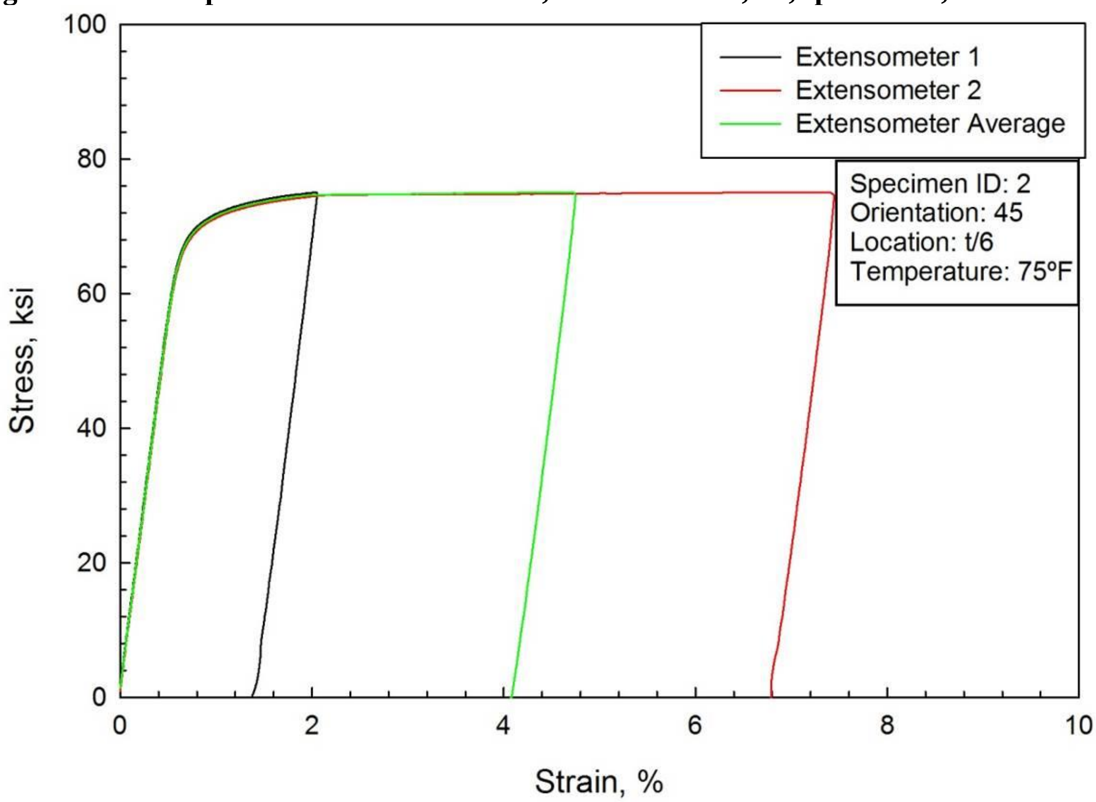

Figure D17. Compression data for 2050-T84, 45º orientation, t/6, specimen 2, tested at 75ºF.

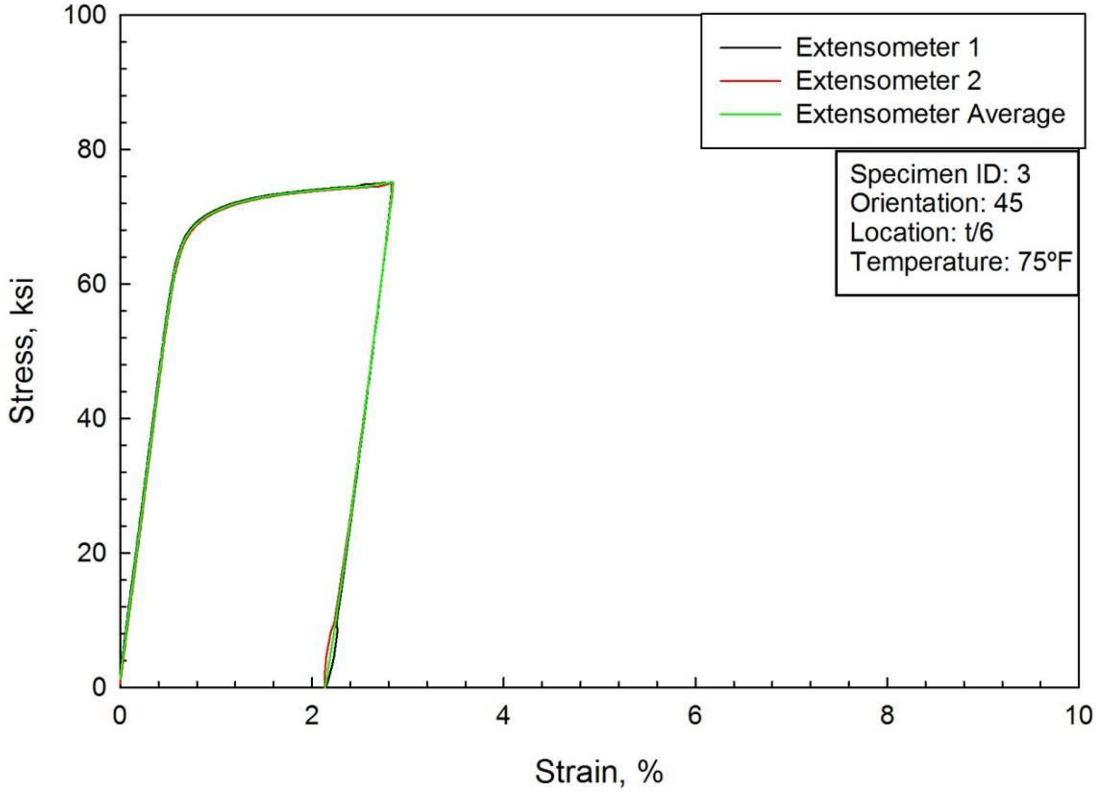

Figure D18. Compression data for 2050-T84, 45º orientation, t/6, specimen 3, tested at 75ºF.

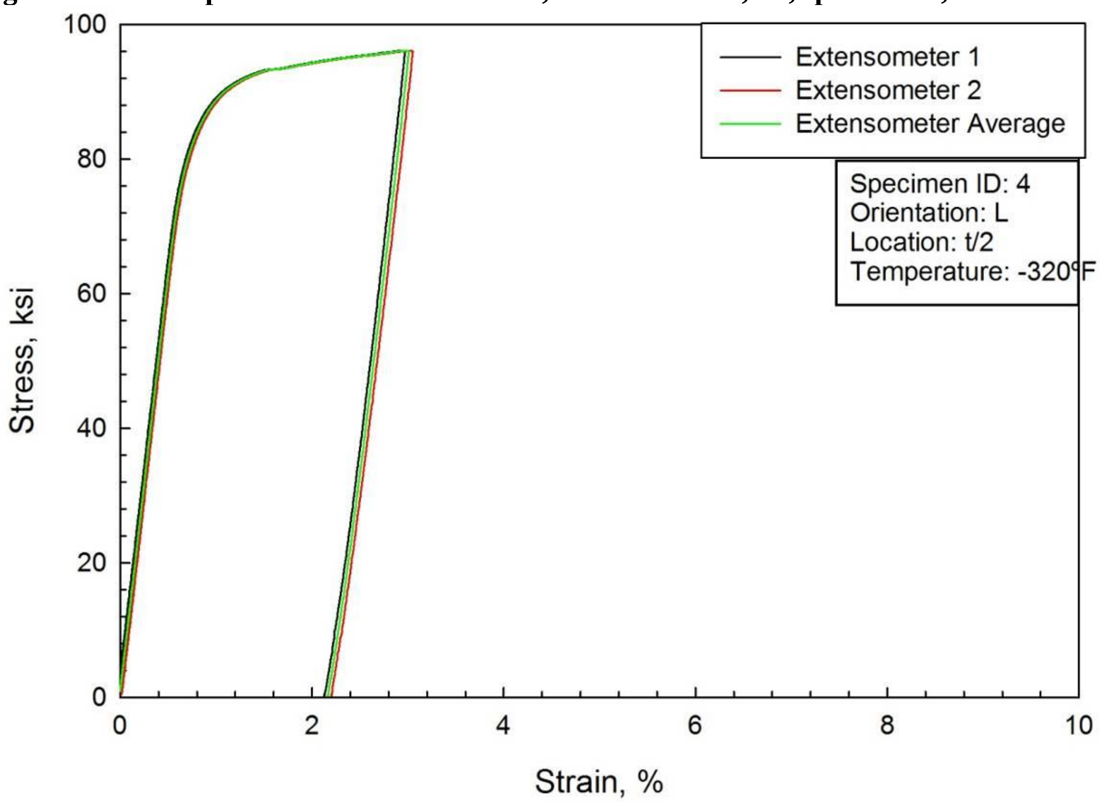

Figure D19. Compression data for 2050-T84, L orientation, t/2, specimen 4, tested at -320ºF.

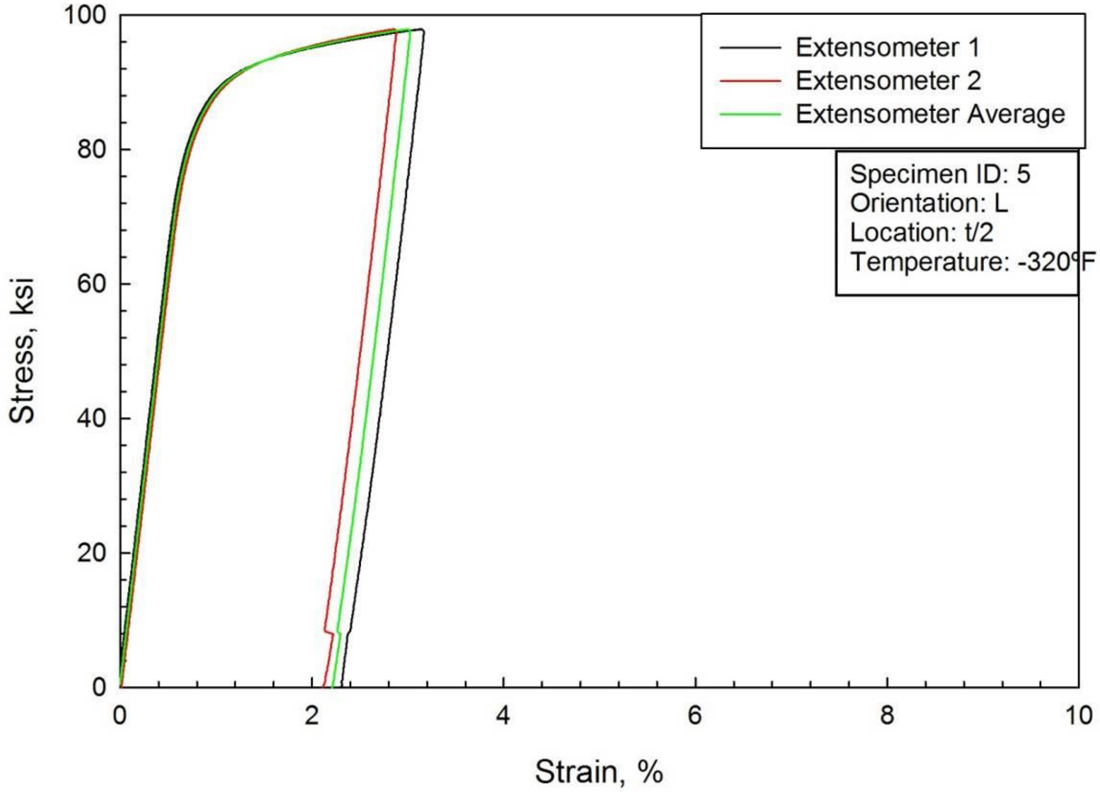

Figure D20. Compression data for 2050-T84, L orientation, t/2, specimen 5, tested at -320ºF.

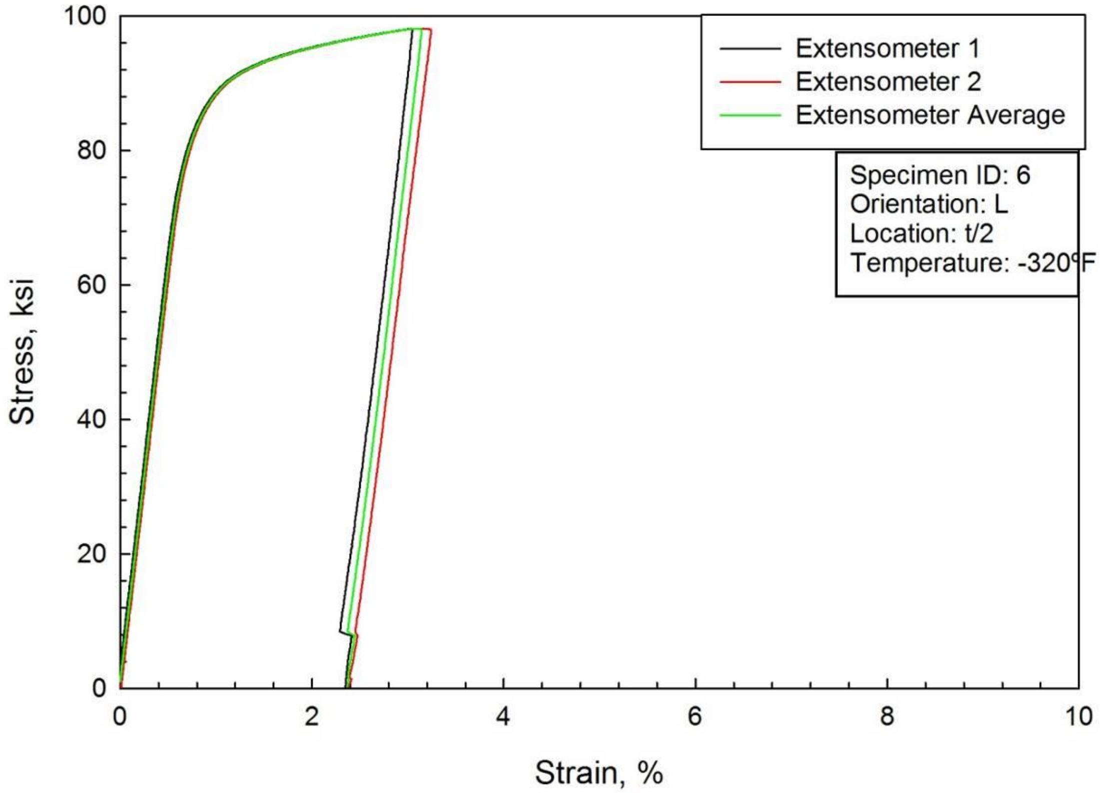

Figure D21. Compression data for 2050-T84, L orientation, t/2, specimen 6, tested at -320ºF.

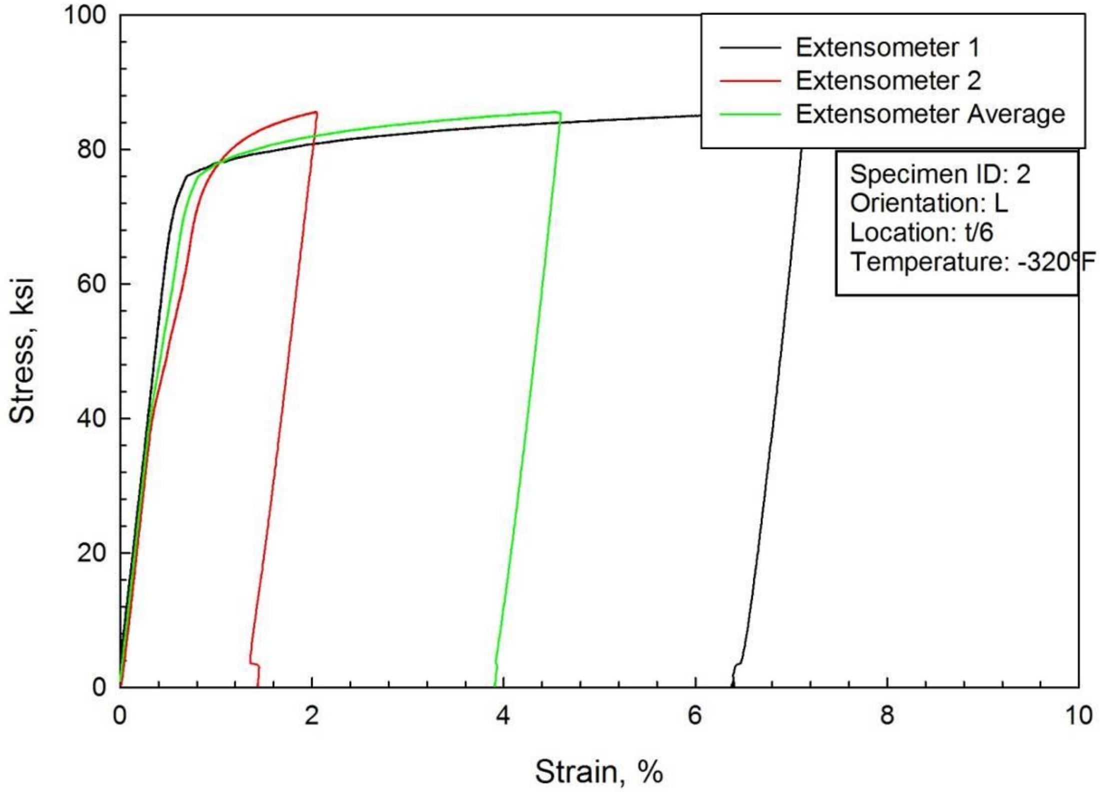

Figure D22. Compression data for 2050-T84, L orientation, t/6, specimen 2, tested at -320ºF.

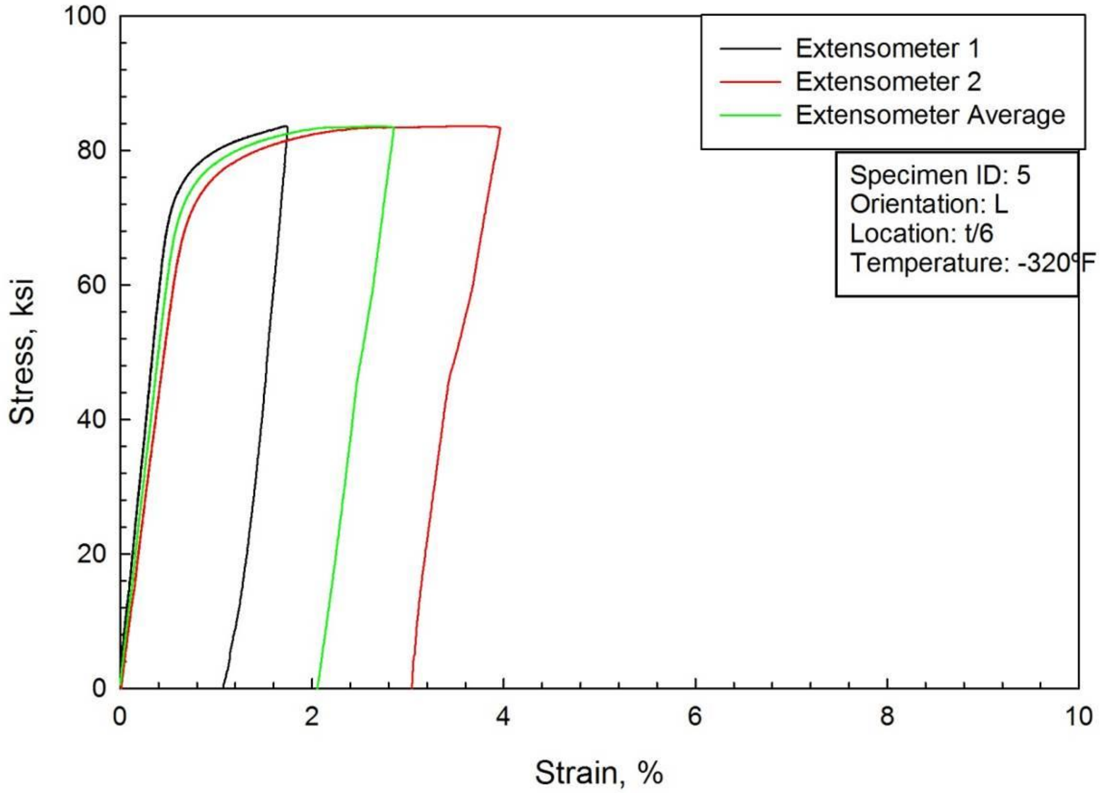

Figure D23. Compression data for 2050-T84, L orientation, t/6, specimen 5, tested at -320ºF.

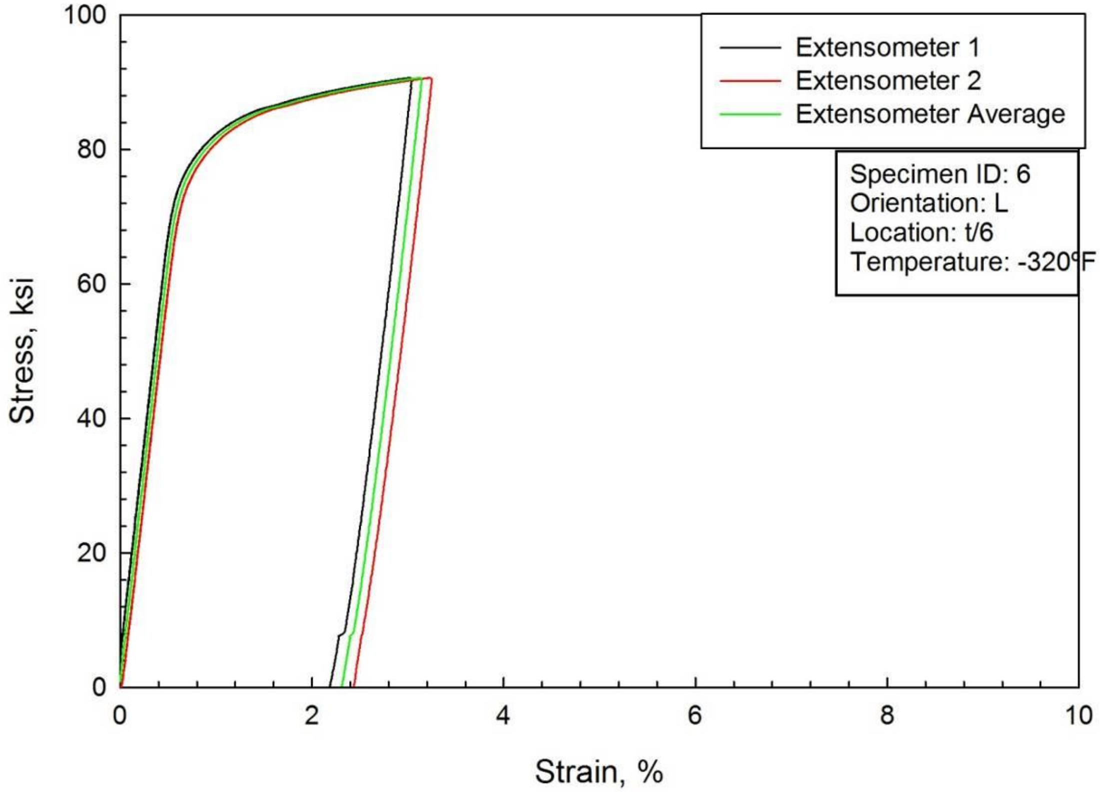

Figure D24. Compression data for 2050-T84, L orientation, t/6, specimen 6, tested at -320ºF.

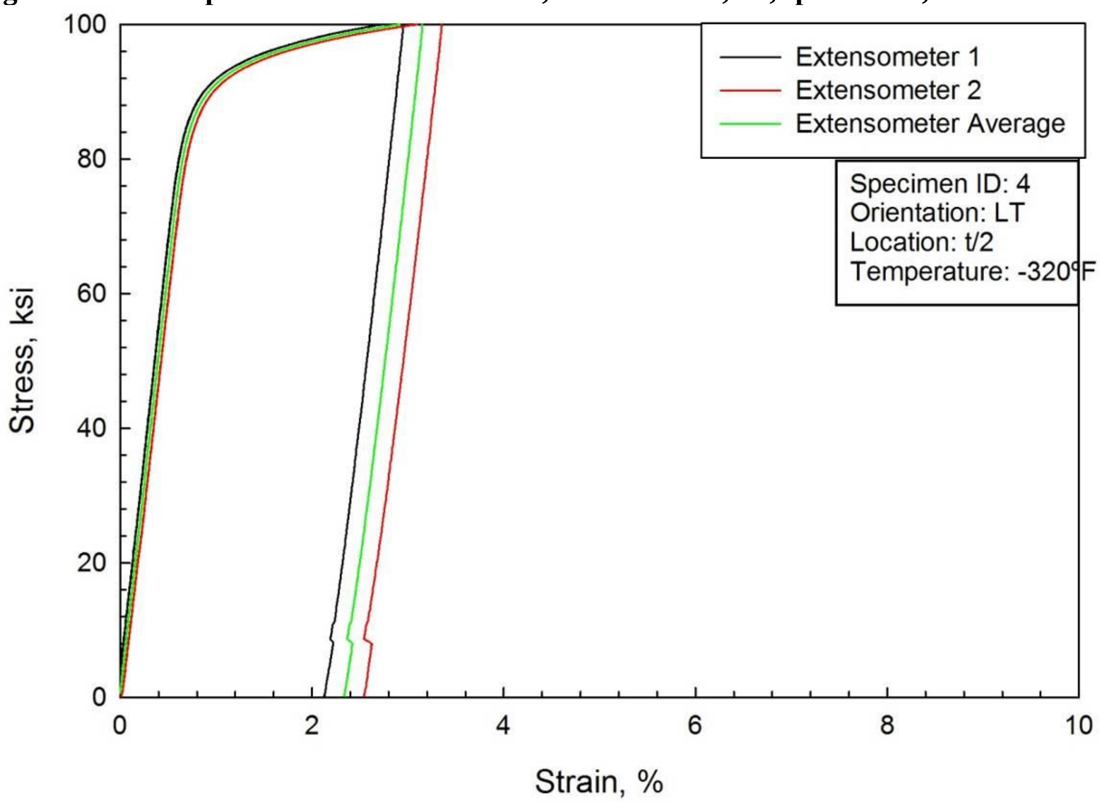

Figure D25. Compression data for 2050-T84, LT orientation, t/2, specimen 4, tested at -320ºF.

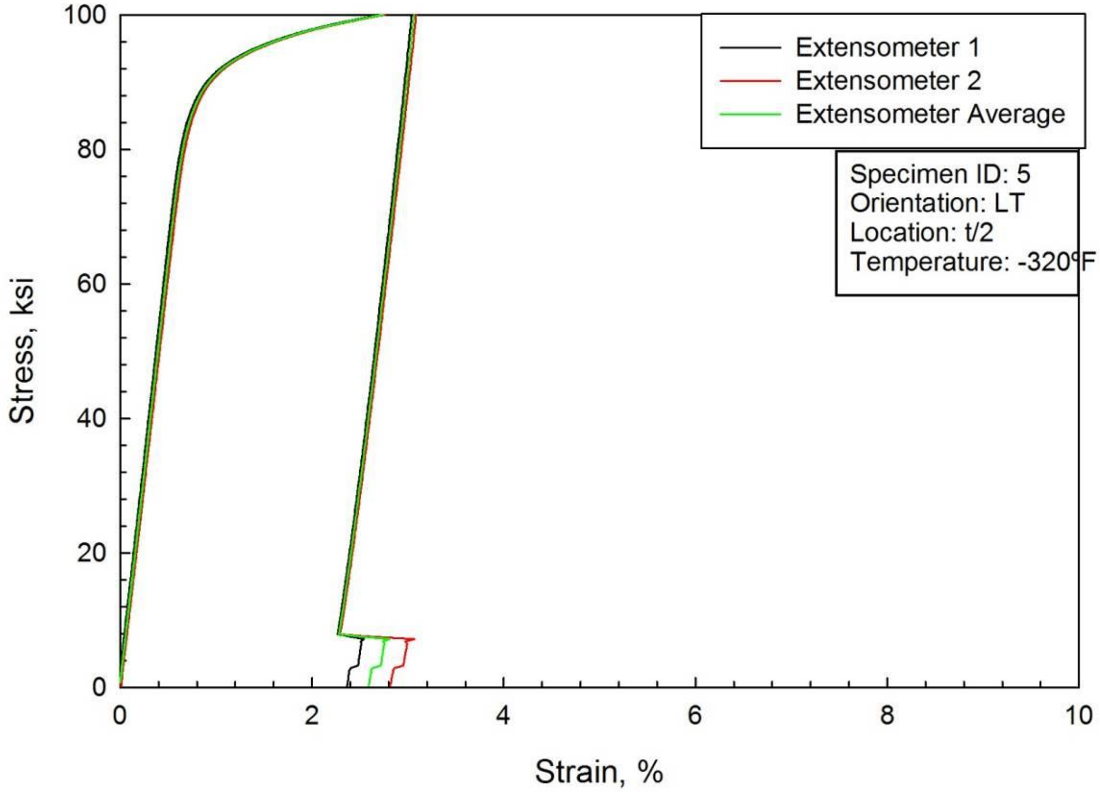

Figure D26. Compression data for 2050-T84, LT orientation, t/2, specimen 5, tested at -320ºF.

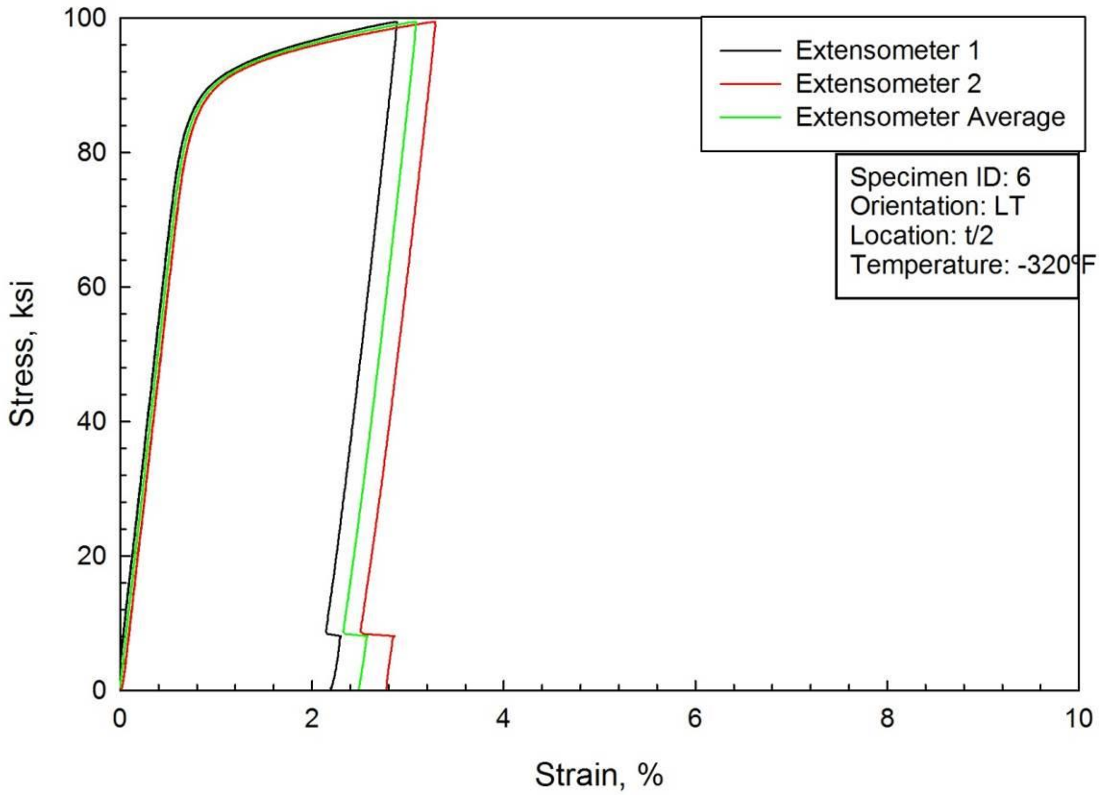

Figure D27. Compression data for 2050-T84, LT orientation, t/2, specimen 6, tested at -320ºF.

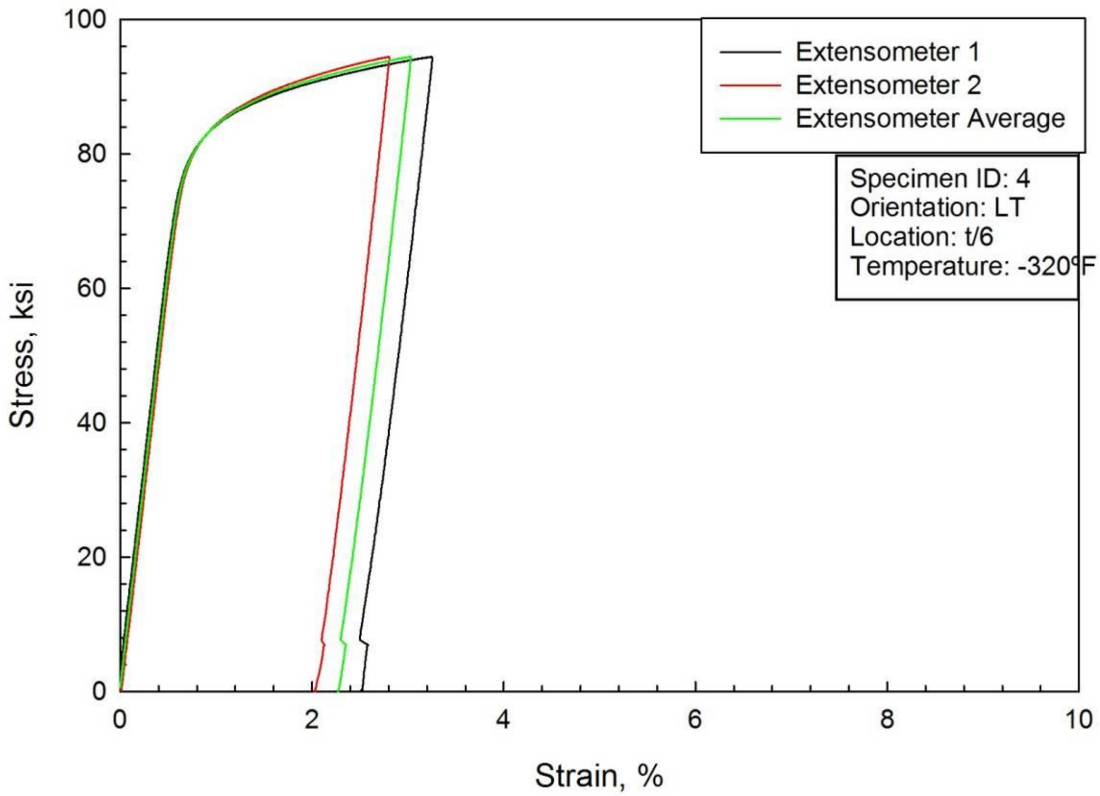

Figure D28. Compression data for 2050-T84, LT orientation, t/6, specimen 4, tested at -320ºF.

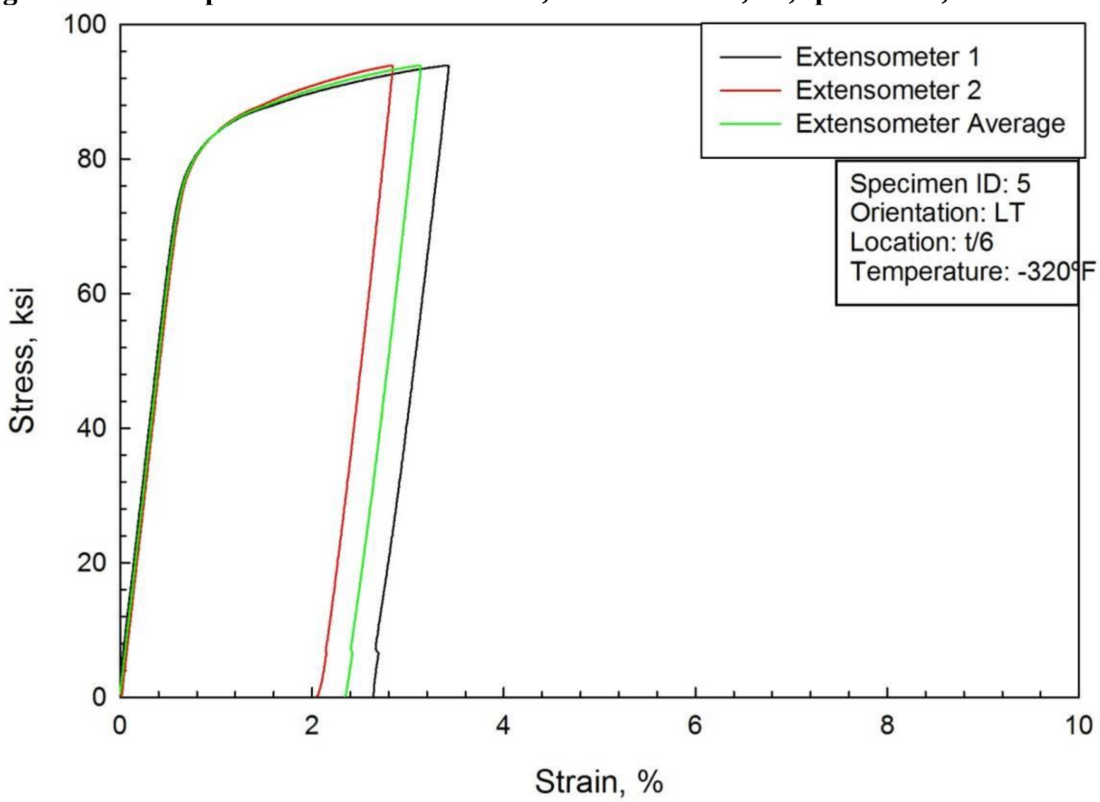

Figure D29. Compression data for 2050-T84, LT orientation, t/6, specimen 5, tested at -320ºF.

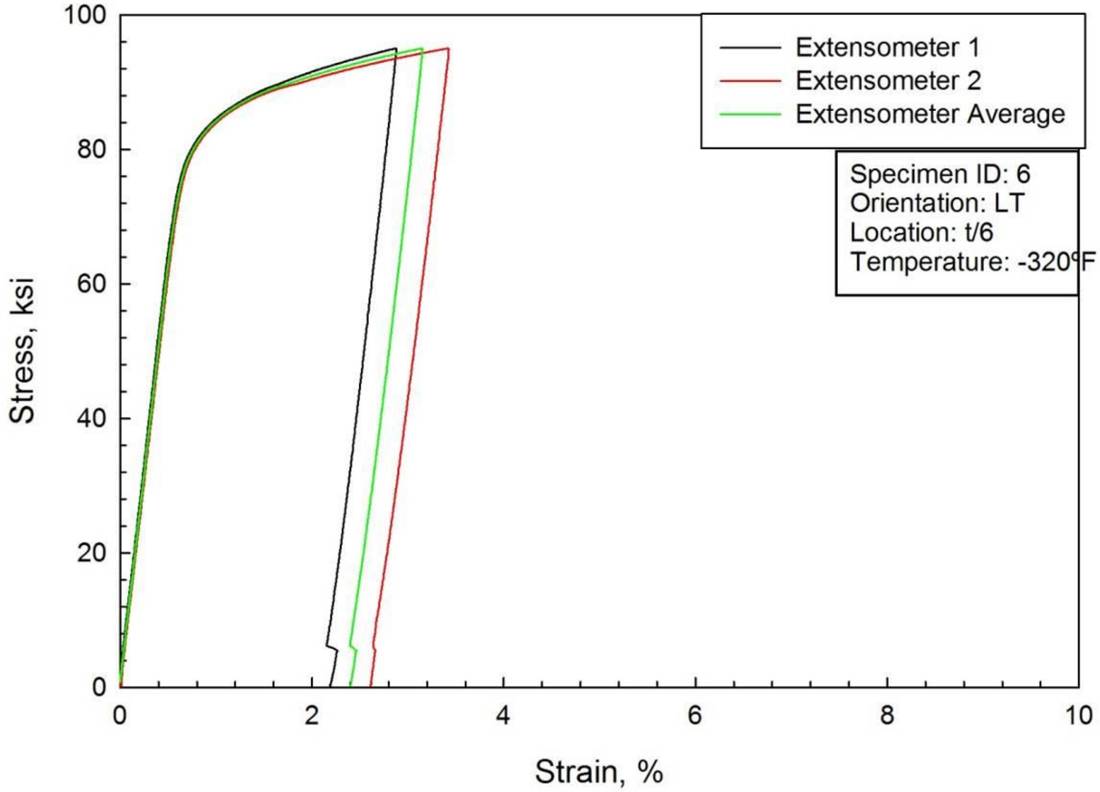

Figure D30. Compression data for 2050-T84, LT orientation, t/6, specimen 6, tested at -320ºF.

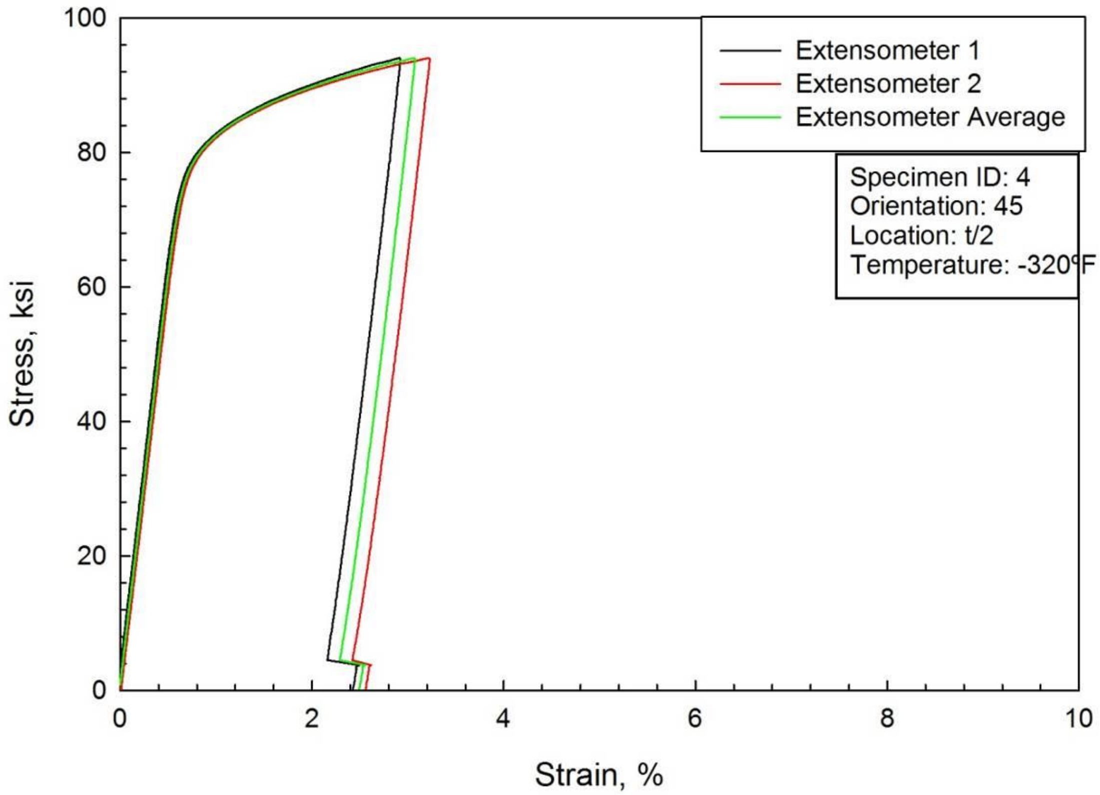

Figure D31. Compression data for 2050-T84, 45º orientation, t/2, specimen 4, tested at -320ºF.

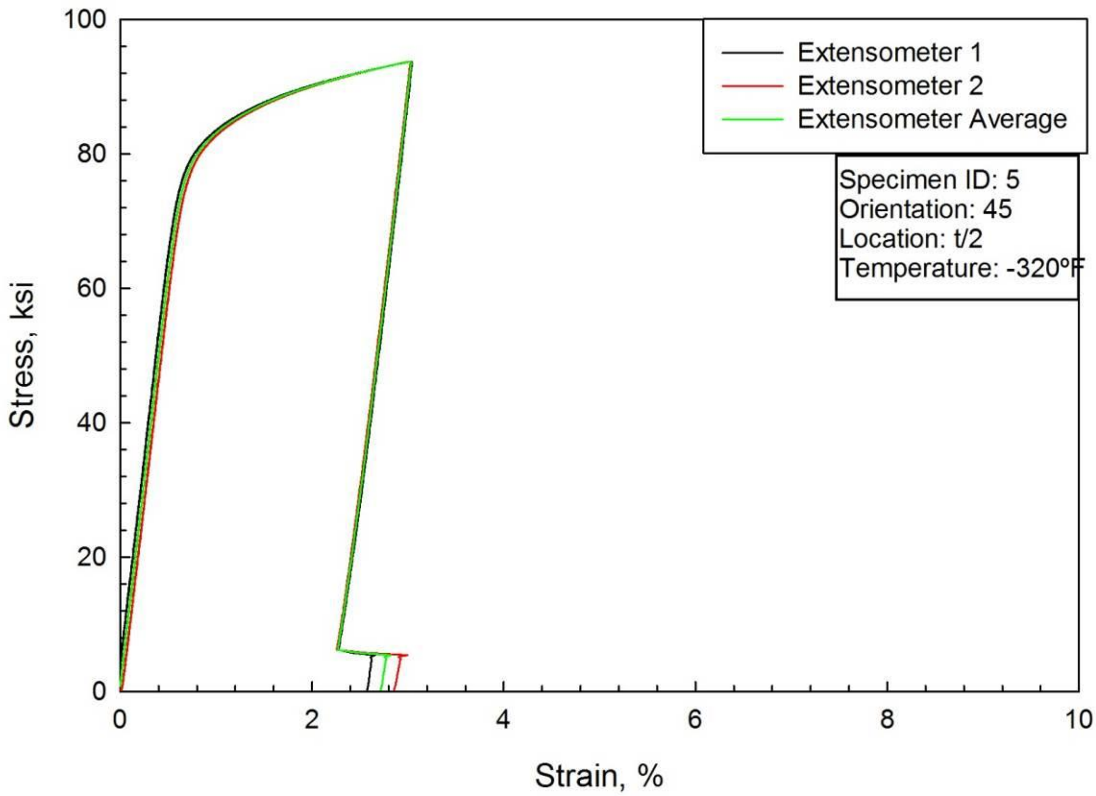

Figure D32 Compression data for 2050-T84, 45º orientation, t/2, specimen 5, tested at -320ºF.

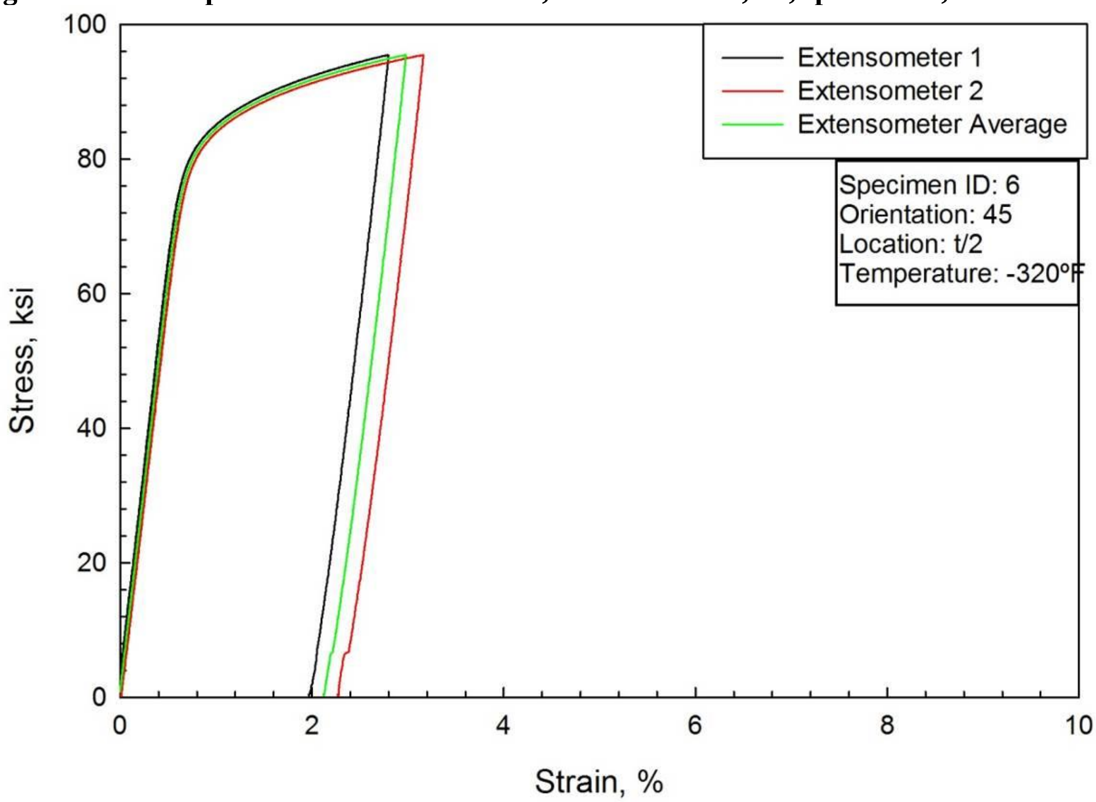

Figure D33. Compression data for 2050-T84, 45º orientation, t/2, specimen 6, tested at -320ºF.

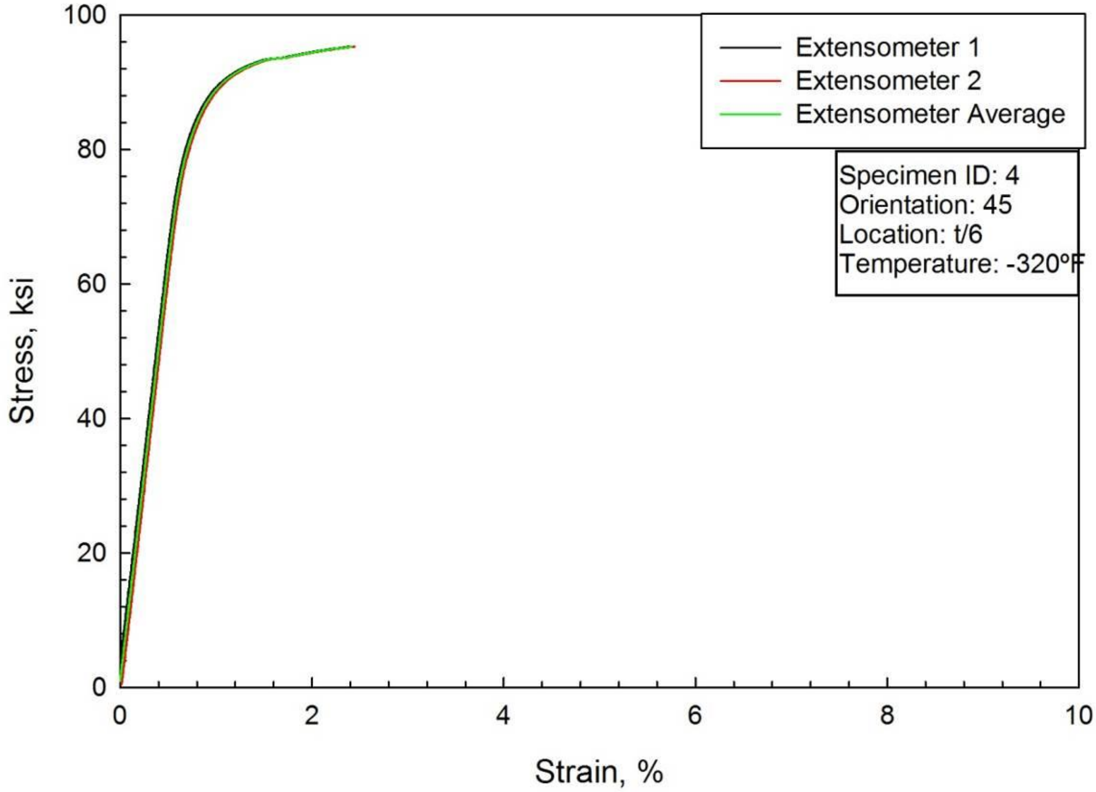

Figure D34. Compression data for 2050-T84, 45º orientation, t/6, specimen 4, tested at -320ºF.

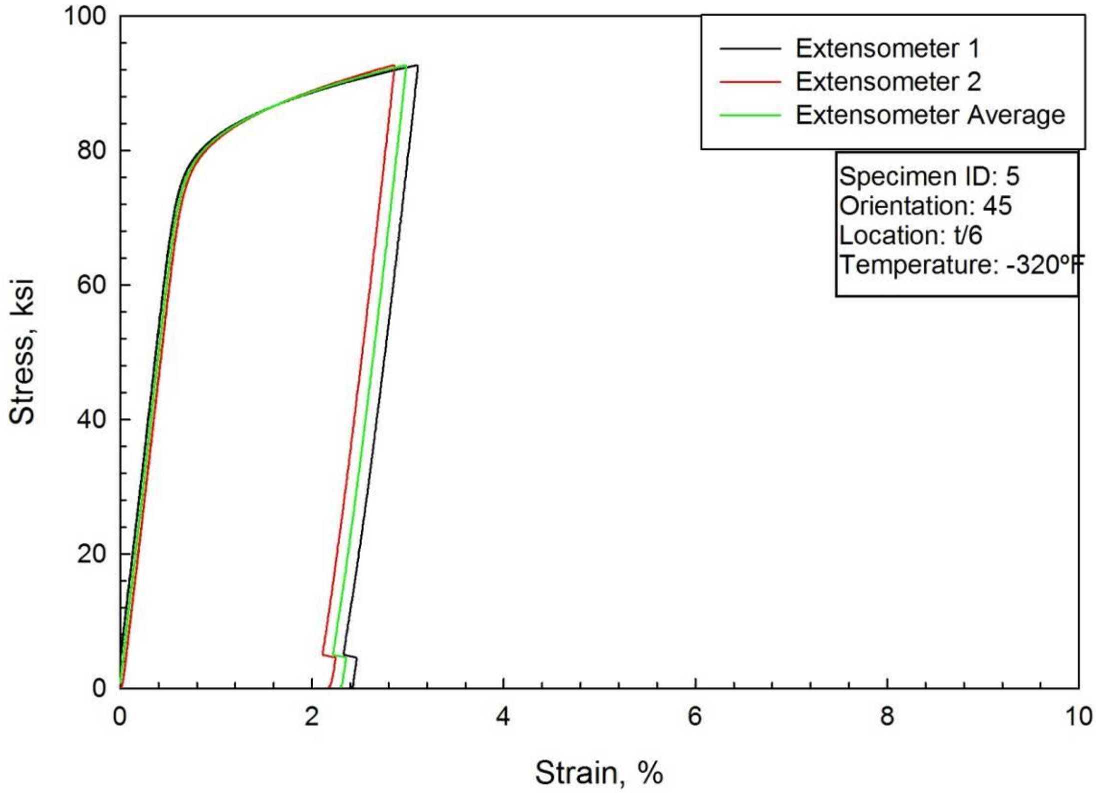

Figure D35. Compression data for 2050-T84, 45º orientation, t/6, specimen 5, tested at -320ºF.

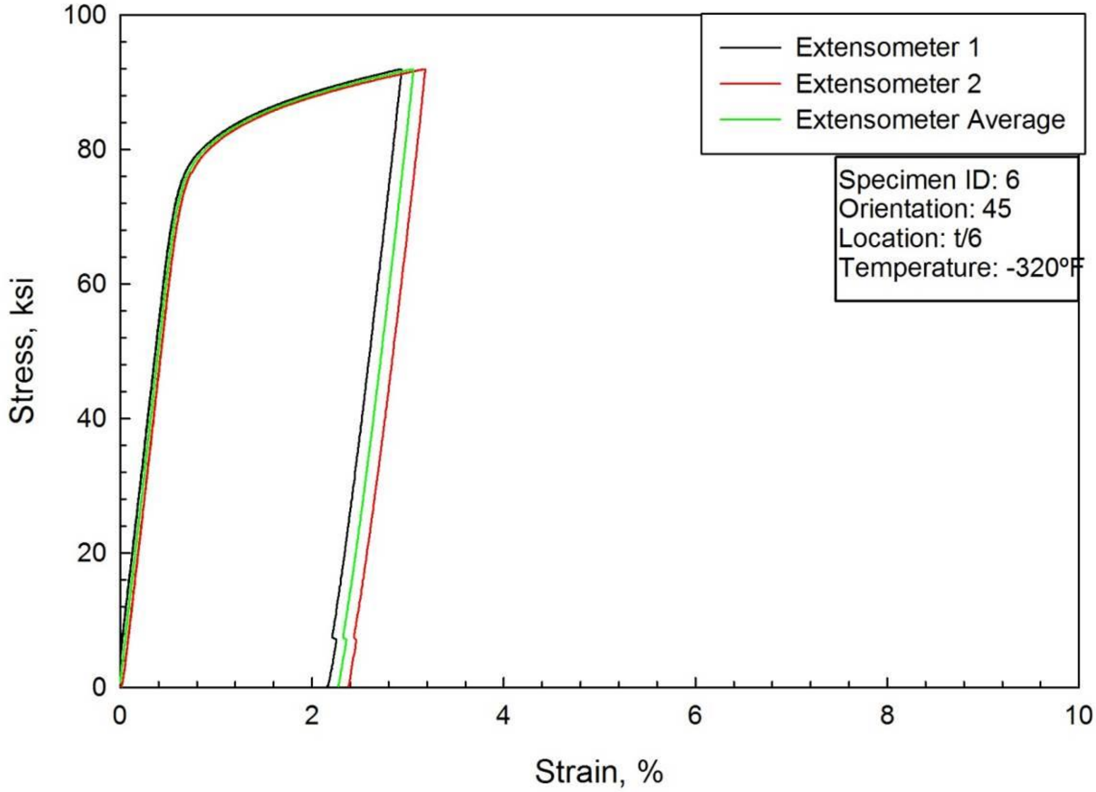

Figure D36. Compression data for 2050-T84, 45º orientation, t/6, specimen 6, tested at -320ºF.

Appendix E: Individual Data, J-Curves, and Specimen Images for Tensile Fracture Toughness Tests on 4 inch thick 2050-T84 Plate

Force lbf	Disp1 inch	Crack inch	Δa inch
266.9	0.00551	1.1970	-0.0017
312.6	0.00648	1.1972	-0.0014
373.9	0.00781	1.1972	-0.0015
436.2	0.00914	1.1968	-0.0018
498.2	0.01048	1.1967	-0.0019
559.0	0.01181	1.1995	0.0009
620.1	0.01316	1.1976	-0.0010
680.5	0.01449	1.1973	-0.0014
739.4	0.01582	1.1977	-0.0009
797.0	0.01717	1.1987	0.0001
851.7	0.01851	1.1991	0.0005
899.9	0.01986	1.2022	0.0035
946.7	0.02123	1.2035	0.0048
994.2	0.02261	1.2065	0.0079
1035.0	0.02403	1.2092	0.0105
1063.8	0.02548	1.2131	0.0144
1104.5	0.02686	1.2161	0.0174
1136.6	0.02823	1.2188	0.0201
1172.8	0.02963	1.2206	0.0219
1206.0	0.03103	1.2213	0.0227
1238.5	0.03241	1.2233	0.0247
1272.0	0.03381	1.2248	0.0261
1303.2	0.03520	1.2261	0.0274
1327.9	0.03659	1.2276	0.0290
1356.6	0.03799	1.2294	0.0307
1383.5	0.03938	1.2311	0.0324
1407.8	0.04077	1.2331	0.0344
1428.4	0.04217	1.2352	0.0366
1450.1	0.04357	1.2373	0.0387
1468.7	0.04497	1.2388	0.0401
1481.7	0.04638	1.2411	0.0424
1499.9	0.04777	1.2430	0.0443
1511.3	0.04918	1.2454	0.0467
1517.9	0.05059	1.2483	0.0496
1522.8	0.05201	1.2509	0.0522
1530.2	0.05342	1.2542	0.0555
1532.7	0.05484	1.2574	0.0587
1531.1	0.05629	1.2623	0.0636
1528.4	0.05771	1.2665	0.0678
1523.0	0.05916	1.2707	0.0721
1512.8	0.06057	1.2757	0.0770
1511.7	0.06201	1.2789	0.0802
1501.8	0.06351	1.2834	0.0848
1495.4	0.06495	1.2865	0.0879
1488.9	0.06638	1.2907	0.0920
1482.7	0.06782	1.2945	0.0959
1454.2	0.06929	1.3018	0.1031
1439.7	0.07074	1.3075	0.1088
1423.8	0.07218	1.3128	0.1141
1410.2	0.07363	1.3180	0.1194
1406.3	0.07507	1.3220	0.1234
1385.8	0.07653	1.3277	0.1290
1364.4	0.07799	1.3336	0.1349
1355.0	0.07942	1.3376	0.1390
1328.9	0.08088	1.3439	0.1452
1312.5	0.08233	1.3483	0.1497
1293.2	0.08377	1.3537	0.1550
1253.4	0.08525	1.3631	0.1645
1233.2	0.08670	1.3688	0.1701
1227.1	0.08815	1.3737	0.1751
1217.7	0.08959	1.3756	0.1770
1208.6	0.09104	1.3786	0.1800
1197.7	0.09251	1.3819	0.1832
1188.7	0.09397	1.3852	0.1865

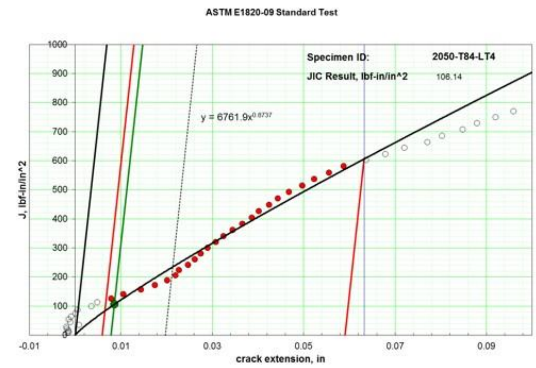

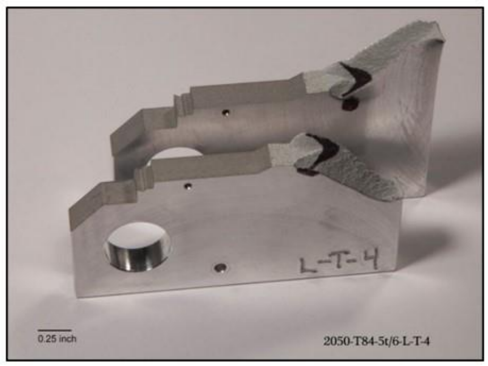

Figure E1. Fracture toughness data, J-curve, and image showing fracture path for 2050-T84, L-T orientation, 5t/6, specimen 4, tested at 75ºF.

Force lbf	Disp1 inch	Crack inch	∆a inch
286.3	0.00584	1.1992	-0.0016
334.6	0.00686	1.1994	-0.0015
547.9	0.01140	1.1996	-0.0012
758.3	0.01602	1.2011	0.0002
947.0	0.02080	1.2082	0.0073
1111.2	0.02580	1.2172	0.0163
1252.1	0.03103	1.2246	0.0237
1372.8	0.03637	1.2320	0.0312
1457.5	0.04190	1.2425	0.0416
1509.9	0.04769	1.2561	0.0552
1542.8	0.05359	1.2719	0.0710
1531.9	0.05980	1.2913	0.0904
1492.6	0.06617	1.3161	0.1153
1403.7	0.07296	1.3427	0.1419
1297.9	0.07965	1.3848	0.1840
1165.7	0.08685	1.4109	0.2101

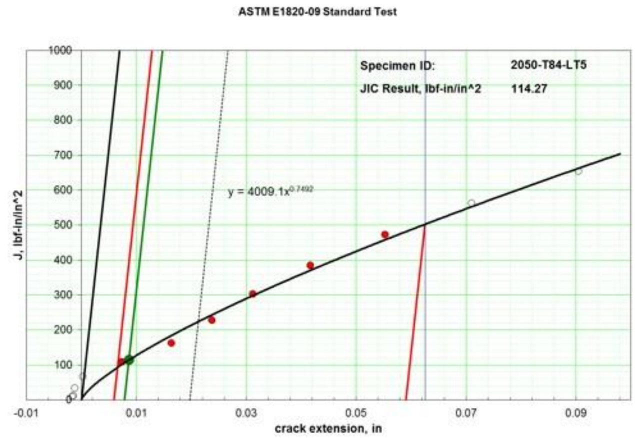

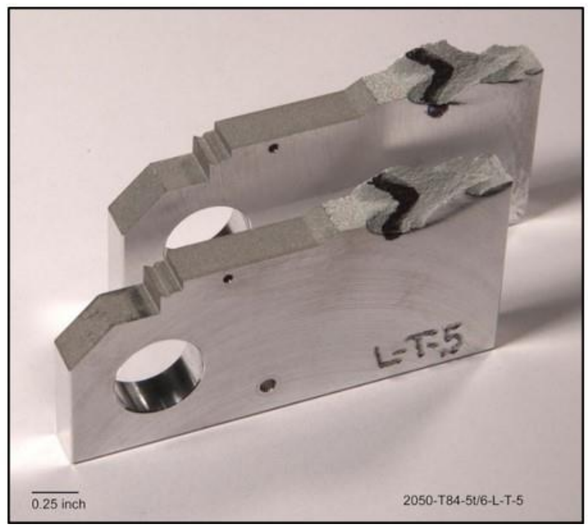

Figure E2 Fracture toughness data, J-curve, and image showing fracture path for 2050-T84, L-T orientation, 5t/6, specimen 5, tested at 75ºF.

Force lbf	Disp1 inch	Crack inch	Δa inch
283.9	0.00608	1.2000	0.0041
332.2	0.00714	1.2006	0.0046
391.6	0.00844	1.2005	0.0046
451.2	0.00975	1.2007	0.0047
510.1	0.01106	1.2007	0.0047
568.4	0.01239	1.2009	0.0049
624.3	0.01372	1.2017	0.0058
659.0	0.01506	1.2110	0.0151
680.0	0.01653	1.2205	0.0246
703.9	0.01795	1.2295	0.0336
737.3	0.01932	1.2373	0.0414
755.2	0.02083	1.2441	0.0482
783.5	0.02227	1.2501	0.0541
798.1	0.02378	1.2574	0.0614
806.3	0.02526	1.2648	0.0689
819.4	0.02668	1.2713	0.0753
831.6	0.02807	1.2801	0.0842
818.0	0.02972	1.2922	0.0963
792.7	0.03130	1.3039	0.1080
762.4	0.03274	1.3247	0.1288
754.1	0.03429	1.3395	0.1436
722.7	0.03602	1.3538	0.1579
560.9	0.03818	1.4127	0.2168

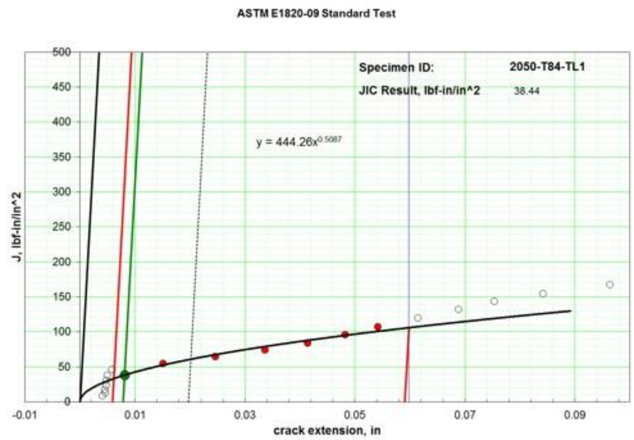

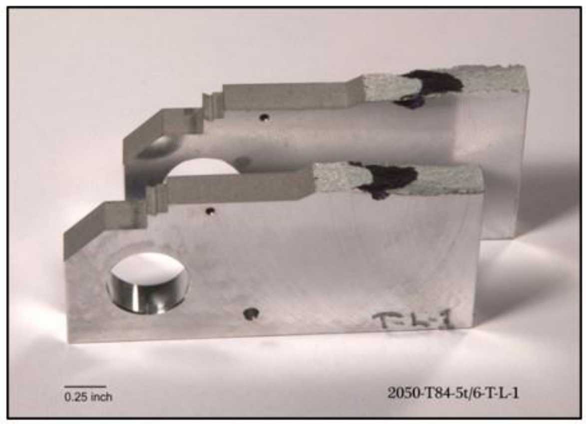

Figure E3. Fracture toughness data, J-curve, and image showing fracture path for 2050-T84, T-L orientation, 5t/6, specimen 1, tested at 75ºF.

Force lbf	Disp1 inch	Crack inch	Δa inch
284.7	0.00582	1.1976	0.0030
333.5	0.00684	1.1979	0.0033
396.0	0.00817	1.1980	0.0034
457.8	0.00949	1.1979	0.0033
519.6	0.01082	1.1977	0.0031
580.5	0.01216	1.1979	0.0033
639.7	0.01351	1.1988	0.0042
686.7	0.01484	1.2028	0.0082
724.8	0.01619	1.2084	0.0138
763.2	0.01758	1.2142	0.0196
795.3	0.01900	1.2207	0.0260
822.7	0.02043	1.2274	0.0328
846.6	0.02190	1.2332	0.0386
871.0	0.02334	1.2389	0.0443
900.4	0.02477	1.2452	0.0506
897.3	0.02627	1.2534	0.0588
921.3	0.02766	1.2586	0.0640
934.8	0.02908	1.2653	0.0706
931.5	0.03056	1.2764	0.0818
905.5	0.03206	1.2898	0.0952
905.4	0.03357	1.3006	0.1060
837.9	0.03525	1.3266	0.1319
835.3	0.03669	1.3440	0.1494
755.9	0.03859	1.3669	0.1723
731.6	0.04003	1.3810	0.1863
696.6	0.04153	1.4108	0.2162

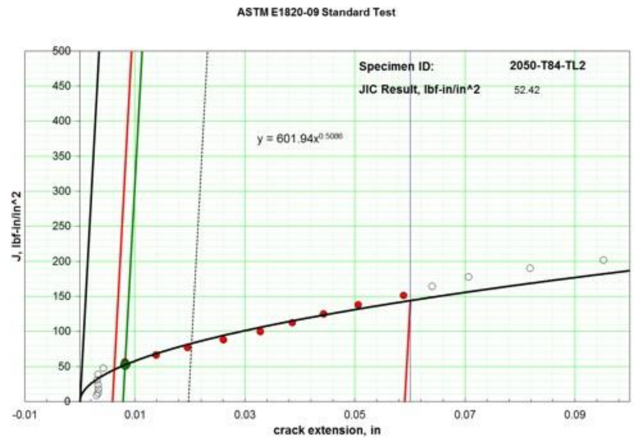

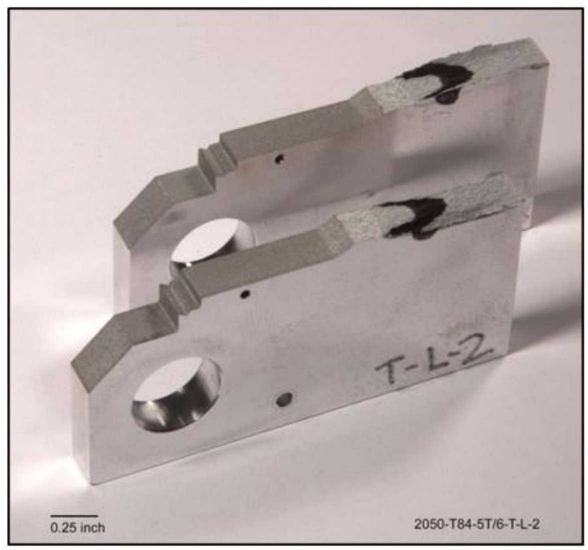

Figure E4. Fracture toughness data, J-curve, and image showing fracture path for 2050-T84, T-L orientation, 5t/6, specimen 2, tested at 75ºF.

Force	Disp1	Crack	Δa
lbf	inch	inch	inch
282.4	0.00600	1.1988	0.0028
329.4	0.00701	1.1992	0.0033
390.1	0.00832	1.1994	0.0035
450.2	0.00963	1.2000	0.0040
510.3	0.01095	1.2000	0.0041
569.5	0.01226	1.2004	0.0044
624.8	0.01358	1.2019	0.0060
671.8	0.01495	1.2057	0.0098
716.3	0.01635	1.2119	0.0159
738.1	0.01787	1.2190	0.0231
746.8	0.01924	1.2282	0.0323
773.8	0.02062	1.2362	0.0402
798.6	0.02206	1.2437	0.0477
788.7	0.02362	1.2597	0.0637
797.0	0.02510	1.2679	0.0719
801.2	0.02654	1.2767	0.0807
803.2	0.02797	1.2867	0.0908
786.1	0.02956	1.3004	0.1044
747.8	0.03107	1.3174	0.1214
750.7	0.03247	1.3279	0.1319
690.9	0.03394	1.3557	0.1597
703.5	0.03534	1.3664	0.1704
625.6	0.03689	1.3951	0.1992
552.3	0.03857	1.4239	0.2280

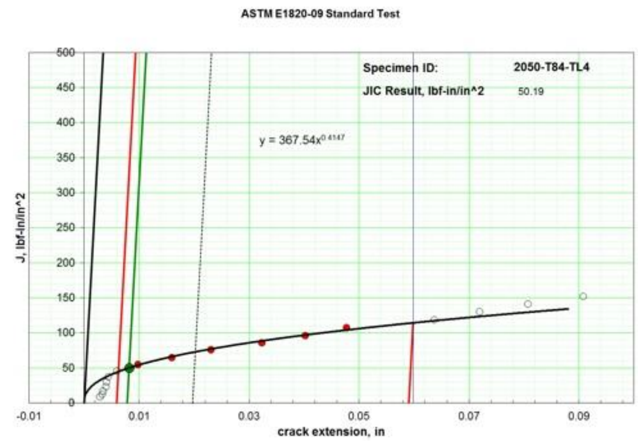

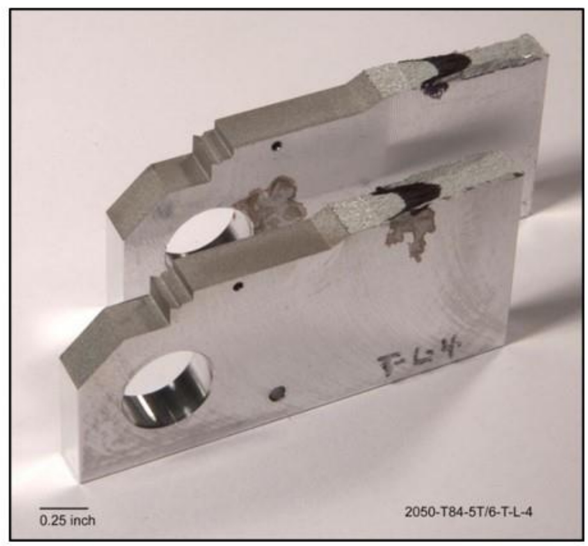

Figure E5. Fracture toughness data, J-curve, and image showing fracture path for 2050-T84, T-L orientation, 5t/6, specimen 4, tested at 75ºF.

Force lbf	Disp1 inch	Crack inch	Δa inch
287.0	0.00570	1.1976	0.0037
338.6	0.00678	1.1980	0.0042
401.2	0.00810	1.1981	0.0042
463.9	0.00943	1.1976	0.0037
526.2	0.01076	1.1975	0.0036
587.9	0.01209	1.1975	0.0037
648.2	0.01342	1.1976	0.0037
707.6	0.01476	1.1982	0.0043
766.5	0.01610	1.1990	0.0051
823.4	0.01744	1.1998	0.0060
880.0	0.01878	1.2006	0.0067
935.0	0.02014	1.2019	0.0080
987.2	0.02148	1.2034	0.0095
1035.3	0.02284	1.2056	0.0117
1068.7	0.02427	1.2099	0.0160
1108.0	0.02568	1.2135	0.0196
1120.4	0.02707	1.2214	0.0275
1164.3	0.02844	1.2241	0.0303
1162.5	0.02985	1.2362	0.0423
1187.1	0.03128	1.2422	0.0483
1223.0	0.03264	1.2484	0.0545
1229.1	0.03418	1.2576	0.0638
1239.9	0.03558	1.2673	0.0734
1264.3	0.03696	1.2744	0.0805
1274.4	0.03850	1.2830	0.0891
1299.4	0.03993	1.2865	0.0926
1276.6	0.04135	1.2996	0.1057
1302.6	0.04274	1.3035	0.1097
1320.9	0.04415	1.3089	0.1150
1306.0	0.04558	1.3218	0.1279
1307.2	0.04709	1.3295	0.1357
1311.0	0.04853	1.3428	0.1490
1206.1	0.05094	1.3698	0.1759
1189.2	0.05238	1.3821	0.1882
1174.6	0.05381	1.3935	0.1996
1173.9	0.05524	1.4013	0.2074

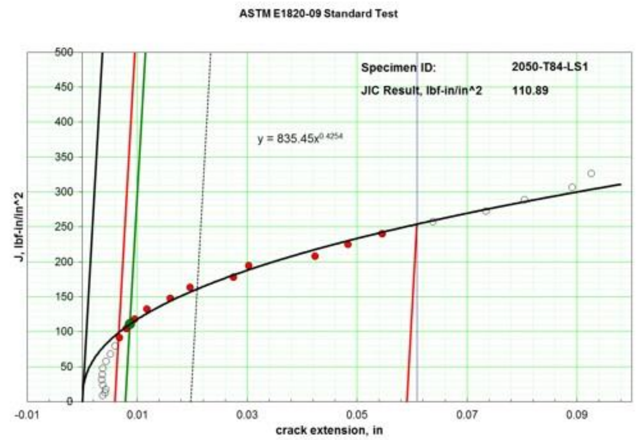

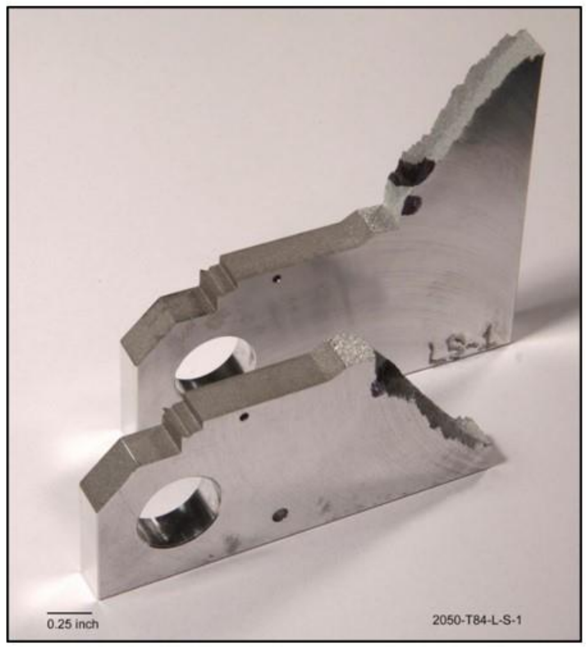

Figure E6. Fracture toughness data, J-curve, and image showing fracture path for 2050-T84, L-S orientation, t/6, specimen 1, tested at 75ºF.

Force lbf	Disp1 inch	Crack inch	Δa inch
288.6	0.00565	1.1979	0.0037
290.8	0.00569	1.1979	0.0036
338.4	0.00669	1.1980	0.0038
401.8	0.00801	1.1983	0.0041
465.3	0.00936	1.1982	0.0040
528.0	0.01068	1.1985	0.0042
590.1	0.01201	1.1985	0.0043
652.2	0.01336	1.1990	0.0048
714.5	0.01470	1.1996	0.0053
776.3	0.01605	1.2002	0.0060
836.1	0.01740	1.2009	0.0067
893.3	0.01875	1.2021	0.0078
947.4	0.02011	1.2038	0.0095
994.3	0.02146	1.2063	0.0121
1042.6	0.02283	1.2101	0.0159
1080.3	0.02430	1.2133	0.0191
1091.2	0.02567	1.2235	0.0292
1119.6	0.02718	1.2295	0.0353
1154.3	0.02860	1.2359	0.0417
1174.7	0.03013	1.2435	0.0493
1197.1	0.03153	1.2509	0.0566
1220.6	0.03295	1.2595	0.0652
1240.1	0.03446	1.2670	0.0728
1261.3	0.03595	1.2727	0.0784
1289.4	0.03736	1.2771	0.0828
1317.7	0.03877	1.2809	0.0867
1340.9	0.04017	1.2846	0.0903
1365.7	0.04157	1.2884	0.0942
1338.2	0.04303	1.3020	0.1078
1347.8	0.04443	1.3093	0.1151
1355.8	0.04593	1.3206	0.1263
1346.6	0.04753	1.3273	0.1331
1345.5	0.04907	1.3402	0.1460
1318.4	0.05075	1.3519	0.1576
1253.2	0.05234	1.3755	0.1813
1120.2	0.05444	1.4232	0.2290

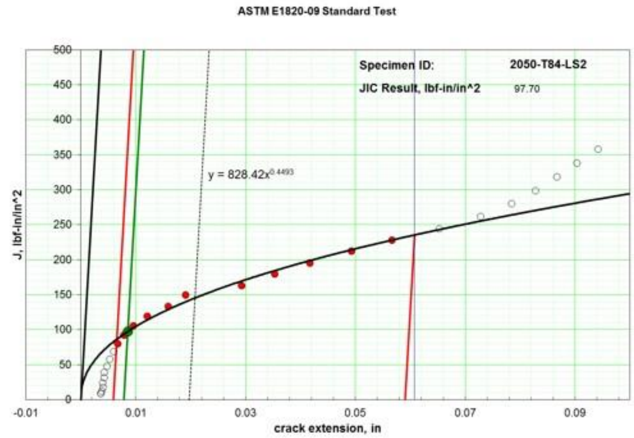

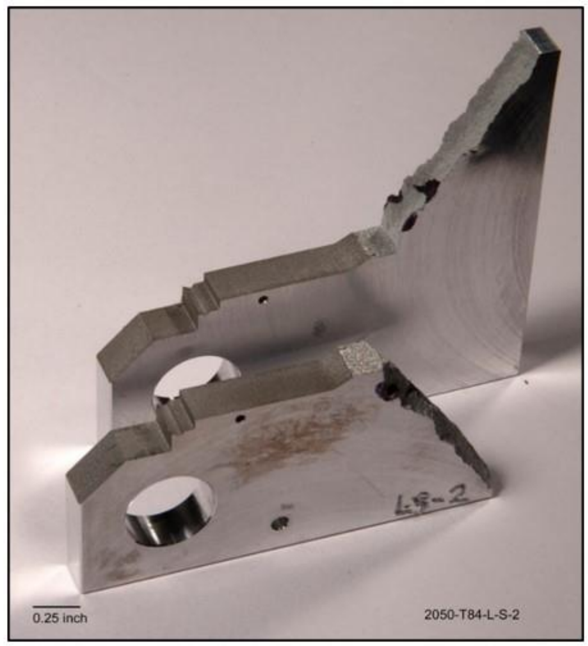

Figure E7. Fracture toughness data, J-curve, and image showing fracture path for 2050-T84, L-S orientation, t/6, specimen 2, tested at 75ºF.

Force lbf	Disp1 inch	Crack inch	Δa inch
296.8	0.00591	1.1959	0.0034
295.6	0.00589	1.1960	0.0035
295.1	0.00588	1.1961	0.0036
294.4	0.00586	1.1962	0.0037
293.3	0.00584	1.1964	0.0039
293.0	0.00583	1.1965	0.0040
292.6	0.00582	1.1967	0.0042
340.4	0.00683	1.1970	0.0046
402.6	0.00815	1.1970	0.0046
464.8	0.00947	1.1970	0.0046
527.0	0.01080	1.1971	0.0046
588.2	0.01212	1.1973	0.0048
649.5	0.01346	1.1975	0.0050
709.4	0.01479	1.1980	0.0056
768.7	0.01614	1.1987	0.0062
825.8	0.01746	1.1991	0.0067
882.6	0.01882	1.2001	0.0076
937.3	0.02016	1.2008	0.0083
990.8	0.02152	1.2022	0.0097
1038.7	0.02288	1.2041	0.0117
1089.0	0.02424	1.2058	0.0134
1128.2	0.02559	1.2088	0.0163
1123.7	0.02698	1.2198	0.0274
1156.3	0.02839	1.2274	0.0349
1162.8	0.03000	1.2377	0.0452
1154.9	0.03138	1.2518	0.0593
1186.1	0.03275	1.2585	0.0660
1204.1	0.03427	1.2653	0.0728
1218.2	0.03568	1.2733	0.0809
1247.8	0.03707	1.2784	0.0859
1274.9	0.03846	1.2832	0.0908
1292.2	0.03986	1.2892	0.0967
1308.4	0.04125	1.2951	0.1026
1329.0	0.04264	1.2988	0.1063
1348.1	0.04405	1.3032	0.1108
1369.5	0.04546	1.3083	0.1158
1385.8	0.04692	1.3121	0.1197
1363.8	0.04832	1.3268	0.1344
1332.9	0.04998	1.3422	0.1498
1351.2	0.05140	1.3459	0.1535
1338.3	0.05282	1.3548	0.1623
1305.5	0.05424	1.3722	0.1798
1279.4	0.05587	1.3837	0.1912
1262.4	0.05754	1.3913	0.1989
1199.0	0.05897	1.4111	0.2187

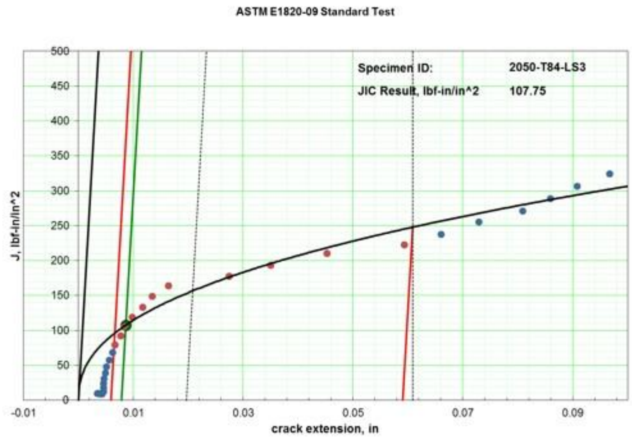

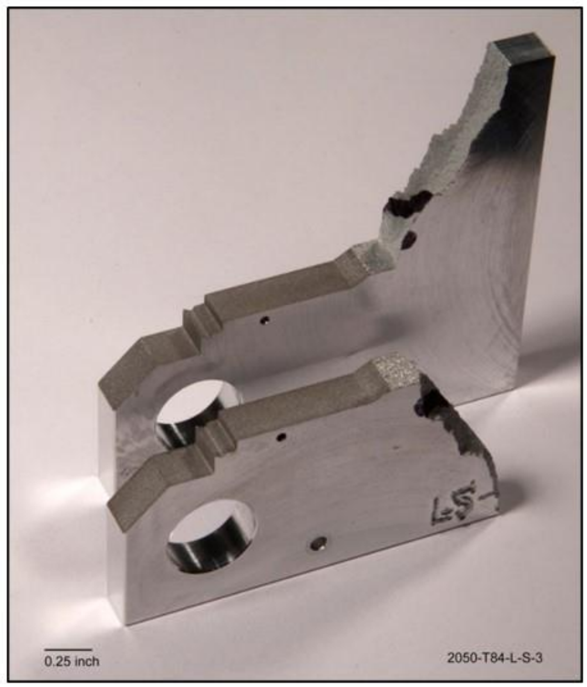

Figure E8. Fracture toughness data, J-curve, and image showing fracture path for 2050-T84, L-S orientation, t/6, specimen 3, tested at 75ºF.

Force lbf	Disp1 inch	Crack inch	Δa inch
288.9	0.00455	1.1988	0.0010
338.4	0.00549	1.1991	0.0013
403.8	0.00675	1.1985	0.0008
469.0	0.00801	1.1988	0.0010
535.0	0.00929	1.1987	0.0009
600.4	0.01056	1.1990	0.0012
666.2	0.01186	1.1991	0.0013
732.7	0.01318	1.1992	0.0014
798.1	0.01450	1.1995	0.0017
861.7	0.01583	1.2001	0.0023
921.0	0.01717	1.2016	0.0038
967.1	0.01853	1.2061	0.0084
1012.7	0.01990	1.2102	0.0124
1041.2	0.02129	1.2175	0.0198
1075.4	0.02268	1.2224	0.0246
1111.8	0.02405	1.2262	0.0284
1145.5	0.02543	1.2299	0.0321
1178.2	0.02682	1.2336	0.0358
1207.0	0.02824	1.2369	0.0392
1241.9	0.02964	1.2398	0.0420
1273.7	0.03103	1.2421	0.0443
1307.4	0.03242	1.2454	0.0476
1336.6	0.03380	1.2477	0.0499
1359.3	0.03523	1.2514	0.0536
1374.4	0.03665	1.2568	0.0590
1387.6	0.03808	1.2611	0.0633
1382.4	0.03956	1.2677	0.0699
1386.6	0.04100	1.2729	0.0751
1390.2	0.04245	1.2784	0.0806
1383.1	0.04393	1.2857	0.0879
1384.7	0.04537	1.2923	0.0945
1367.9	0.04683	1.3022	0.1044
1357.1	0.04830	1.3113	0.1135
1350.3	0.04979	1.3186	0.1208
1345.6	0.05126	1.3245	0.1267
1310.3	0.05273	1.3412	0.1435
1258.7	0.05447	1.3527	0.1549
1245.5	0.05598	1.3602	0.1624
1235.1	0.05745	1.3694	0.1716
1214.2	0.05890	1.3783	0.1805
1204.8	0.06037	1.3857	0.1879
1188.3	0.06189	1.3929	0.1951
1168.1	0.06337	1.4001	0.2023

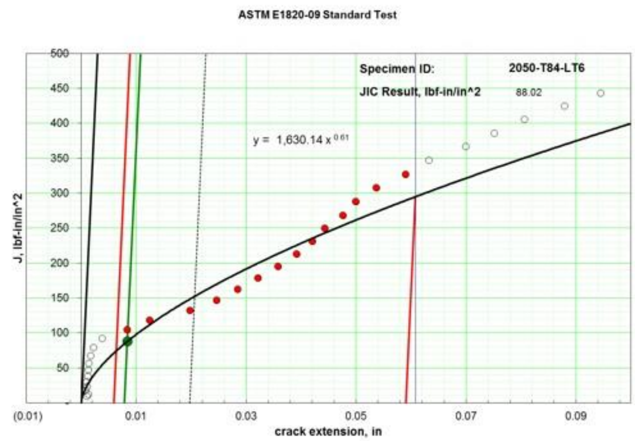

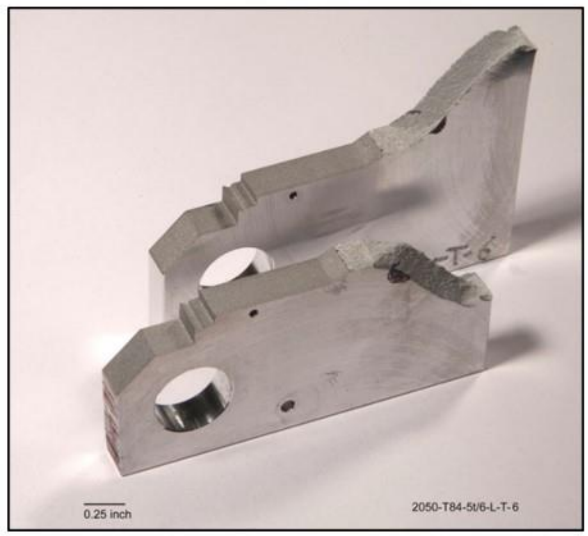

Figure E9. Fracture toughness data, J-curve, and image showing fracture path for 2050-T84, L-T orientation, 5t/6, specimen 6, tested at -320ºF.

Force lbf	Disp1 inch	Crack inch	Δa inch
285.3	0.00453	1.2018	0.0006
335.5	0.00549	1.2016	0.0004
400.6	0.00677	1.2011	-0.0001
466.0	0.00805	1.2013	0.0000
532.2	0.00935	1.2018	0.0006
597.3	0.01064	1.2021	0.0009
663.2	0.01196	1.2019	0.0007
728.7	0.01328	1.2025	0.0012
793.4	0.01461	1.2035	0.0023
855.9	0.01593	1.2045	0.0033
908.5	0.01725	1.2068	0.0056
958.2	0.01858	1.2100	0.0087
1009.8	0.01993	1.2129	0.0116
1051.7	0.02130	1.2178	0.0165
1075.1	0.02270	1.2247	0.0234
1102.3	0.02408	1.2293	0.0281
1136.5	0.02545	1.2336	0.0324
1169.3	0.02686	1.2375	0.0362
1199.3	0.02826	1.2404	0.0391
1226.6	0.02967	1.2434	0.0421
1254.0	0.03107	1.2473	0.0461
1284.5	0.03248	1.2502	0.0489
1299.0	0.03387	1.2550	0.0537
1322.0	0.03528	1.2579	0.0566
1345.2	0.03672	1.2616	0.0604
1361.5	0.03813	1.2643	0.0630
1370.2	0.03955	1.2693	0.0681
1374.8	0.04104	1.2731	0.0719
1386.3	0.04246	1.2762	0.0750
1389.4	0.04389	1.2812	0.0800
1394.3	0.04533	1.2861	0.0849
1400.2	0.04677	1.2893	0.0880
1392.6	0.04821	1.2960	0.0948
1387.3	0.04966	1.3019	0.1007
1371.2	0.05110	1.3094	0.1082
1333.0	0.05261	1.3204	0.1192
1312.5	0.05409	1.3279	0.1267
1289.7	0.05557	1.3371	0.1359
1285.8	0.05704	1.3426	0.1414
1262.1	0.05853	1.3499	0.1486
1242.4	0.06002	1.3589	0.1576
1217.8	0.06151	1.3685	0.1672
1192.7	0.06300	1.3785	0.1772
1164.8	0.06449	1.3881	0.1869
1139.4	0.06597	1.3961	0.1948
1109.5	0.06752	1.4039	0.2026

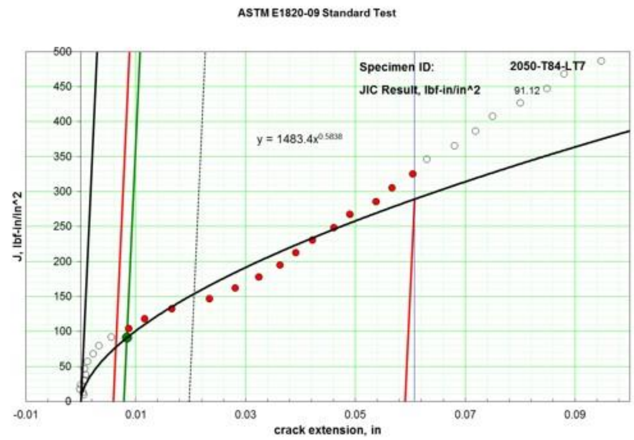

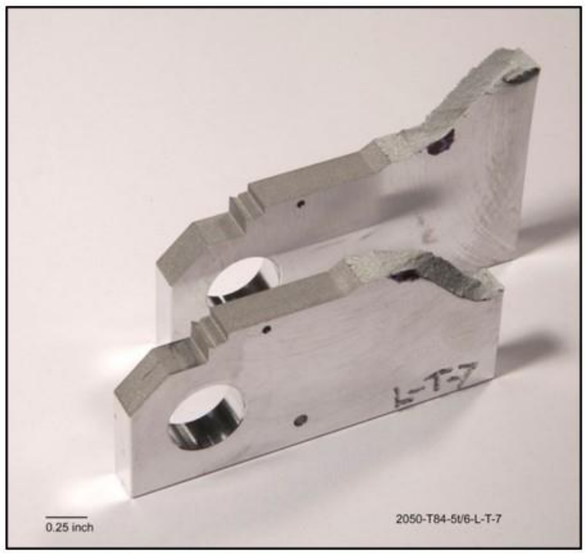

Figure E10. Fracture toughness data, J-curve, and image showing fracture path for 2050-T84, L-T orientation, 5t/6, specimen 7, tested at -320ºF.

Force lbf	Disp1 inch	Crack inch	Δa inch
281.1	0.00440	1.2039	0.0020
330.1	0.00536	1.2037	0.0018
395.7	0.00664	1.2036	0.0017
461.0	0.00792	1.2031	0.0012
526.7	0.00921	1.2024	0.0005
592.4	0.01052	1.2014	-0.0005
658.3	0.01184	1.2002	-0.0016
721.9	0.01317	1.2010	-0.0009
777.1	0.01450	1.2037	0.0018
827.5	0.01585	1.2073	0.0054
875.7	0.01720	1.2127	0.0108
911.0	0.01860	1.2190	0.0171
949.9	0.01997	1.2237	0.0218
986.0	0.02136	1.2282	0.0263
1020.4	0.02275	1.2325	0.0306
1055.6	0.02411	1.2355	0.0336
1088.4	0.02549	1.2391	0.0372
1117.3	0.02689	1.2429	0.0410
1141.0	0.02827	1.2465	0.0446
1160.8	0.02967	1.2509	0.0490
1186.5	0.03108	1.2546	0.0527
1207.3	0.03248	1.2585	0.0566
1228.0	0.03389	1.2626	0.0608
1227.1	0.03531	1.2704	0.0685
1221.8	0.03677	1.2783	0.0764
1231.5	0.03822	1.2848	0.0829
1232.1	0.03969	1.2912	0.0893
1218.3	0.04118	1.2997	0.0978
1190.4	0.04265	1.3114	0.1095
1171.6	0.04412	1.3220	0.1202
1161.3	0.04561	1.3286	0.1267
1142.0	0.04706	1.3380	0.1361
1096.3	0.04864	1.3557	0.1538
1052.2	0.05021	1.3685	0.1666
1009.5	0.05171	1.3851	0.1833
974.2	0.05324	1.3992	0.1973
947.3	0.05477	1.4086	0.2067

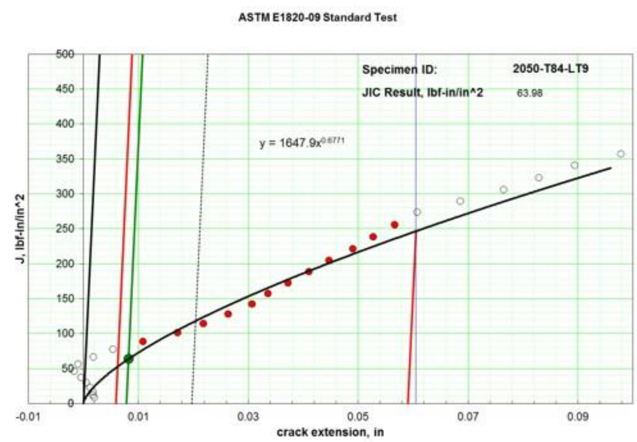

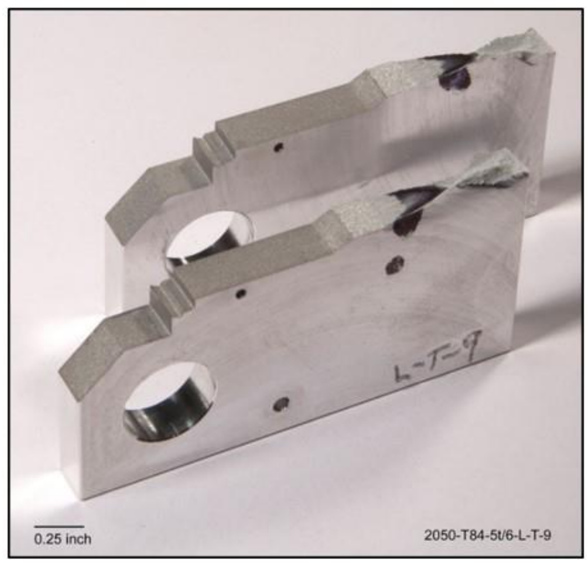

Figure E11. Fracture toughness data, J-curve, and image showing fracture path for 2050-T84, L-T orientation, 5t/6, specimen 9, tested at -320ºF.

Force lbf	Disp1 inch	Crack inch	Δa inch
283.5	0.00439	1.1982	0.0021
334.0	0.00535	1.1984	0.0023
399.9	0.00662	1.1986	0.0025
466.5	0.00791	1.1988	0.0027
532.9	0.00920	1.1989	0.0028
599.3	0.01051	1.1994	0.0033
664.4	0.01185	1.2003	0.0042
720.1	0.01319	1.2040	0.0079
763.0	0.01457	1.2097	0.0136
790.7	0.01594	1.2203	0.0242
825.2	0.01734	1.2269	0.0308
827.9	0.01871	1.2406	0.0445
850.5	0.02013	1.2485	0.0524
874.9	0.02157	1.2569	0.0608
869.1	0.02302	1.2706	0.0746
850.8	0.02449	1.2867	0.0906
784.7	0.02603	1.3153	0.1192
772.4	0.02752	1.3301	0.1341
723.4	0.02903	1.3573	0.1612
680.9	0.03060	1.3825	0.1864
606.2	0.03229	1.4152	0.2191

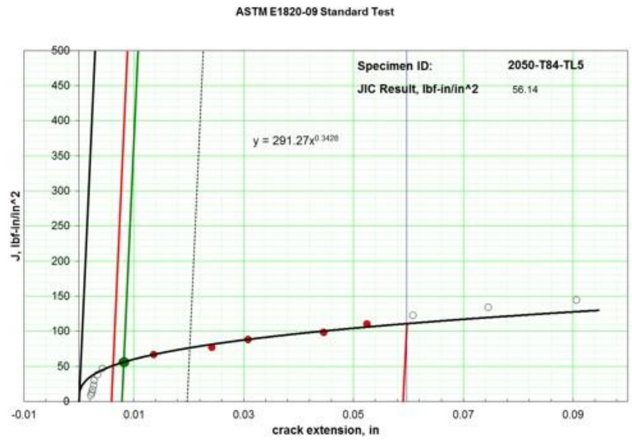

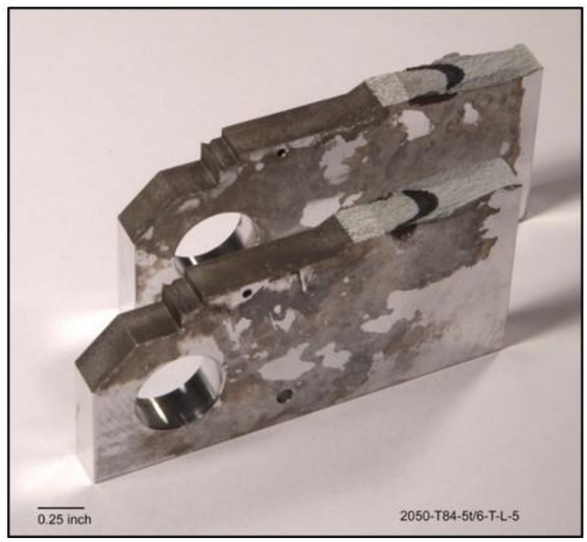

Figure E12. Fracture toughness data, J-curve, and image showing fracture path for 2050-T84, T-L orientation, 5t/6, specimen 5, tested at -320ºF.

Force	Disp1	Crack	Δa
lbf	inch	inch	inch
281.5	0.00442	1.1976	0.0021
327.8	0.00531	1.1978	0.0023
393.5	0.00658	1.1970	0.0015
460.1	0.00786	1.1971	0.0016
526.8	0.00917	1.1975	0.0021
593.3	0.01049	1.1969	0.0015
658.5	0.01182	1.1980	0.0025
715.6	0.01316	1.2007	0.0053
759.8	0.01449	1.2055	0.0101
781.4	0.01585	1.2164	0.0209
814.1	0.01724	1.2247	0.0293
831.8	0.01863	1.2357	0.0403
850.8	0.02005	1.2446	0.0492
861.0	0.02145	1.2560	0.0606
859.8	0.02288	1.2703	0.0748
848.6	0.02437	1.2841	0.0887
808.6	0.02584	1.3065	0.1110
795.4	0.02733	1.3257	0.1302
739.6	0.02901	1.3545	0.1591
713.0	0.03055	1.3735	0.1781
650.5	0.03204	1.4058	0.2103

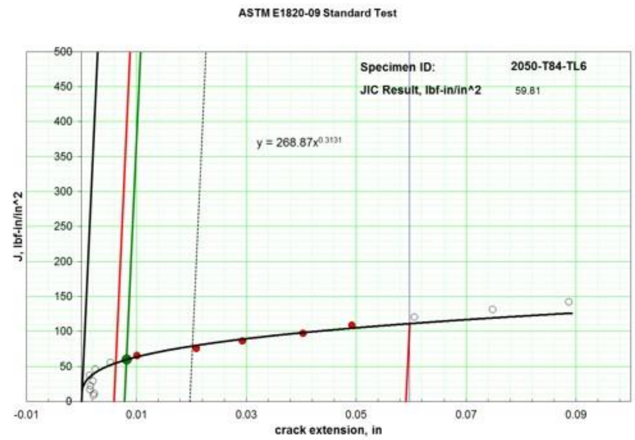

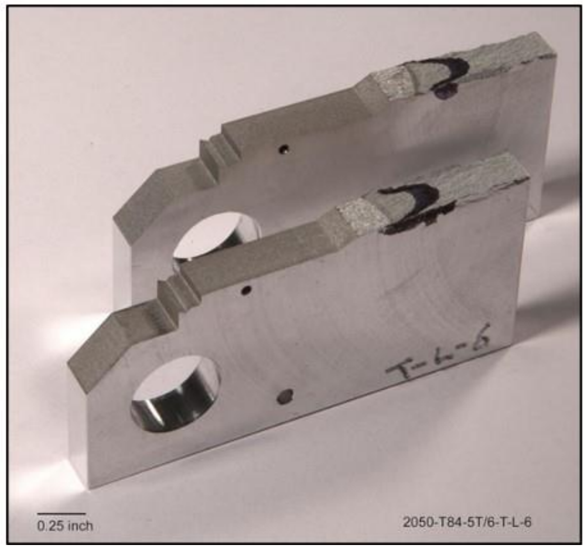

Figure E13. Fracture toughness data, J-curve, and image showing fracture path for 2050-T84, T-L orientation, 5t/6, specimen 6, tested at -320ºF.

Force lbf	Disp1 inch	Crack inch	∆a inch
276.1	0.00447	1.2039	0.0036
323.6	0.00540	1.2044	0.0041
390.4	0.00672	1.2038	0.0036
457.4	0.00805	1.2033	0.0030
523.4	0.00936	1.2033	0.0030
589.8	0.01069	1.2029	0.0026
655.7	0.01202	1.2037	0.0034
718.3	0.01337	1.2039	0.0037
774.9	0.01472	1.2073	0.0070
820.8	0.01608	1.2125	0.0122
856.3	0.01748	1.2189	0.0187
877.9	0.01883	1.2293	0.0290
904.2	0.02023	1.2358	0.0355
933.7	0.02161	1.2428	0.0426
956.6	0.02304	1.2502	0.0499
970.0	0.02454	1.2567	0.0565
977.4	0.02593	1.2656	0.0653
993.8	0.02735	1.2736	0.0734
993.3	0.02884	1.2844	0.0842
978.5	0.03043	1.2950	0.0948
971.1	0.03190	1.3057	0.1055
955.2	0.03337	1.3199	0.1196
920.8	0.03492	1.3351	0.1349
876.2	0.03644	1.3552	0.1550
849.8	0.03794	1.3684	0.1681
807.0	0.03943	1.3847	0.1844
778.7	0.04095	1.3982	0.1979

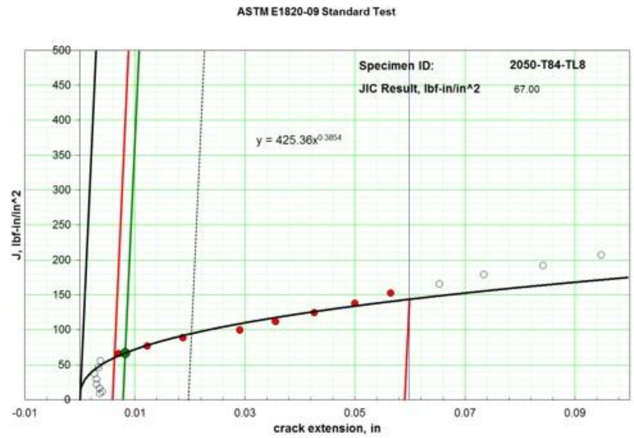

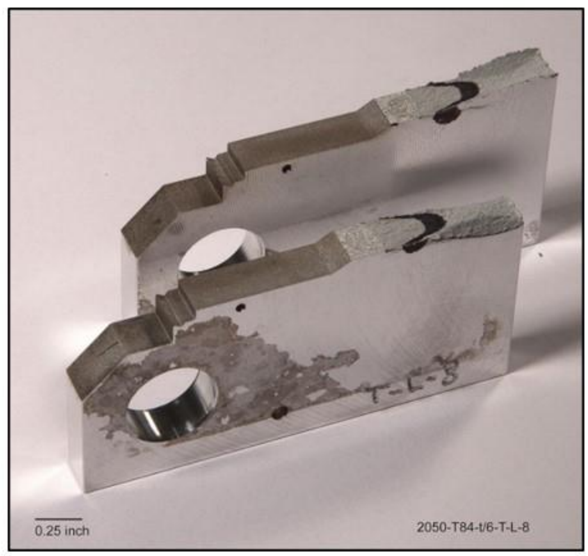

Figure E14. Fracture toughness data, J-curve, and image showing fracture path for 2050-T84, T-L orientation, t/6, specimen 8, tested at -320ºF.

Force lbf	Disp1 inch	Crack inch	∆a inch
285.3	0.00470	1.1988	-0.0006
335.5	0.00565	1.1988	-0.0005
402.3	0.00691	1.2004	0.0010
469.9	0.00819	1.1988	-0.0006
537.6	0.00948	1.1991	-0.0003
605.1	0.01076	1.1999	0.0005
672.8	0.01206	1.2005	0.0011
740.4	0.01338	1.2001	0.0007
807.6	0.01470	1.2000	0.0006
875.4	0.01597	1.2006	0.0012
939.7	0.01732	1.2011	0.0018
1001.7	0.01868	1.2013	0.0019
1062.8	0.02003	1.2030	0.0037
1119.7	0.02139	1.2049	0.0055
1152.9	0.02276	1.2098	0.0104
1166.3	0.02419	1.2180	0.0186
1215.5	0.02557	1.2212	0.0218
1214.8	0.02695	1.2309	0.0315
1239.1	0.02835	1.2402	0.0408
1237.9	0.02980	1.2520	0.0526
1246.6	0.03120	1.2640	0.0646
1250.2	0.03271	1.2739	0.0745
1244.9	0.03419	1.2865	0.0871
1147.2	0.03585	1.3304	0.1311
923.2	0.03842	1.3861	0.1867
883.1	0.04014	1.4120	0.2126

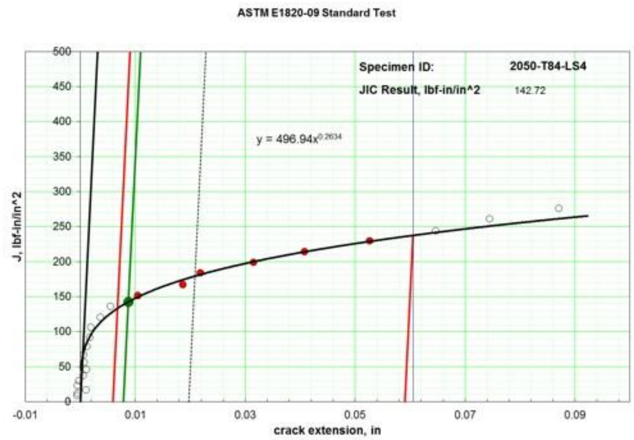

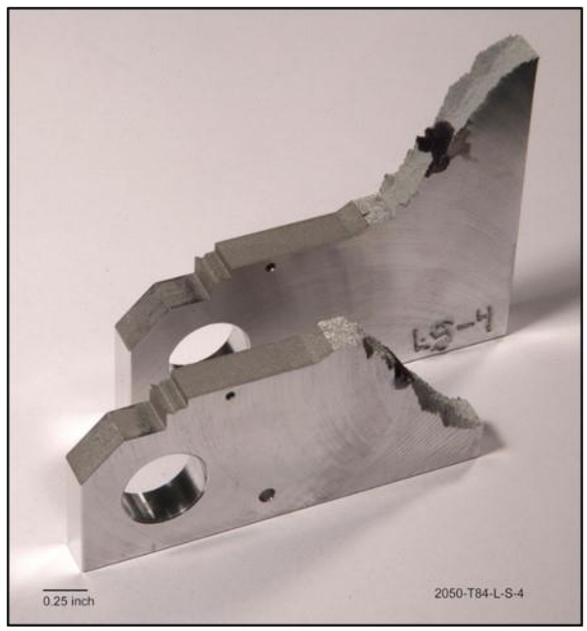

Figure E15. Fracture toughness data, J-curve, and image showing fracture path for 2050-T84, L-S orientation, t/6, specimen 4, tested at -320ºF.

Force	Disp1	Crack	Δa
lbf	inch	inch	inch
281.5	0.00430	1.1973	-0.0003
330.9	0.00524	1.1973	-0.0003
396.4	0.00649	1.1973	-0.0003
461.7	0.00775	1.1971	-0.0005
527.6	0.00902	1.1970	-0.0006
593.0	0.01029	1.1971	-0.0004
658.4	0.01157	1.1976	0.0000
724.2	0.01288	1.1977	0.0001
790.0	0.01420	1.1983	0.0008
854.1	0.01552	1.1990	0.0014
916.7	0.01684	1.1994	0.0018
978.5	0.01817	1.2001	0.0025
1039.1	0.01950	1.2017	0.0041
1095.9	0.02085	1.2036	0.0060
1150.8	0.02221	1.2056	0.0080
1196.0	0.02360	1.2087	0.0111
1236.1	0.02499	1.2126	0.0150
1237.4	0.02638	1.2237	0.0261
1263.9	0.02778	1.2306	0.0330
1262.4	0.02916	1.2420	0.0444
1297.2	0.03057	1.2484	0.0508
1274.3	0.03199	1.2638	0.0662
1288.9	0.03342	1.2738	0.0762
1252.1	0.03484	1.3110	0.1134
982.5	0.03751	1.4012	0.2036

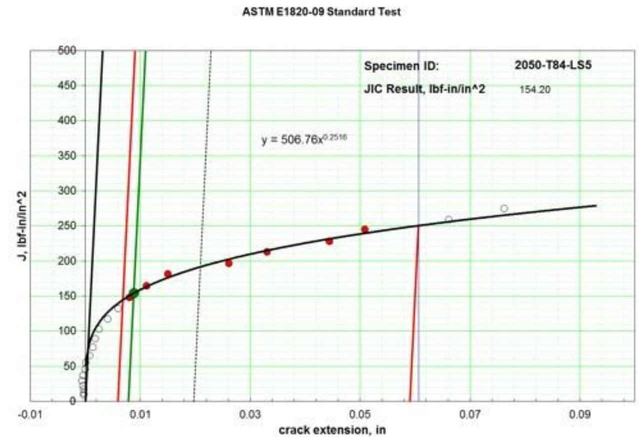

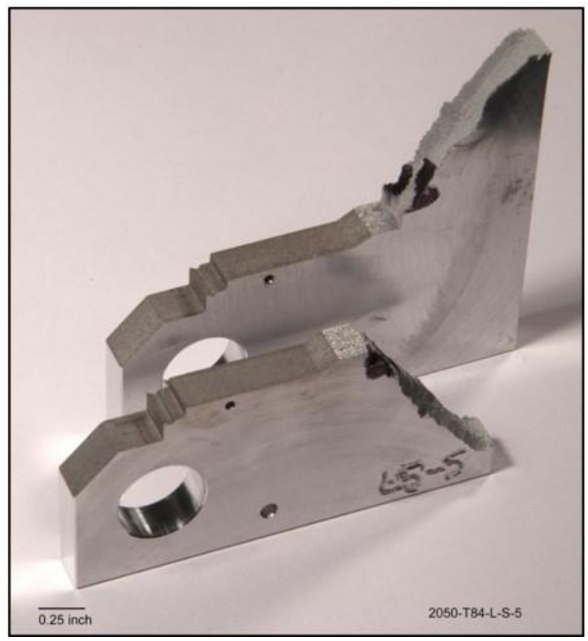

Figure E16. Fracture toughness data, J-curve, and image showing fracture path for 2050-T84, L-S orientation, t/6, specimen 5, tested at -320ºF.

Force lbf	Disp1 inch	Crack inch	Δa inch
274.7	0.00411	1.1958	-0.0005
321.1	0.00498	1.1955	-0.0008
387.0	0.00622	1.1960	-0.0004
453.3	0.00745	1.1960	-0.0003
519.4	0.00870	1.1963	-0.0001
585.6	0.00996	1.1961	-0.0002
652.2	0.01123	1.1962	-0.0001
718.6	0.01250	1.1972	0.0009
784.8	0.01377	1.1974	0.0011
851.1	0.01508	1.1988	0.0025
918.1	0.01641	1.1995	0.0032
984.8	0.01775	1.2004	0.0041
1048.7	0.01910	1.2010	0.0047
1109.3	0.02045	1.2025	0.0062
1166.9	0.02180	1.2043	0.0080
1182.1	0.02317	1.2142	0.0178
1211.5	0.02463	1.2216	0.0253
1237.3	0.02603	1.2291	0.0328
1250.6	0.02746	1.2385	0.0422
1257.7	0.02889	1.2489	0.0526
1261.4	0.03029	1.2617	0.0653
1244.5	0.03168	1.2775	0.0812
1226.0	0.03321	1.2962	0.0999
1168.8	0.03486	1.3297	0.1334
1140.1	0.03644	1.3459	0.1496
1086.7	0.03801	1.3834	0.1871
870.1	0.04050	1.4479	0.2516

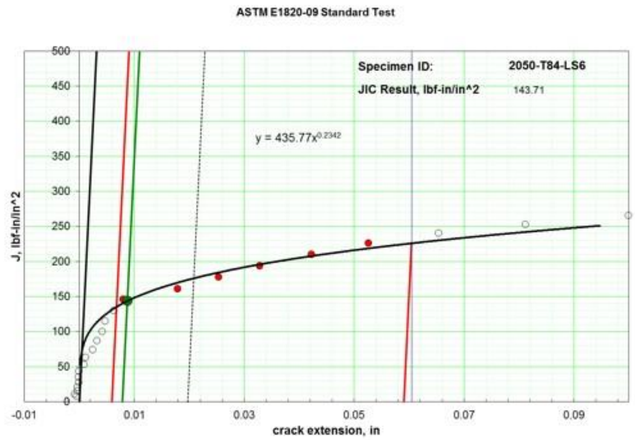

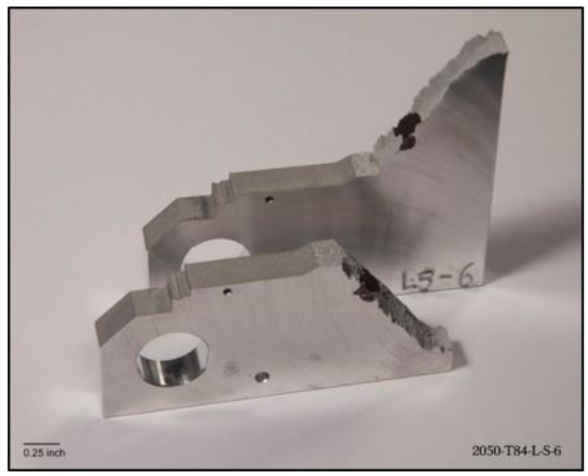

Figure E17. Fracture toughness data, J-curve, and image showing fracture path for 2050-T84, L-S orientation, t/6, specimen 6, tested at -320ºF.

REPORT DOCUMENTATION PAGE	*Form Approved OMB No. 0704-0188*

	2. REPORT TYPE	**3. DATES COVERED** *(From - To)*
	Technical Memorandum	

4. TITLE AND SUBTITLE	**5a. CONTRACT NUMBER**
Evaluation of Aluminum Alloy 2050-T84 Microstructure Mechanical Properties at Ambient and Cryogenic Temperatures	**5b. GRANT NUMBER**
	5c. PROGRAM ELEMENT NUMBER
6. AUTHOR(S)	**5d. PROJECT NUMBER**
Hafley, Robert A.; Domack, Marcia S.; Hales, Stephen J.; Shenoy, Ravi N.	**5e. TASK NUMBER**
	5f. WORK UNIT NUMBER 869021.04.07.01.013

7. PERFORMING ORGANIZATION NAME(S) AND ADDRESS(ES)	**8. PERFORMING ORGANIZATION REPORT NUMBER**
NASA Langley Research Center Hampton, VA 23681-2199	L-20041
9. SPONSORING/MONITORING AGENCY NAME(S) AND ADDRESS(ES)	**10. SPONSOR/MONITOR'S ACRONYM(S)**
National Aeronautics and Space Administration Washington, DC 20546-0001	NASA
	11. SPONSOR/MONITOR'S REPORT NUMBER(S) NASA/TM-2011-217163(Corrected Copy)

12. DISTRIBUTION/AVAILABILITY STATEMENT
Unclassified Unlimited
Subject Category 26
Availability: NASA STI Program (757) 864-9658

13. SUPPLEMENTARY NOTES

14. ABSTRACT

Aluminum alloy 2050 is being considered for the fabrication of cryogenic propellant tanks to reduce the mass of future heavy-lift launch vehicles. The alloy is available in section thicknesses greater than that of the incumbent aluminum alloy, 2195, which will enable designs with greater structural efficiency. While ambient temperature design allowable properties are available for alloy 2050, cryogenic properties are not available. To determine its suitability for use in cryogenic propellant tanks, tensile, compression and fracture tests were conducted on 4 inch thick 2050–T84 plate at ambient temperature and at -320°F. Various metallurgical analyses were also performed in order to provide an understanding of the compositional homogeneity and microstructure of 2050.

15. SUBJECT TERMS

Al-Cu-Li alloy, compression properties, cryogenic properties, tensile properties

16. SECURITY CLASSIFICATION OF: a. REPORT	b. ABSTRACT	c. THIS PAGE	**17. LIMITATION OF ABSTRACT**	**18. NUMBER OF PAGES**	**19a. NAME OF RESPONSIBLE PERSON**
					STI Help Desk (email: help@sti.nasa.gov)
					19b. TELEPHONE NUMBER *(Include area code)*
U	U	U	UU	99	(757) 864-9658

Standard Form 298 (Rev. 8-98)
Prescribed by ANSI Std. Z39.18